The analysis and mathematical modelling of the parameters influencing cathodic deposits in copper refining electrolysis

Dipl.-Ing. Iris Filzwieser

Dissertation zur Erlangung des akademischen Grades eines
Doktors der montanistischen Wissenschaften
an der Montanuniversität Leoben

Leoben, Juni 2005

Hiermit erkläre ich Eides Statt,
die vorliegenden Arbeit selbst verfasst
und nur unter Verwendung der angegebenen Hilfsmittel
durchgeführt zu haben.

Dipl.-Ing. Iris Filzwieser

Leoben, Juni 2005

Danksagung

Die vorliegende Arbeit wurde in der Zeit von 2002 bis 2005 am Department für Metallurgie mit dem Arbeitsbereich Nichteisenmetallurgie der Montanuniversität angefertigt.

Besonderer Dank gilt Herrn O.Univ.Prof.Dipl.-Ing.Dr.mont Peter Paschen für die Übertragung und Begutachtung der Arbeit. Außerdem möchte ich mich für seine unermüdliche Bereitschaft, nicht nur der wissenschaftliche, sondern auch in sehr vielen anderen Lebensbereichen ein Mentor gewesen zu sein, bedanken.

Gleichzeitig danke ich Herrn Prof.Dipl.-Ing.Dr.-Ing.Dr.mont.h.c. Klaus Hein für seine wertvollen Anregungen, sowie für die Betreuung und Begutachtung der Arbeit. Auch ihm danke ich ganz herzlich für sein Verständnis und seine unermüdliche Diskussionsbereitschaft.

Ich möchte mich weiters bei meinen Diplomanden bedanken, die mit Ihrer Arbeit auch zum Entstehen der vorliegenden Arbeit beigetragen haben.

Ein herzliches Dankesschön gilt auch allen Mitgliedern des Institutes für Nichteisenmetallurgie für die gute Zusammenarbeit, die ständige Diskussionsbereitschaft und dem ausgezeichneten Arbeitsklima. Besonders hervorheben möchte ich Herrn Erich Troger, für seine wertvolle Unterstützung im Aufbau der Versuchsanlage und Frau Claudia Pelka, die mir bei so manchen administrativen Schwierigkeiten immer mit Rat und Tat zur Seite stand.

Ganz besonders möchte ich noch meinen Eltern danken, die mich immer unterstütz haben. Sie haben es mir ermöglicht eine gute schulische Ausbildung zu genießen und in sehr vielen Lebenslagen ihre uneingeschränkte Liebe gezeigt. Danke! Weiters danke ich auch meinen lieben Schwiegereltern, die zu jeder Zeit abrufbar waren und auch geholfen haben, wo es nur ging.

Schließlich möchte ich aber auch noch „meinen“ Männern danken. Florian, Sebastian und Felix waren mir immer eine große Hilfe und für jegliche wissenschaftliche Diskussionen sehr aufgeschlossen.

Zu letzt möchte ich meinem geliebten Mann danke sagen. Er war es, der mich unentwegt motivierte und nicht aufhörte an mich zu glauben. Danke!

1 INTRODUCTION

During the last decades, copper production methods have been subjected to a continual selection process because of the requirement for increased productivity through rationalization, lower energy consumption, raised environmental protection, increased operational reliability, and improved operational safety. The selection of a particular production method depends essentially on the type of raw materials available, which are usually ore or concentrate, and on the specific plant conditions. Globally, approximately 80 % of primary copper is produced from low-grade or poor sulphide ores, which are usually treated by pyrometallurgical methods, typically in the following sequence:

- Beneficiation of the ore to copper concentrate by froth flotation
- Optional partial roasting to obtain oxidized material
- Two-stage pyrometallurgical extraction
    - Smelting concentrates to matte
    - Converting matte to crude copper by oxidation
- Refining the crude copper, usually in two steps
    - Pyrometallurgically to fire-refined copper
    - Electrolytically to high-purity electrolytic copper

In addition, approximately 15 % of primary copper is produced from low-grade oxidized or mixed ores /1/ and these materials are generally treated by hydrometallurgical methods. Figure 1-1 depicts the flow diagram of a modern copper smelter, from the concentration process to production of the pure copper cathode.

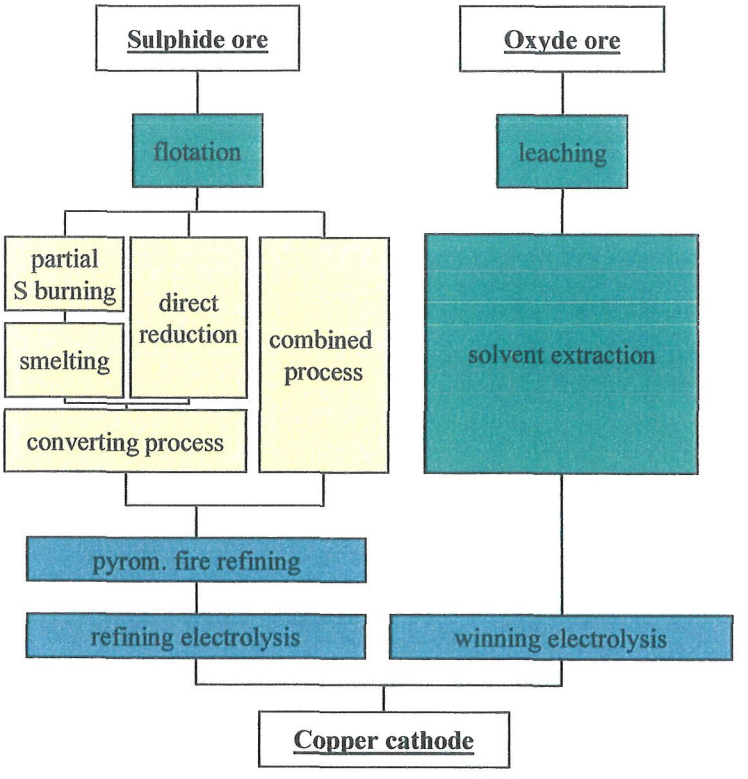

Figure 1-1: Typical flow diagram of pyrometallurgical copper production from ore concentrates

Nearly all pyrometallurgical copper processes are based on the principle of partial oxidation of the sulphide ore concentrates. Methods based on the total oxidation of sulphidic ores with the subsequent reduction to the metal, thereby avoiding the formation of copper matte, are rarely employed because of the high fuel consumption, the formation of copper-rich slags, and the production of crude copper with high impurity levels.

The flash smelting process with subsequent converting has become the most important process set-up. The costs of this hydrometallurgical processing depend on the copper content; however, typically the capital costs are up to 50 % less than for conventional processing. Energy requirements have a significant effect on operating costs and the step that requires the largest proportion of energy for pyrometallurgical copper production is the smelting itself /2/.

Step	Energy required per 1 t Cu [GJ]	Deviation [%]
Mining	5.5	35
Beneficiation	3.8	35
Smelting (Outokumpu flash)	8.4	20
Converting	0.0	-
Anode casting	0.2	10
Electrolysis	1.3	10
Cathode casting	1.7	10
total	20.9	

Table 1-1: Energy as required /3/

The amount of energy required to produce copper pyrometallurgically depends on the process.

Process	Energy required per 1 t Cu [GJ]
INCO, flash smelting (95 % O_2)	1.7
Electric furnace	6.7
Noranda process (30 % O_2)	6.7
Outokumpu flash smelting	8.4
Mitsubishi process	10.1
Reverberatory furnace with roasted concentrate	13.4
Brixlegg process	19.3
Reverberatory furnace with raw concentrate	21.8

Table 1-2: Amount of energy required for different pyrometallurgical processes /3/

After the pyrometallurgical smelting process, conventional refining comprises two stages:

- Pyrometallurgical or fire refining
- Electrolytic refining

The refining without electrolysis is adequate if the fire-refined copper has the purity and if the precious metal content can be neglected. Extremely high-purity copper is occasionally required for research purposes; in such cases, zone melting or repeated electrolysis is employed.

1.1 Pyrometallurgical refining

The fire refining of blister copper to anode copper for electrolysis or commercial fire-refined copper has the following functions:

- Removing impurities by slagging and volatilization, with the precious metals remaining entirely in the metallic copper
- Reducing the sulphur content by oxidation to approximately 0.002 wt % or 20 ppm
- Decreasing the oxygen content by reduction to < 0.15 % or < 1500 ppm, thereby producing a flat surface as a result of the water-gas equilibrium in the molten copper

After fire refining, anode casting can be performed continuously or discontinuously. The conventional anode production method is discontinuous casting on casting wheel machines. The pure copper moulds must be sprayed with a mould coating that prevents the solidified anodes sticking, and barite, alumina, or silica are suitable for this application. The casting rate can reach 80 t/h /4/. The anode weights vary between 160 and 400 kg, depending on the specific refinery. Another possibility is to produce uniform anodes using the continuous Hazelett twin-belt casting system.

1.2 Electrolytic refining

More than 80 % of global copper production is refined by electrolysis. This treatment generates copper with a high electrical conductivity and enables the separation of valuable impurities, in particular precious metals.

Several half-reactions can possibly occur at the electrodes:

Anode reactions				Cathode reactions				E^0 (25°C) [mV]
Cu	$\rightarrow$	Cu^{2+}	$+ 2e^-$	Cu^{2+}	$+ 2e^-$	$\rightarrow$	Cu	0.337
Cu	$\rightarrow$	Cu^{+}	$+ e^-$	Cu^{+}	$+ e^-$	$\rightarrow$	Cu	0.521
Cu^{+}	$\rightarrow$	Cu^{2+}	$+ e^-$	Cu^{2+}	$+ e^-$	$\rightarrow$	Cu^{+}	0.153

Table 1-3: Reactions at electrodes

Whilst the following secondary reactions occur in the electrolyte:

				$2\ Cu^{+}$	$\rightarrow$	Cu^{2+}	+	Cu	disproportionation
$2\ Cu^{+}$	+	$2\ H^{+}$	+	$\frac{1}{2}\ O_2$	$\rightarrow$	$2Cu^{2+}$	+	H_2O	air oxidation
		Cu_2O	+	$2\ H^{+}$	$\rightarrow$	$2\ Cu^{+}$	+	H_2O	dissolution of Cu_2O

Table 1-4: Secondary reactions

Oxidation of air and disproportionation of copper(I)ions generates a surplus of copper(II)ions in the electrolyte, Table 1-4. The copper metal powder formed by the disproportionation of Cu^{+} contributes to the accumulation of anode slime. The electrochemical equivalent of copper depends on the oxidation state, Table 1-5.

Species	g/Ah	mg/C
Cu^{2+}	1.185	0.3294
Cu^{+}	2.371	0.6588

Table 1-5: Electrochemical equivalent

The two most important electrical parameters in electrolytic copper refining operations are the cell voltage and the current density. The cell voltage, which usually ranges between 0.25 and 0.3 V, is determined by several factors:

- Ohmic electrolyte resistance, which is dependent on the composition, temperature, and electrode distance
- Polarization, especially overvoltage of electrodes, which is dependent on the rate of electrolyte circulation and temperature
- Polarization due to organic additives
- Voltage loss in the circuit
- Anode passivity, which may occur at high current densities and impurities

The interaction of these effects is difficult to predict. At any particular electrolytic facility, a continual effort is made to optimize the cell voltage. With increasing current density the production of copper increases and the current efficiency decreases.

The behaviour of impurities also influences the process and is dependent on their position in the electrochemical series: elements more electropositive than copper are insoluble, while less electropositive elements dissolve in or react with the electrolyte. Therefore, electrolysis distributes the anode material among three phases: cathode copper, electrolyte, and anode slime.

Insoluble substances account for < 1 % of the anode weight and they collect on the cell bottom as anode slime. The slime contains precious metals including selenides; tellurides of copper and silver; and complex compounds of lead, arsenic, antimony, bismuth, and nickel. Although the separation techniques differ significantly from plant to plant, anode slimes are generally treated as part of the production process.

In the various plants the electrolyte composition for copper electrolysis is generally similar. As a result of secondary reactions during electrolysis the concentration of copper(II)ions increases slowly; therefore, the copper surplus must be recovered by cathodic deposition in a few liberator cells equipped with insoluble anodes, usually of antimonial lead. Soluble impurities such as iron, cobalt, zinc, manganese, most of nickel, and some arsenic and antimony, are also enriched in the electrolyte /5/.
Currently, cathode copper is produced at purity between 99.97 and 99.99 %.

2 TASK DESCRIPTION

A constant problem in copper refining electrolysis is establishing a sufficiently high current whilst maintaining the lowest specific energy consumption and highest current density. A high current can be obtained if no short circuits occur during electrolysis. A short circuit results if the two electrodes connect due to dendritic growth. Under these conditions the electricity is no longer used for precipitation, but is converted into heat. In practice, dendrites, which always exist to a greater or lesser extent, must be identified and removed daily by a plant employee. To minimize the probability of short circuits it is important to avoid dendrites; therefore, it is necessary to determine the influence of the electrolysis conditions on dendrite growth, the crystallization mechanisms of dendrites, and the interdependence of the electrolysis parameters.

To evaluate the influences on cathode dendrite formation, the "Sponsor Group" initiated the "CESAR" project at the Department of Nonferrous Metallurgy, University of Leoben, Austria. The Sponsor Group consisted of seven international partners: Atlantic Copper (Spain), Codelco (Chile), New Boliden (Sweden), Noranda (Canada, until 2003), Norddeutsche Affinerie (Germany), Outokumpu (Finland - since 2004 part of New Boliden), and Umicore (Belgium).

CESAR is the abbreviation for Copper Electrolysis Shorts Avoidance Research. This project was defined for a three year period (September 2002–September 2005), and this PhD thesis was part of the project.

In addition to this project the following work was accomplished:

***General literature study** /6, 7, 8/*

Evaluation of the actual tankhouse parameters

Metallographic investigations

Analysis of dendritic cathodes provided by the partners
Summary of the electrolysis parameters and conditions, especially for the analysed dendritic cathodes
Metallographic discussion and analysis of the dendrites

Establishment of a near technical scale cell

The cell design and electrode arrangement was optimized using computational fluid dynamic (CFD) mathematical modelling

Investigations

Different chemical anode qualities
Different current densities
Anode slimes derived from different anodes (with different chemical compositions)
Variation of the anode-cathode distance and geometry

Defining a mathematical model to describe the interrelationships of the different parameters

3 ACTUAL DATA FROM INDUSTRY

It is well established that the appearance of short circuits (or shorts) negatively influences cathode production in a persistent manner. Cataloguing and avoiding shorts is a decisive and important objective for industrial plants. To address this issue from a laboratory research perspective requires adequate details of the circumstances and conditions of the respective cell houses by inspections at the different companies. Therefore, a detailed investigation of the seven partners' individual conditions was performed by means of a questionnaire. The answers to these questionnaires had to give a general overall view on the refineries /9/.

The questionnaire included the basic data concerning the following issues:

- Copper production
- Anodes
- Anode slime
- Electrolytic cells and cell inspections
- Short circuits (shorts)
- Electrolyte
- Additives
- Cathodes

The data from all the questionnaires was compiled and Table 3-1 details the most important plant characteristics. All abbreviations and symbols used are explained in page 149.

	A	B	C				E	F	G			H
Electrolyte , g/l												
Cu	45	50	40 to 43				46	46	45			42
Free H2SO4	180	172	190 to 205				175	50	175			165
As	6	1.5	5 to10				8 to 10	7	7			2.5
Sb	0.4	0.3	0.4 to 0.5				0.5 to 0.6	0.5	0.5			0.5
Bi	0.5	0.04					0.1 to 0.2	0.2	0.2			0.15
Ni	5	20	0.1 to 0.5				12 to 18	13	12			16
Fe	1.3						1.2		0.2			
Cl	0.04	0.5	0.03 to 0.06				0.04	0.05	0.04			0.04
Inlet temperature, °C	64	65	60				63	67 to 68	65			65
Outlet temperature, °C	66	69					63 to 68	65 to 67	63			65
Circulation, l/min/cell	18 to 24	15 to 20	20				25	17	20			20
Addition Agents:												
Glue g/tonne of cathode	80	75	35	35			25	100	100			60
Thiourea	60	78	60	60			53	70	60			45
Avitone A	No	No	22	10			No	No	No			0.5
HCl, NaCl, g/t	50	70 NaCl					35 to 40	50 HCl				HCl 0.040 g/l
Other	No	No					No	No	No			No
CATHODES												
Cu starting sheet/stainless steel	SS						SS	Cu SS	SS			SS
Copper Starting Sheets:												
L, mm								969				
W, mm								960				
T, mm								0.7				
Mass, kg								5.5				
Starting blanks								SS				
Isa or Kidd	ISA	ISA					ISA		ISA			Kidd
Stainless steel	316L						3167 L		316L			316L
L, mm	1092	1018							1092			1092
W, mm	966	946							966			967
T, mm	3.25								3.25			3
Mass, kg	36						36		36			35
Life, days	6						5 to 8		7			7
Final Cu mass, kg	50	40 to 50					50 to 70		55			100
System of stripping?	ISA	ISA					ISA		ISA			KIDD

	A	B	C				E	F	G			H
			CI	CII	CIII	CIV			GI	GII	GIII	
Capacity of t of cathodes/year	245 000	240 000					[illegible]	[illegible]	340 000			360 000
Production of cathodes t 2000	257 593	133 000	192 000	491 000			[illegible]	[illegible]	320 000			313 000
Production of cathodes t 2001	235 280	217 000						115 471				323 023
Anode Furnance												
Conv./ conti. cast	Conv.	Conv.					Conv.	Conv.	Conv.			Conv.
Automatic weight control	Yes	Yes					Yes	Yes	Auto			Yes
Weight tolerance of anodes,kg	10	[illegible]	5				[illegible]	10	12			[illegible]
Casting mould coating	$BaSO_4$	$BaSO_4$					$BaSO_4$	$BaSO_4$ +water	SiO_2			$BaSO_4$
Anode preparation machine	Wenmec	Wenmec					Yes	No	Yes			Yes
Anodes L, mm	937	995	1 218	[illegible]			1 046	[illegible]	960			1 049
Anodes W, mm	864	882	[illegible]	856			914	900	[illegible]			890
Anodes T, mm	49	[illegible]	42	[illegible]				45	[illegible]			46
Mass, kg	357	335	400				[illegible]	300 to 320	400			[illegible]
Life, days	18	[illegible]	[illegible]				21	[illegible]	21			21
Scrap, %	15	20	[illegible]				[illegible]	20 to 22	16			18
Anode Analysis												
Cu%	99.50	[illegible]	99.59	99.60	[illegible]	99.65	> 99.50	99.00				
Ag ppm	203	2 000	495	366	[illegible]	287	800	322				[illegible]
Au ppm	57.00	60.00	2.03	3.93	[illegible]	12.83	50.00	51.00				[illegible]
S ppm	[illegible]	< 50	[illegible]		17							
Se ppm	360	400	137	[illegible]	240	109	400	425				[illegible]
Te ppm	60	110	34	26	[illegible]	28	100	171				[illegible]
As ppm	870	900	1 547	1 164	1 235	911	800	[illegible]				[illegible]
Sb ppm	160	[illegible]	145	130	111	180	450	[illegible]				371
Bi ppm	110	100	62	40	[illegible]	20	100	[illegible]				150
Pb ppm	260	[illegible]	94	72	[illegible]	62	500	114				1 038
Fe ppm		[illegible]	12	[illegible]	27	10						
Ni ppm	190	[illegible]	[illegible]	41	65	105	1 000	2 630				1 582
O ppm	[illegible]	1,800 to 2,200	1 350	1 760	1 419	1 523	1 400	2 000				[illegible]

	A	B	C				E	F	G			H
Anode Slime												
kg per tonne of anode	2.4	8					6	5.9				10
removed after ? days	18	16										
Analysis, %												
Cu	17.0	12.0	34.3	33.7	40.3	34.6	15.0		25.6	30.2	26.4	17.0
Ag	9.0	25.0	15.7	16.7	10.0	13.5	10.5	8.7	3.2		12.2	
Au	3.5	0.8	0.1	0.2	0.1	0.4	0.7	1.0				1.0
S									9.5	10.6		
Se	15.0	3.9	6.1	5.7	8.1	5.9	5.0	8.8		5.7	6.3	7.0
Te	1.0	2.2	1.2	1.3	0.7	1.1	2.0	1.4		0.5	2.4	
As	1.0	1.4	7.3	7.9	7.8	7.6	4.5		2.2	1.8	3.2	1.5
Sb	2.0	3.7	3.2	3.9	3.0	4.5			7		1.6	1.0
Bi		0.7	0.9	0.2	0.6	0.7			0.9	0.3	0.8	0.5
Pb		0.7	2.2	2.1	3.3	5.1			1.8	2.2	3.4	10.0
Fe			0.04	0.05	0.04	0.05					0.04	
Ni		2.7	45.0	21.0		39.0	0.7		10.0	1.3	1.5	0.8
Cell principal:												
Commercial cells, numbers	1 120	896	750	1920			1 075	692	911			
Stripper cells, numbers		896						68				6
Liberator cells, numbers	46							20	9			18
Cell construction:												
Electrolyte inlet, position	Down	Bottom					Bottom	Bottom	~1 m below Bot.			Bottom
Electrolyte outlet, position	Top	Top					Top	Top	Top			Top
Inside size L, mm	4 100	4 490										
Inside size W, mm	1 050	1 102						1 090				
Inside size D, mm	1 300	1 330										
Anodes/cathodes per cell	40 / 39	44/43					57 / 56					48/47
A/A centre to centre, mm	98	100	114						100			102
A/C face, mm (min)	20						18		24			
A/C face, mm (max.)							37		38			
Current density, A/m²	330	330	240					316	310			275
Cathode current efficiency, %	96								92 - 96			95
Periodic current reverse?	No	No					No	Yes	No			No
Stop and go?	No						No					
Time efficiency, %	97.50						96.70	97.00				

	A	B	C				E	F	G			H
10. CATHODE ANALYSIS:												
Cu %	99.99		99.99				> 99.99	99.997				
Ag ppm	17.3	16	7.3				10	9.4	10			13.98
S ppm	4	5	2.3				< 3	4.3	4			
Se ppm	< 0.5	0.3	0.1					0.6				0.23
Te ppm	< 0.5	0.3	0.1					0.3				0.2
As ppm	< 0.8	0.3	3.1				0.75	0.6				< 0.2
Sb ppm	< 0.8	0.4	0.1				1					0.2
Bi ppm	0.3	0.05	0.1				0.2	0.2				< 0.1
Pb ppm	< 0.5	0.5	0.47				< 0.5	0.3				3.2
Fe ppm		3	0.99					1.5	< 1			1.7
Ni ppm	< 0.5	0.7	0.1					0.8				

Table 3-1: Questionnaire data

Table 3-1 provides a good overview of the important parameters at the individual electrolysis plants. In the table significant values are highlighted in red or green, whereby red values represent the maxima and green values the minima. In the following paragraphs the individual values and their dispersion are discussed briefly.

The anode casting was performed using conventional casting machines. The facing material for the moulds was barium sulphate with one exception: silica.

A decisive point for the final anode geometry and their arrangement was the casting weight tolerance, which showed a variation from 4 to 15 kg. In dependent of the dimensions this results in different thicknesses. In the cell house this led to different anode-cathode distances with the consequence of various current density distributions at the electrodes. In these cases the existing different current densities resulted in irregular crystal growth (dendrite formation).

The anode thickness varied from 37 to 50 mm. This dimension and the weight of the anodes dictated the length of an anode period in the electrolysis. The cathode crops in the partner plants were very different with a minimum of 5 days and a maximum of 12 days. Therefore, the conditions in the cells were very different. In addition, the initial anode-cathode distance varied by more than 10 mm per side.

Both copper starting sheets as well as stainless steel blanks have been employed as cathode blanks. The current densities fluctuated between 242 and 337 A/m^2, which is considered a large variation.

The type of inhibitors were the same in all plants, however, the dosage was very different. The proportion glue/thiourea varied between 0.58 and 1.71 g per ton of cathodic copper. This means that the dosage relation fluctuates by 300 %! The absolute figures for glue were between 31 g/t and 120 g/t and the values for thiourea were 45 g/t to 70 g/t. The amount of added chlorine ions was between 35 and 50 mg/l.

The electrolyte temperature was 60 to 68 °C.

The cell volume exchange also had a broad variation range of 50 %. Furthermore, the number of anodes per cell was very different. In conclusion, these factors indicated that there were very different process conditions in use in the plants of the various companies.

Extremely variable was the chemical composition of the anodes with nickel levels from 24 to 4100 ppm, and oxygen amounts from 1140 to 3500 ppm. The critical elements Sb, As, Bi, Se, and Te also fluctuated enormously.

The attempt was made to determine certain collection and description of shorts with the aid of the questionnaires. However, this was only effective for a few parameters and the data and information provided were not sufficient for this. A comprehensive statistical evaluation and overview on the problematic nature of shorts occurrence was not possible at this time. Furthermore, the search for shorts was handled in a rather different way. Partly there was a search for shorts in one shift and partly this search was performed by a certain number of employees continuously.

With these data characteristics like the mole fraction ratio MFR I As/(Sb+Bi), and the mole fraction ratio MFR II Ag/(Se+Te) were calculated to compare the conditions in the plants. These figures are shown in Table 3-2 and Table 3-3 /10/.

	A	B	C/I	C/II	C/III	C/IV	E	F	G/I	G/II	G/III	H
MFR A	6.31	2.62	13.85	12.36	17.38	7.72	2.56	[illegible]	[illegible]	4.15	6.76	2.01
MFR AS	0.81	0.55	3.26	3.19	[illegible]	2.52	1.08	2.75	[illegible]	3.15	1.02	1.89
MFR C	1.33	1.14	1.63	[illegible]	[illegible]	[illegible]	1.09	[illegible]	1.03	1.03	1.03	1.26
MFR E	14.10	[illegible]	20.32	32.50	[illegible]	[illegible]	21.94	[illegible]	18.45	18.45	18.45	7.56

Table 3-2: MFR I As/(Sb+Bi)

MFR: MFR
MFR A: MFR anode
MFR AS: MFR anode slime
MFR C: MFR cathode
MFR E: MFR electrolyte

A high MFR I ratio is an advantage in the refining plant. A high As level prevents the Sb^{3+} from being oxidized to Sb^{5+} due to the higher oxygen affinity of As^{3+} compared to Sb^{3+}. In fact Sb^{5+} is a main component of the drifting slimes. All MFR < 1 are critical because there is too little As and the existence of Sb^{5+} is very possible /11/.

	A	B	C/I	C/II	C/III	C/IV	D	E	F	G/I	G/II	G/III	H
MFR	0.48	[illegible]	2.89	2.46	0.56	2.09		1.60	0.54	3.50	[illegible]	1.34	3.29

Table 3-3: MFR II Ag/(Se+Te)

If Se and Te are surplus in the anode then the Ag content in the anode is too low to combine Se and Te with Ag; therefore, the formation of Cu_2Se and Cu_2Te occurs. Alternatively, Ag will go directly to the cathode if there is too little Se and Te in the anode /12, 13/.

The discussed Se and Te form difficult dissolving complexes in the anode slime. The anode slime that is whirled up will go to the cathode and thereby they will be responsible for many problems in the refinery.

With relation to the cathode and anode distances it was possible to see large variations. The minimum distance between the anode and cathode was 18.5 mm and the maximum distance was 33.5 mm, a variation of 15 mm.

The evaluation of Table 3-2 and Table 3-3 indicated that between the individual electrolysis plants large differences exist. In Chapter 4 the different reasons for dendrite growth are discussed and the relationship to the existing evaluation is given to the individual electrolysis conditions.

4 METALLOGRAPHICAL ANALYSIS OF NODULATED COPPER ELECTRODEPOSITS

Metallographical investigations were performed on the nodulated cathode samples received from the five companies: A, B, E, F, and G. The factors considered when selecting nodules for the metallography studies included the appearance and the position of the nodule on the cathode surface either on the top-region, mid-region, or bottom-region of cathode so that the samples were representative of the nodulation behaviour over the entire cathode surface. The partners filled out a metallographic questionnaire and the conditions in the electrolytic cell at the time of the appearance of the nodules were recorded. In this chapter, all the reasons for dendrite formation will initially be investigated, for example impurities in the anode slime, floating slime, and $BaSO_4$, as well as inhibitor problems including the transportation and amount. Subsequently, a link between these facts and the conditions in the tankhouse will be discussed.

4.1 Introduction

There are two possibilities for buds and dendrites formation during cathodic precipitation in the copper refining electrolysis. These are:

1) The crystallization changes for certain reasons with the result that cavities (spherical or streaky) are formed. Subsequently, particles (anode slime and drifting slimes) are mechanically enclosed in the hollow space. Whilst the inclusions are the consequence of a disturbed crystallization they are not the cause of it.

2) Particles (metals, oxides, and compounds) are deposited on the copper precipitate for certain reasons (mechanically, chemically, and electrochemically) with the consequence that the crystallization behaviour changes towards bud formation. Whilst the particles are the reason for the disturbed crystallization they are not the consequence of it.

The further bud growth towards dendrite formation, which finally leads to shorts, appears to be independent from the events at the bud roots. This growth is mainly caused by the higher current density at the summit of the paunch. The following literature summary was performed principally on the basis of these assumptions; therefore, the order is in reverse.

- Buds and dendrites and their roots
- Analysis of inclusions
- Electrocrystallization
- Electrolysis parameters (inhibitors, chemical analysis, mass transfer, current density, and temperature)
- Anode slime and drifting slimes
- Anodic dissolution
- Anode casting and preparation
- Anode composition
- Anode furnace refining

Dendrites may have already been produced after the nucleation stage when the separate crystallites start their growth to merge into a compact layer. In this collective growth the anisotropy of growth begins. A geometrical selection takes place and a favourable orientation in the electric field lines occurs. This causes faster growth in a predominant direction and a columnar structure is formed /14/.

The nodulation has often started on the surface of the starter sheet, although a layer of smooth copper is deposited before nodulation commences /15/. Whilst the roots may exhibit a pronounced dendritic structure without cavities, most nodules display roots with microcavities, where slime particles may be encapsulated. The size of these slimes clusters, rather than their composition, appears to be the important factor determining further nodule formation and growth. Subsequently, the nodulation can effect all parts of the cathode deposit. The very fine crystals in the first zone (FT type) are very compact; with increasing time the grains become coarser, bud formation begins, sometimes with small cracks in between. The cracks then become wider and the electrolyte becomes enclosed.

/16/ illustrates that the cathodic surface structure corresponds directly to the cathode quality and/or purity. The original cathode itself normally has a polycrystalline metal surface with different crystallographic orientations. Furthermore there are grain boundaries, crystal defects, inclusions, adsorbed molecules, oxides, and different grain sizes /17/. On such surfaces the nucleation of cathodic discharge and deposition has to take place.

All electrolyte additions can be partly included in the cathodic copper, especially the sulphur from the thiourea /18/, which originates from the decomposition of $CS(NH_2)_2$. A thiourea balance stated that 20 to 27 % of the additive goes into the cathodes, with the exact amount being directly proportional to the amount added to the electrolyte. Up to 0.6 % of thiourea sulphur could be detected. No increase could be found between the cathode crops.

Following /11/, Sb (and As, Bi and their compounds) can precipitate on the cathode surface as colloidal solids that then lead to a faulty copper nucleation. In the case of entrapped anode slime particles in the cathode, the analysis of the inclusions corresponds to the anode slime analysis.

Electrocrystallization is based on the electrostatic attraction of ions. The first step is nucleation. Nucleation is the surface build-up and requires energy (activation energy and polarization at the cathode). However, because the activation energy is smaller at preferential points of the lattice, the formation of nuclei occurs at these "active places".

A high nucleation number produces a fine grain size and a high crystallization speed produces dendrites. In the case of rapid growth (oversaturation) the build-up of crystals takes place primarily at the edges and corners. The structure of the precipitates depends on the number of crystallites per area and their orientation. The main parameters are:

- Velocity of ion supply to the cathode
- Mobility of cations on the cathode surface (insertion into the lattice)
- Presence of other constituents in the electrolyte (inhibitors, slimes, undissolved and dissolved elements/compounds)
- Cathodic polarization

The most important possibilities for influencing these processes are:

- Current density
- Electrolyte composition
- Fluid dynamics
- Temperature

The Galvani tension (dependent on the chemical potentials, activities, and concentration of metal ions in the two adjoining phases) and the polarization are related to the number of nuclei per cm^2. The number of nuclei is inversely proportional to the nucleation energy and is increased by higher polarization, whereby the crystal size decreases. The so-called thread-crystals must be avoided, which can be achieved by enlarging the basis plane of the crystal, which means a slower growth in the vertical direction. This can be performed by a slow and steady increase in the current density /19/.

The crystallization polarization is attributed to an inhibition of the metal ion transfer from the "ad-atomic" state into the lattice order /20/. This transport by diffusion requires an activation energy, the nucleation energy U.I.t. The higher the polarization is, the greater the nucleation probability. At low current densities this polarization is small. A complication is the fact that the polarization changes with time due to changes in the metal surface by the deposition itself. At the beginning, the nucleus growth is three-dimensional up to a certain thickness. Subsequently, the surface parallel to the base becomes more passive because the formation of new lattice planes is inhibited; this is possibly caused by adsorption or insertion of foreign substances.

Influencing the polarization appears to be difficult: /21/ states that the polarization increases with a decrease of ions at the cathode and decreases with an increase in temperature. /22/, however, states that the polarization increases with temperature.

If the copper ion concentration in the electrochemical double layer approaches zero, the limiting current density for this ion (Cu^{2+}) is reached and the discharge of other ions is made possible. The depletion of the original ions can be prevented by higher flow conditions and higher bath exchange values. It was formulated by /23/ that an increasing I/C (current density divided by copper concentration) results in an increase of nucleation rate and finer grain size. An increased copper concentration favours more the growth of already existing crystals as well as the more turbulent flow and higher temperature, the cathodic polarization and polarization decrease /24/.

The cathodic polarization is a very complex parameter, composed of four additive terms:

- Charge transfer polarization
- Diffusion polarization
- Reaction polarization
- Crystallization polarization

/22/ proposed the following five main growth types of polycrystalline deposits:

- Field-oriented isolated crystal type (FI)
- Basis-oriented reproduction type (BR)
- Twinning intermediate type (Z)

- Field-oriented texture type (FT)
- Unoriented dispersion type (UD)

The influence of inhibitors on the growth type is discussed in literature /25, 26, 27, 28, 29/. An inhibitor is a substance, which due to its adsorption at the electrode surface, reduces the speed of an electrochemical reaction by increasing the polarization. This is attributed to a decrease in the effective electrode surface and blocking of the active sites. The ions have to be discharged at less active places. This requires high activation energy.

Therefore, the inhibitors have to stop preferential unidirectional crystal growth and they have to cover any outjutting site on the cathodic surface and passivate it. No crystallization takes place at these sites. Alternatively, the effective current density at the free sites is increased, providing higher polarization and better nuclei formation conditions /30/.

Glue is an organic adhesive and forms colloid-disperse systems with particles between 1 and 100 µm in an overlapping field between true single-phase solutions and heterogeneous multi-phase mixtures. Glue is unstable and has the tendency to turn into either a real solution or disperse but in heterogeneous mixtures. Thiourea is a H_2N-C-S compound that is reduced at high cathodic polarizations to sulphide compounds that act as inhibitors.

Glue and thiourea are often repeatedly described as a deactivator and an activator, respectively. However, this explanation appears too simple as the effects would cancel each other out. More probable is that thiourea preserves the passivating activity of the glue for a certain time. Definitely, the incorrect concentration of these additives can lead to larger nodules at the cathode, as well in absolute concentrations as in improper ratios thiourea/glue/chloride. The different limited lifetimes of these additives is also a big uncertainty to control, for example with systems such as Collamat /31/. Influencing parameters for the lifetimes are the initial concentration, time, temperature, and forced convection. The parameters are not constant over the electrolysis time. The cathodic crystallization and the change of the deposit structure are dependent on all of these factors.

Electrolysis takes place under the flow of direct current that causes mass transfer and transformation. The driving force for mass transfer is concentration, temperature, and pressure gradients. Mass transfer by diffusion and by convection is the only valuable mass transfer mechanisms. Diffusion is governed by Flick's Law, whilst convection can be "free" or "forced". The mass transfer coefficient (m/s) or ($m^3/s.m^2$) depends on the concentration difference /32/.

Forced convection of the electrolyte improves the morphology of the cathodic copper deposit /33, 34, 35/. The concentration of impurities in the cathode may increase because of a low copper ion concentration. This concentration can be increased by forced convection and the deposition of impurities on the cathode is decreased.

Cathode potential measurements give quantitative indications. In the case where the consumption rate of copper at the cathode is higher than the supply rate a concentration polarization will occur. The remedy is a high fluid flow velocity. A high electrolyte fluid flow velocity decreases the contents of the As, Sb, Bi impurities in cathodic copper. The differences become decisively bigger with higher current density.

The formation of compact and smooth cathodic deposits depends on the electrocrystallization process during the electrolysis. The electrocrystallization is determined by the nucleation and the crystal growth. A certain ratio between the nucleation rate and speed of crystal growth is necessary for the generation of high cathodic copper deposits /36, 37/. This proportion is dependent on factors including:

- Current density
- Electrolyte composition
- Electrolyte temperature
- Electrolyte circulation
- Inhibitor dosage
- Type of starting sheet

Energetically, the formation of a new nucleus is less probable than the growth of a previous crystal, because additional energy is required for the formation of a new nucleus. The single source for an energy surplus on the surface of the electrode is the energy of the polarization in the electrolysis, which is liberated during the ion discharge ($zF\eta$). If this amount of energy is sufficiently large, it can be transferred into surface formation energy for three-dimensional nuclei; otherwise this energy is transformed into heat at the electrode surface.

The relationship for the three-dimensional nucleus formation is as follows:

$$\sigma S \leq zF\eta$$

Equation 4-1

σ...surface tension metal-electrolyte
S...surface of the nucleus being formed
η...polarization at the metal ion discharge
z...number of electrons involved
F...Faraday constant

The probability of new nuclei formation increases the higher $zF\eta$ is in relation to σS.

The exchange energy liberated, related to the unit area of the cathode, is given by the following equation (for two-valent metals):

$$z\,F\,\eta = -4.6\,RT\lg i_0 - 2.3\,RT\lg c_0 + 2.3\,RT\lg\left[\frac{i_K^2 \cdot i_{Gr}}{i_{Gr} - i_K}\right] + zF\Psi_1$$

Equation 4-2

i_0...standard exchange current density
i_K...cathodic current density
i_{Gr}...limiting current density
c_0...concentration of dischargeable ions in the electrolyte
Ψ_1...external electric potential

The growth of a metal crystal does not take place at lattice planes but in step-lines with microscopic thick growth layers. After a three-dimensional nucleus has formed with a certain thickness (10^{-6} – 10^{-7} m vertical to the base surface), the basic plane parallel to the electrode surface becomes passive. The nucleus can only grow further in a tangential direction. The reason for the growth blockage in a vertical direction is seen in the adsorption and insertion of foreign substances /20/.

4.1.1 Current density and polarization

With an increasing current density the deposit becomes finer because the amount of energy $zF\eta$ increases. The same is true for the effect of polarization η since high current densities generally result in high polarizations. If both parameters become so high that hydrogen is precipitated together with the metal (at the limiting current density), then porous and spongy deposits are generated because of gas bubble formation. The discharge of H^+ ions leads to a higher pH value of electrolyte near to the cathode surface. This enables the formation of solid hydroxides or basic salts, which are inserted into the metal deposit.

4.1.2 Electrolyte composition

The nucleus formation probability is decisively related to the metal ion concentration in the bath. The same is true for the further growth of the cathodically formed three-dimensional nuclei. In the case of a lower metal ion concentration the phase boundary layer at the cathode will be impoverished and $zF\eta$ will become bigger. The probability of nucleus formation is increased. However, a higher ion concentration leads to a lower $zF\eta$. This factor can be kept constant by an increased current density but a metal concentration increase is limited by the solubility of metal salts in the electrolyte.

4.1.3 Electrolyte temperature

A higher temperature increases the term $zF\eta$ and therefore should cause a fine-crystalline deposit. On the other hand, higher temperatures improve the activity of the metal ions in the electrolyte and in the phase boundary layer and diffusion and convection are also increased. This means a higher concentration of metal ions at the cathode surface and, as a consequence, the diffusion polarization and the term $zF\eta$ are decreased.

4.1.4 Addition of inhibitors

Often inhibitors are the reason for higher polarization. This is due to the effect that the inhibitors cover parts of the cathode and decrease the effective surface, leading to a higher effective current density. By the inhibitors' adsorption the most active parts of the surface are blocked with the consequence that the ions have to be deposited at less active spots – or the ions have to drive away the inhibitors. Both processes require higher activation energy. The blockage of the active spots primarily results in a strongly increased crystallization polarization because the ions are forced to discharge on the crystal surface due to the formation of many new nuclei. The inhibitors may also block chemical side reactions, including a further reaction polarization.

4.2 Metallographical questionnaire

The summary of the metallographic questionnaire is detailed in Table 4-1. The significant differences were evident in the mould coatings. The anode casting was performed on conventional casting machines with barium sulphate as the facing material for the moulds, with the one exception of silica. Furthermore, the current densities fluctuated between 310 and 337 A/m². The dosage of the inhibitors fluctuated between 35 g/t and 110 g/t for glue and between 50 g/t and 70 g/t for thiourea. The amount of added chlorine ions ranged between 32 and 50 mg/l. The temperature was between 62 °C and 69 °C. An extremely variable parameter was the anode chemical composition with oxygen ranging from 848 to 2388 ppm, lead from 19 to 1311 ppm, and silver from 254 ppm to 2600 ppm. The critical elements were Sb (53 – 1259), As (420 – 3456), Bi (27 – 285), Se (15 – 624), and Te (3 – 284).
Most of these values differ from those which were mentioned in chapter 3; they are exclusively related to the conditions which were valid in producing the samples for the metallography.

	A					B					E				F		G			
Casting mould coating	$BaSO_4$					$BaSO_4$					$BaSO_4$				$BaSO_4$		SiO_2	SiO_2	$BaSO_4$	SiO_2
Mass, kg	348					335					404				310					
Life, days	18					16														
Scrap, %	18.64					20									20					
Decription of the anode rest	anodic passivation was observed on the anode faces										for all anodes signs of passivation				smooth surface and in shape		samples were taken during the first run			
Sample Nr.	1	2	3	4	5	1	2	3	4	5	1	2	3	4	1	2	1	2	3	4
Anode Analysis																				
Cu%	99.4	99.4	99.36	99.37	99.38	99.3	99.3	99.3	[illegible]						[illegible]	[illegible]				
Ag ppm	373	373	286.5	260	285	[illegible]	1 800	2 200	2 100		385	385	1 078	1 027	503	432	[illegible]	259	340	233
Au ppm	55.5	55.5	60.9	46.4	59.0	51	49	55	47		13	13	42	37	62	58	1.3	27	[illegible]	
S ppm	73	73	47	27	40	70	[illegible]	61	73								[illegible]	8	38	13
Se ppm	313.5	313.5	478	436	460	280	300	280	260		315	315	363	514	369	550	[illegible]	307	[illegible]	113
Te ppm	80	80	106.3	80	110	182	202	190	183		13	13	103	102	197	[illegible]	[illegible]	35	51	
As ppm	1 004	1 004	1 444	1 065	1 472	790	1 200	1 200	1 100		631	631	1 212	956	[illegible]	2 643	[illegible]	484	532	1 126
Sb ppm	53	53	75	73	77	400	500	450	570		132	132	644	169	212	195	[illegible]	76	117	68
Bi ppm	75.5	75.5	88	57	85	50	80	90	60		56	56	74	134	210	[illegible]	140	101	207	
Pb ppm	101	101	565	213	521	820	780	590	530		[illegible]	[illegible]	774	419	293	338	408	987	1 285	
Fe ppm	26	26	32.5	[illegible]	45	30	30	15	30								19	[illegible]	39	30
Ni ppm	548	548	570	151	612	2 000	2 300	1 700	1 700		1 457	1 457	2 050	1 538	3 400	3 400	[illegible]	380	81	
O ppm	1 252	1 252	1 453	[illegible]	1 212	2 200	1 900	2 300	2 300		1 600	1 600	1 300	1 200	1 900	2 200	2 388	2 795	[illegible]	2 412
Anode Slime																				
kg per tonne of anode	[illegible]					[illegible]					6.2				5.6		4.5	[illegible]	5.2	
removed after ? days	18					16					[illegible]									
Analysis, %																				
Cu															28.2	[illegible]	30	29	27	
Ag															[illegible]	7.5	[illegible]	5.8	5.1	8.7
Au															[illegible]	[illegible]				
S																	[illegible]	3.7	[illegible]	1.6
Se															6.8	[illegible]	[illegible]	7.2	8.9	4.7
Te															3.6	[illegible]	[illegible]	1.2	0.9	0.4
As															[illegible]	4.9	[illegible]	5.6	3.6	12
Sb															2.3	2.2	[illegible]	1	0.9	
Bi															1.1	[illegible]	0.5	1.8	1.5	
Pb															5.4	5.9	5	[illegible]	15	
Fe																	[illegible]	0.15	0.077	[illegible]
Ni															7.9	7.4	[illegible]	0.09	0.07	[illegible]

	A					B				E				F		G			
Cell construction:																			
Voltage at the electrodes[mV]	277.4	277.4	296.4	245.5	355.2	312	446	286	362	317	317	254	263	320					
Current at the electrodes [A]														700					
Anodes/cathodes per cell	40/39					44/43				56/57				81/80		61/60			
Distance anode face to cathode face, mm Air side/Mould side	25/20.4									26	26					25			
Amps/mm2 of busbar area [A/mm2]	1					1				0.47						0.6			
the bath was covered	8 h	8 h	16 h	8 h	16 h	all time				60%	60%	80%	80%	all time		removed 3 times/day			
how was the dentrite found	infrared gun					Gauss meter				Gauss meter						hand held infrared camera			
Cell temperature, °C	64	64	64	65	64	62 to 69				65	65	63	62.8	67		Inlet: 64 Outlet: 61			
Position of the cathode in the cell	middle of the cell, Nr. 20 from inlet					Nr 30	Nr 10	Nr 22	Nr 12	30 AS		20 MS	22 AS	middle		23rd	41st	45th	42nd
at which time in the cathode life	3rd	3rd	end of each crop			3rd	6th	5th	5th	4d 2nd	4d 2nd	6d 1st	4d 1 st	full time		2,82 d	5.61	4.54	1.53
Cathode current efficiency [%]	73.5	73.5	90.5	[illegible]	94.9					[illegible]	[illegible]	91.9	89.8	93		83	89	95	95
stainless steel cathodes in use since	1995					1995				2001				3 years		8 years			
Cathode Analysis:						global arc										sample it self (bulk of the crop)			
Cu %														99.99	99.99				
Ag ppm	6.6	6.6	[illegible]	7.6	7.6	8	15	11	12					10.5	9.8	9.1	6.8	[illegible]	7.4
S ppm	[illegible]	[illegible]	[illegible]	[illegible]	[illegible]									5.7	7.5	9.8	6.6	[illegible]	9.7
Se ppm	0.5	0.5	0.5	0.5	0.5	0.2	[illegible]	[illegible]	[illegible]					0.7	0.6	0.5	0.8	[illegible]	0.7
Te ppm	0.5	0.5	0.5	0.5	0.5	0.4	0.3	[illegible]	0.4					0.6	0.5	< 0.3	< 0.3	[illegible]	< 0.3
As ppm	0.8	0.8	0.8	0.8	0.8	2.5	0.5	[illegible]	0.9					0.9	0.8	2.2	1.3	[illegible]	1.9
Sb ppm	0.8	0.8	0.8	0.8	0.8	5.1	1.2	1.1	1.8					[illegible]	[illegible]	[illegible]	< 0.5	3.8	0.5
Bi ppm	0.2					[illegible]	[illegible]	[illegible]	0.3					0.2	0.2	0.56	0.24	> 1	0.27
Pb ppm	0.5													0.8	[illegible]	3.5	2	[illegible]	0.6
Fe ppm														[illegible]	0.5	3.4	2.8	[illegible]	3.4
Ni ppm	0.8	0.8	0.8	0.8	0.8	2.8	0.8	[illegible]	1.1					0.7	[illegible]	[illegible]	[illegible]	7.1	1.6
O ppm																0.6	[illegible]	[illegible]	0.6
Other																[illegible]	[illegible]	0.7	

	A					B				E				F		G			
Electrolyte , g/l																			
Circulation, l/min/cell	17.6	17.6	26	20.2		20	25	20	21	27				2x25		40			
Electrolyte filtered	each 2 days, Scheibler filter					daily, Scheibler filter								no filtering		during U-pull (every 3 weeks)			
Cu	52.11	52.11	50.97	43.15	50.97	48.8	46.1	48.6	49.1	46.5		45	47	58	60	48	43	45	50
Free H_2SO_4	168.5	168.5	176.5	169.66	176.5	179.5	183	180	179	172		174	165	140	149	177	175	178	169
As	11.19	11.19	13.35	10.25	13.35	4.3	4.4	4.3	4.3	8.2		10.1	8.3	18	21	4.9	4.7	4.8	4.8
Sb	0.14	0.14	0.14	0.17	0.14	453	472	473	455	0.46		0.52	0.4	133	150	0.3	0.2	0.3	0.3
Bi	0.14	0.14	0.15	0.15	0.15	149	150	148	146	0.28		0.32	0.28	62	87	0.2	0.3	0.2	0.2
Ni	10.9	10.9	13.7	11	13.7	17.3	16.9	17	16.7	14.6		18	14.8	18	22	8.5	8	8.5	7.4
Fe	0.75	0.75	0.93	0.74	0.93	144	144	142	141	0.15		0.15	0.15	0		0.2	0.2	0.2	0.2
Cl	50	50	41	54	41	50.8	45.8	4.1	45.8	0.064		0.06	0.06	39	45	47	47	40	45
Addition Agents:																			
Glue g/tonne of cathode	90	90	90	90	90	78	78	78	78	35	35	35	35	100	100	110	110	110	110
Thiourea g/tonne of cathode	60	60	60	60	60	70	70	70	70	50	50	50	50	70	70	65	65	65	65
Cl, g/t	50	50	50	50	50	50	50	50	50	32		47	32	50	50	up to 45			

There were only small differences in the As content of the electrolytes from four of the companies (from 4.3 to 13.35 ppm). Only F had significantly higher values (18 to 21 ppm). This was understandable from the extremely high As contents in their anodes.

A, E and G had Sb contents < 1 ppm in the electrolyte, whereas F has 133 to 150 ppm and B 453 to 473 ppm. B had by far the highest Sb contents in the electrolyte, due to the high starting levels in the anodes.

The Bi contents in the electrolytes differed from 0.14 to 150 ppm (factor 1000), with B having the highest levels.

Referring to the MFR I in the anodes is not meaningful, because all companies had a MFR I of > 2 in their anodes.

Ag, Se, Te, and Pb: These four elements were not detected in the electrolyte.

Characteristics including the MFR I As/(Sb+Bi) and the MFR II Ag/(Se+Te) were calculated to compare the conditions in the plants. These values are detailed in Table 4-2.

	Company	A				B				E			F		G			
	Sample Nr.	1/2	3	4	5	1/2	3	4	5	1/2	3	4	1	2	1	2	3	4
Anode	MFR I	16.82	18.59			2.99	3.57	3.88	2.96	6.23	2.87	6.29	16.80	11.90		5.83	3.64	
	MFR II	1.17	0.60			7.60	4.86	6.36	6.47	1.35	2.88	2.02	1.17	0.68		0.89		2.29
Anode Slime	MFR I												3.54	2.18		4.44	3.30	
	MFR II												1.17	6.77		0.83		1.99
Cathode	MFR I	1.42	1.42	1.42	1.42	0.69	0.63		0.74				1.02	0.95	0.57	3.30	1.85	
	MFR II	9.41	8.70	10.84	10.84	20.85		39.23	31.28				11.29	12.41	5.76	4.93		4.62
Electrolyte	MFR I	82.08		64.72		4.63	4.80	4.87	4.75	21.39	23.24	23.24	2.98	2.44	0.09		0.09	0.11

Table 4-2: MFR I = As/(Sb+Bi), and MFR II = Ag/(Se+Te)

A high MFR I ratio is always an advantage in the refining plant because it is responsible for not forming Sb^{5+} and Sb^{5+} is a main part of the drifting slimes. All MFR I <1 are critically values, because there is too little As and the existence of Sb^{5+} is very possible. All anodes except G have a MFR I ratio higher than 2 and this appears to cause no problems with so called floating slimes.

4.3 Cathode samples

The cathodes from the five companies are described in the next chapters. The initial photographs indicate the location of the samples taken. Therefore, it is possible to explain the type and numbers of dendrites in relation to their location. Many dendrites were cut out and ground sections were prepared. Subsequently, all the samples were evaluated under the microscope. Having analysed the inclusions with a scanning electron microscopy (SEM) a discussion of the different reasons for the resulting inclusions can be provided.

4.3.1 Company A

In Figure 4-1 the cathodes from A are illustrated with photos sent from the company.

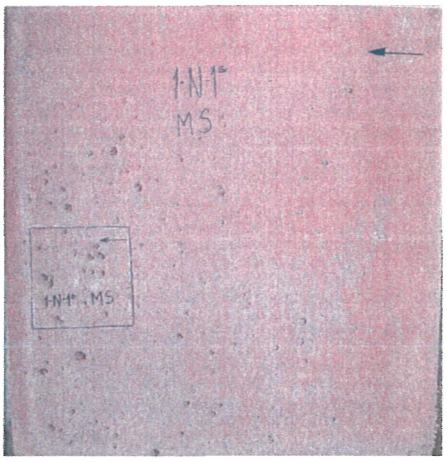

(a) Cathode A 1

(b) Cathode A 2

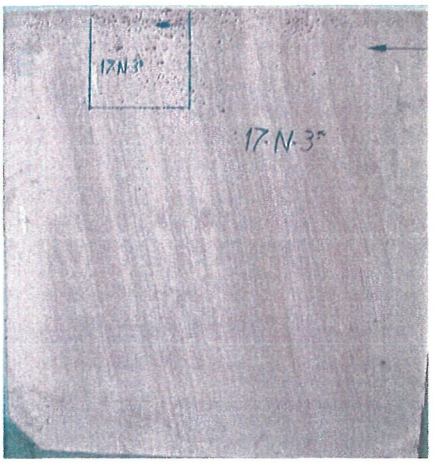

(c) Cathode A 3

(d) Cathode A 4

(e) Cathode A 5

Figure 4-1: Cathodes with selected dendrite samples

Different dendrite locations were chosen from the top-region, mid-region, and bottom-region of the cathode. From the five cathodes five pieces of 200 mm x 200 mm were cut (each containing a significant number of dendrites). From these samples nodules were chosen for microscopic examination. Figure 4-2 depicts photographs of the nodule locations on the cathode surface, as well as the sample pieces used for metallography. The current density, anode composition, inhibitor composition, and other parameters at the A refining plant were obtained from the questionnaire results and are provided in Table 4-1. Microstructures of the samples are presented that include the microstructure in the entire deposit region and in the area "suspected" as the root of the nodule or inside it.

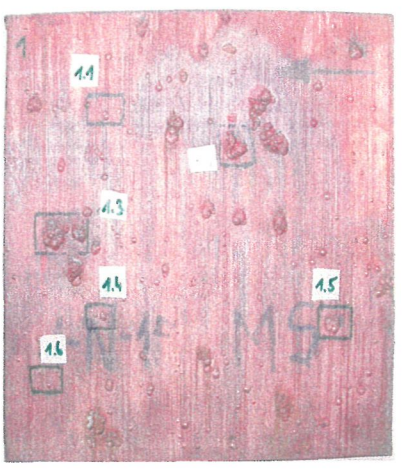

(a) Sample A 1

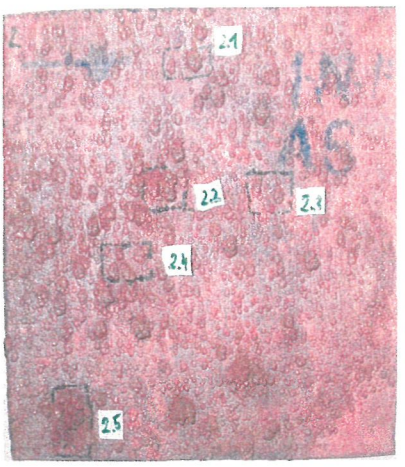

(b) Sample A 2

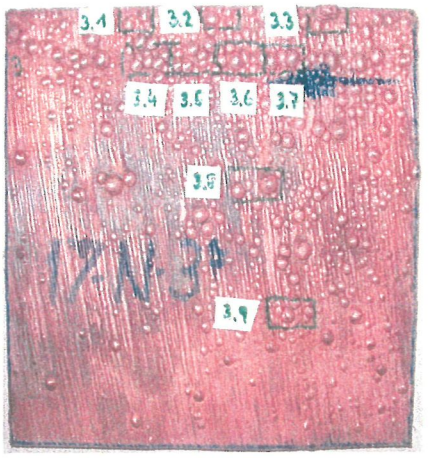

(c) Sample A 3

(d) Sample A 4

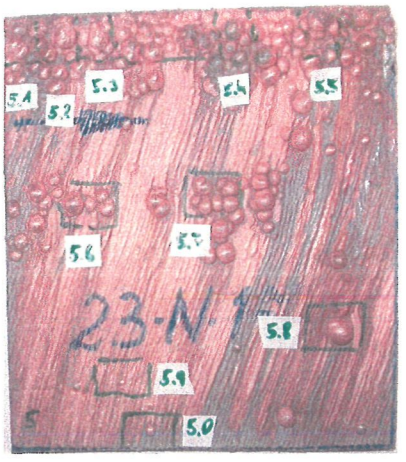

(e) Sample A 5

Figure 4-2: Cathode samples from A

In Figure 4-2 (a) a cathode piece from the mid-region is illustrated. The dendrites were evenly distributed and they were a mixture of globular and crystal growth type. Many of the dendrites were < 5 mm with only some of them being quite big, about ~ 10 mm. The stripes, caused by the glue dosage, were clearly evident and vertical over the entire area.

In the following pictures the metallographic copper cross sections are shown. In the first column the entire cross section is illustrated. At the second column the beginning of the copper crystallization at the cathodic starter sheet can be seen. In the columns afterwards the enlargement of the existing dendrites is shown.

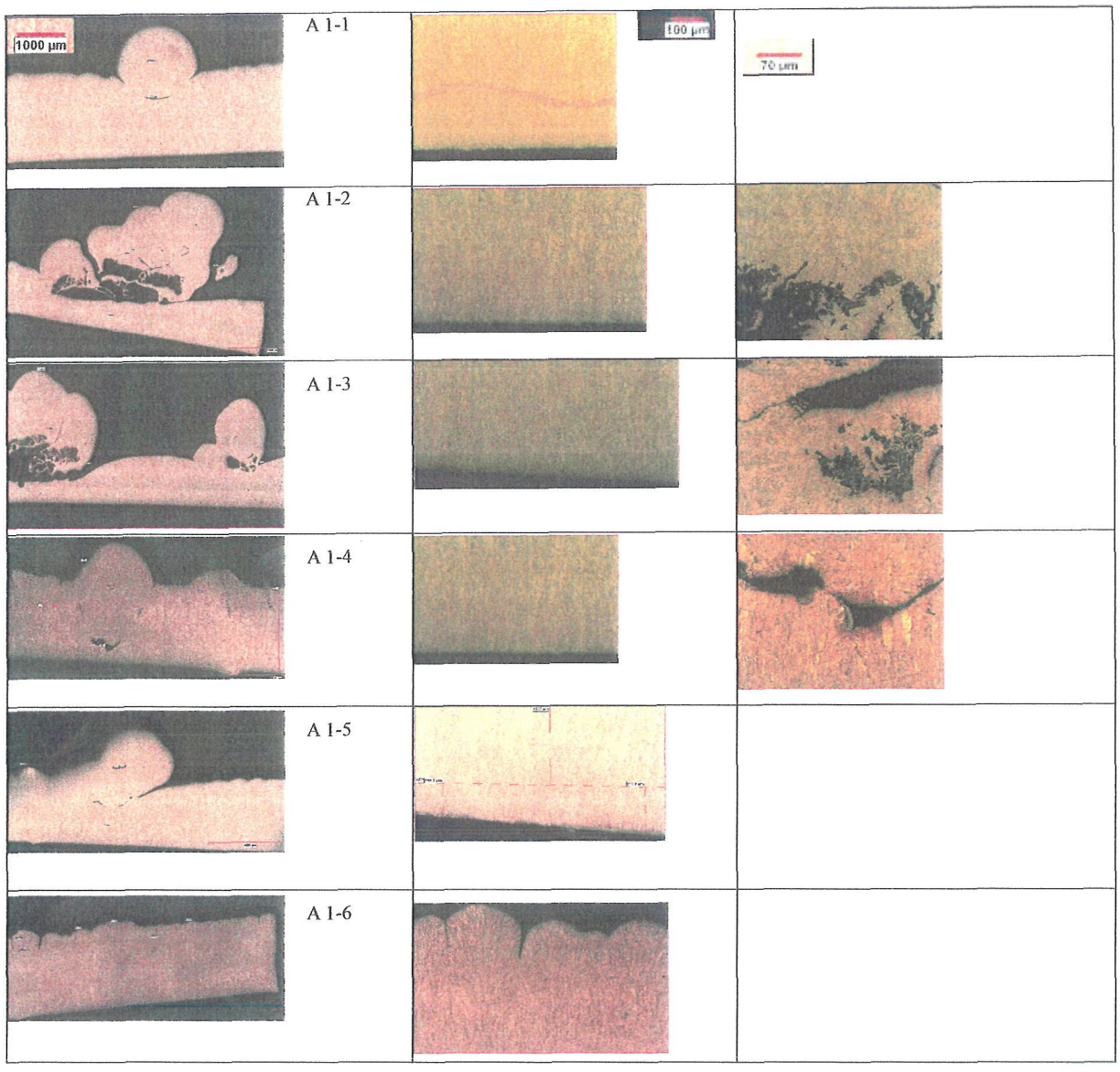

Figure 4-3: Metallographic samples from cathode 1, mid-region

Six samples (A 1-1 to A 1-6) were taken from cathode 1 and prepared for microscopic and SEM analysis. In all six ground sections the very first layer at the stainless steel cathode was without holes and impurities, a compact copper precipitation and by using SEM no impurities were detected in these first layers. After the BR type the FT type was predominant until an inclusion has disturbed the regular cathodic precipitation. All existing dendrites had holes and many inclusions.

In Figure 4-4 three spots were picked out to analyse the dendrite formation. In (a) many small dark spots were recognizable that consist of Se, Te, and Sn. No silver was detected. In (b) the very bright ring forms are the Se and Te inclusions. The matrix around these inclusions consists of Ba. In (c) much Ba (bright areas) and Se, Te and a little bit of Ag could be detected.

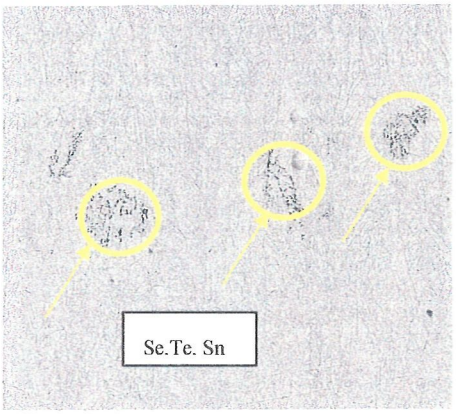

(a) Sample 1-2, spot 1

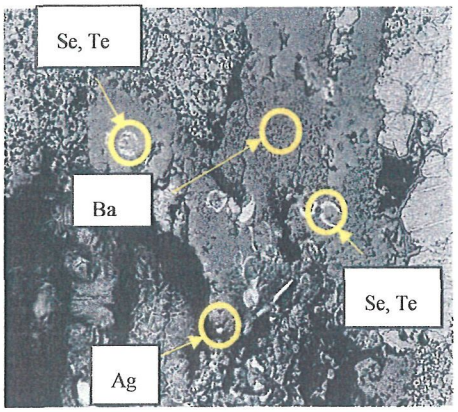

(b) Sample 1-2, spot 2

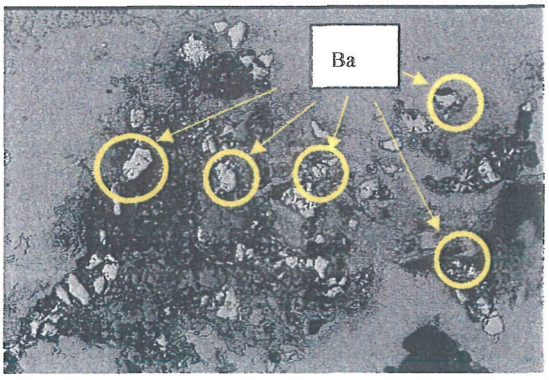

(c) Sample 1-3, spot 1

Figure 4-4: SEM analysis of cathode sample 1

In Figure 4-1 (a) and (b) cathode samples from the bottom-part are shown. The dendrites are distributed over the total area. The size and the form of the dendrites are in both samples similar and seem to be like dendritic form. No strips are recognizable at these cathode samples.

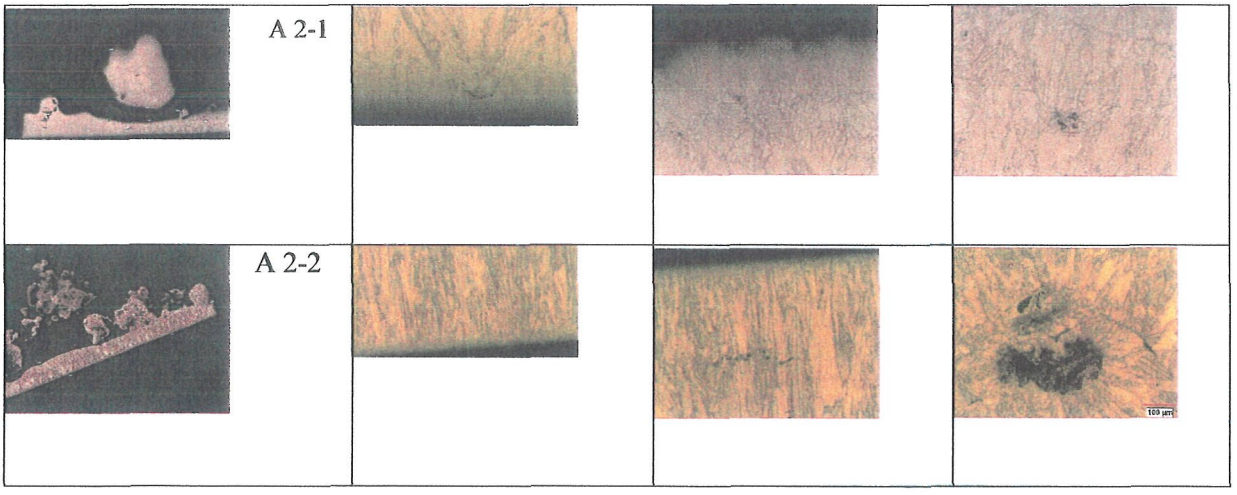

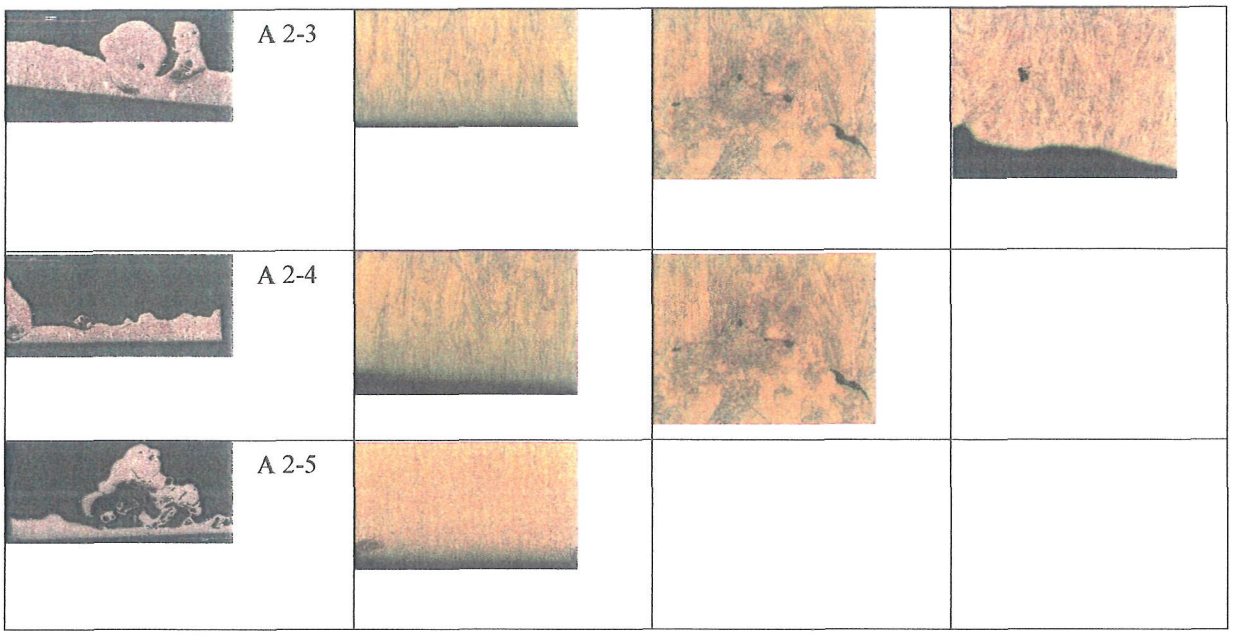

Figure 4-5: Metallographical samples from cathode 2 bottom-part

In both cases the ground layer is without any inclusions. After this layer the dendrite growing is started and many big dendrites with a quite high number of holes are present. The analysis at the SEM gives for all samples the same results. Much Ba inclusions and only few anodic slime particles could be found. In (a) to (d) singular examples are picked out to show the kind of impurities. Big bright particles are mounted in the copper matrix at each sample. In Figure 4-6 the analysis shows that these inclusions are mainly Ba.

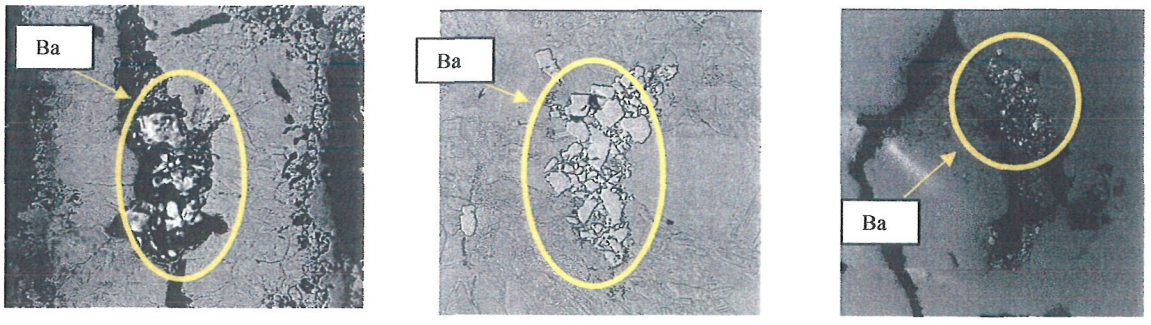

(a) Sample 2-2, spot 1 (b) Sample 2-3, spot 2 (c) Sample 2-4, spot 1

Figure 4-6: SEM analysis of cathode sample 2

In Figure 4-7 cathode samples from the top-part are shown. The dendrites are distributed mainly near the day-night line (electrolyte surface). The size and the form of the dendrites are in both samples similar and seem to be globular. The first copper layer at the stainless steel cathode is with many inclusions and holes. The dendrite growing starts immediately at the very first copper layer.

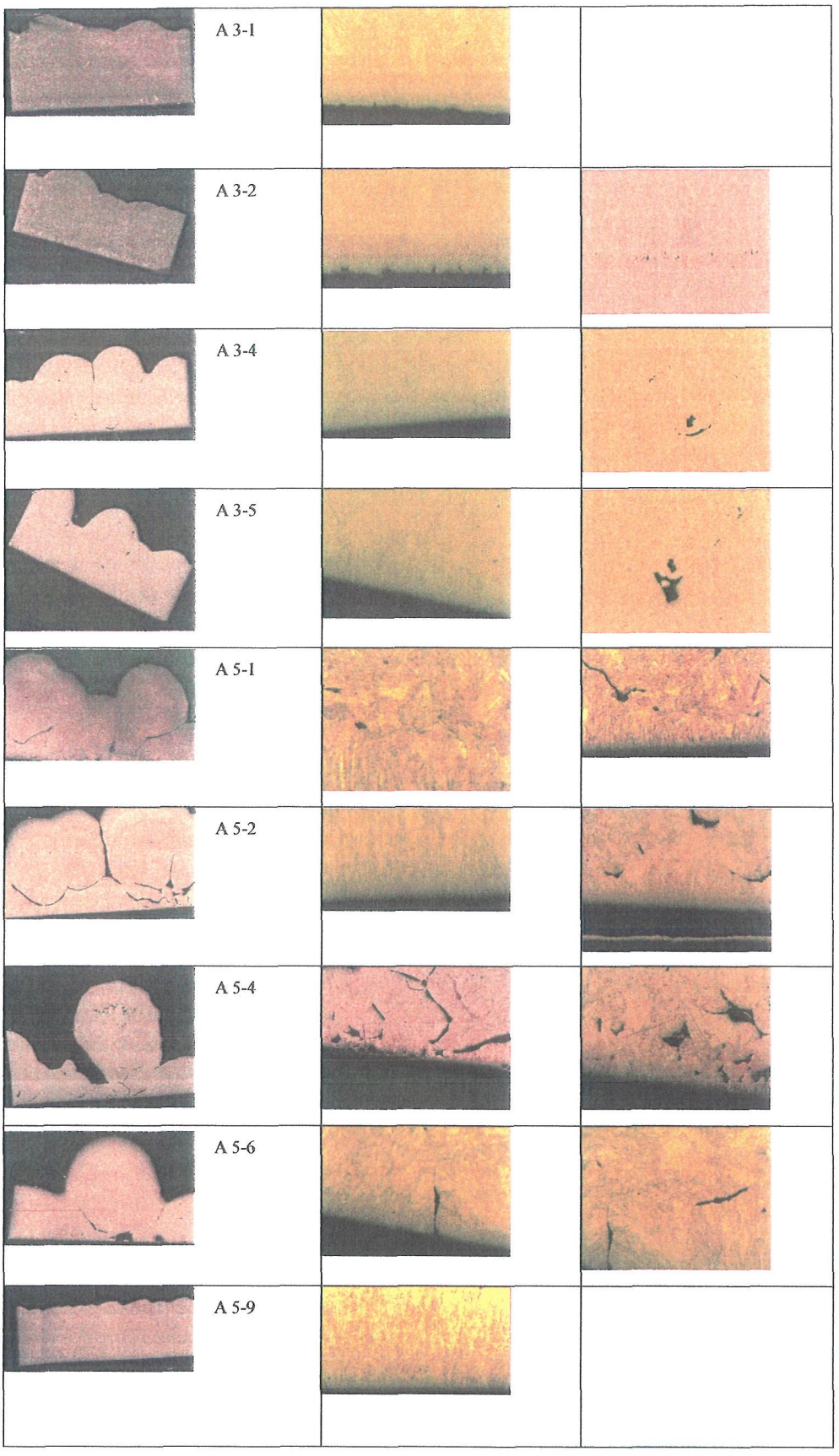

Figure 4-7: Metallographical samples from cathode 3 and 5, top-part

The metallographic ground sections in Figure 4-7 show at many samples holes at the starting layer of copper precipitation where the dendrite growing started. In Figure 4-8 (f) the inclusions near to the stainless steel sheet are shown. Big bright particles were found there and their analyses showed Ba. At (a) a typical Se, Te and Ag inclusion is shown. Many small white spots could be detected. These are all silver inclusions. The Se and Te particles are looking like a crescent.

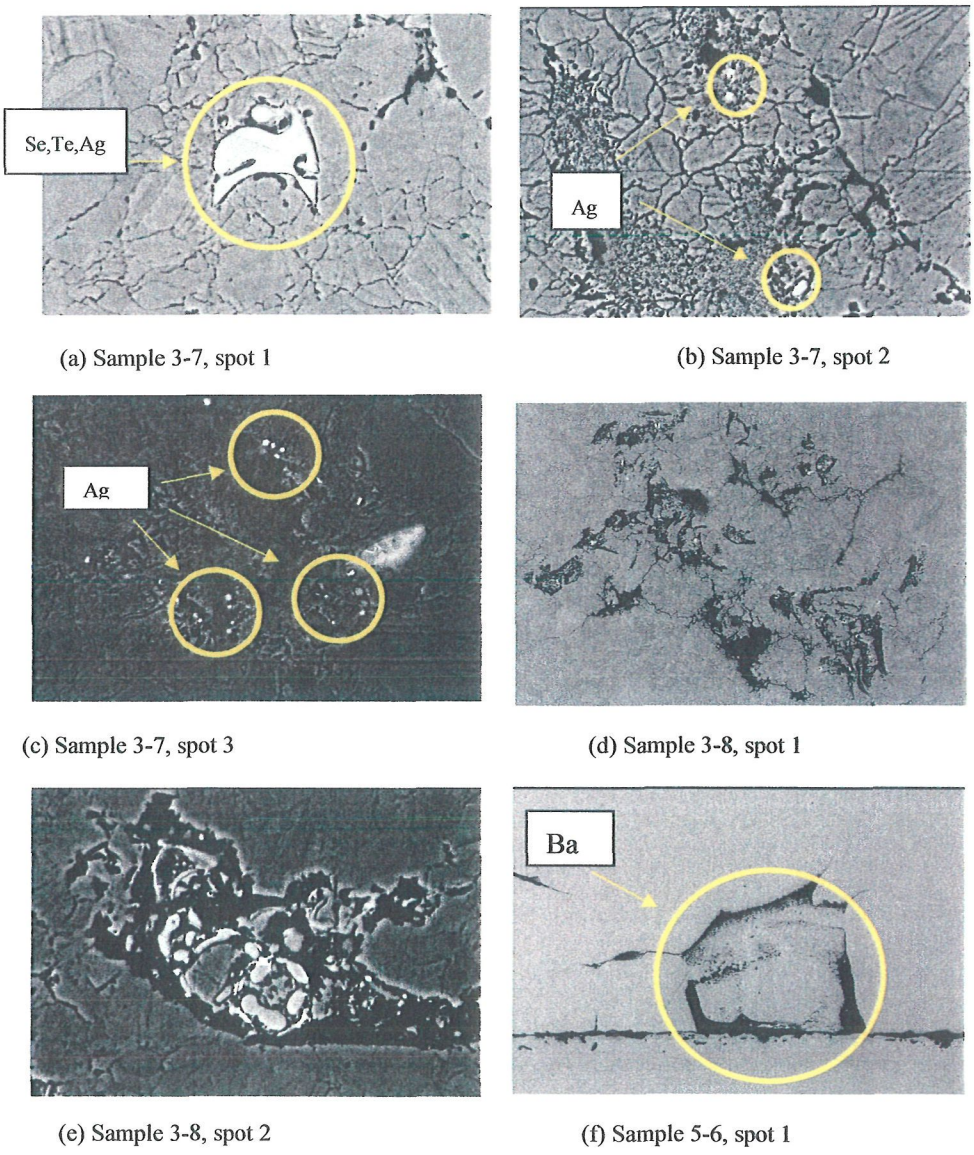

(a) Sample 3-7, spot 1

(b) Sample 3-7, spot 2

(c) Sample 3-7, spot 3

(d) Sample 3-8, spot 1

(e) Sample 3-8, spot 2

(f) Sample 5-6, spot 1

Figure 4-8: SEM analysis of cathode sample 3 and 5

4.3.2 Company E

In Figure 4-9 the cathodes from E are shown. Here also different locations of the dendrites were chosen, bottom-part of the cathode and two middle sections. From the three cathodes four pieces with 200 mm x 200 mm were cut (each containing a significant amount of dendrites), too. From these samples nodules were chosen and imbedded for microscopic examination.

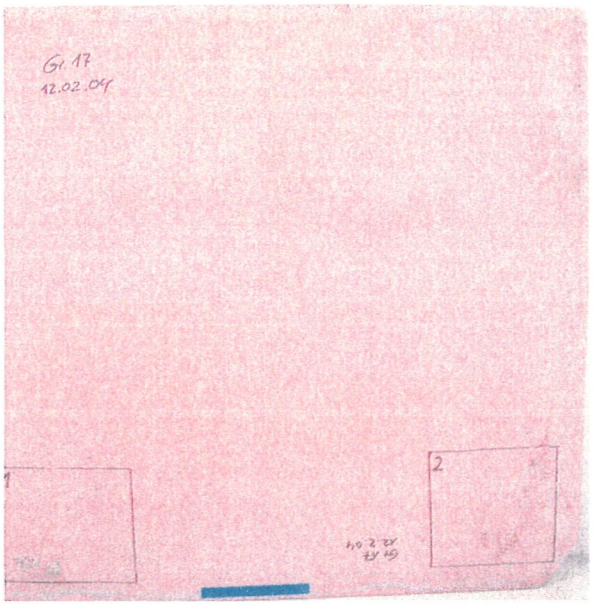

(a) Cathode E 1

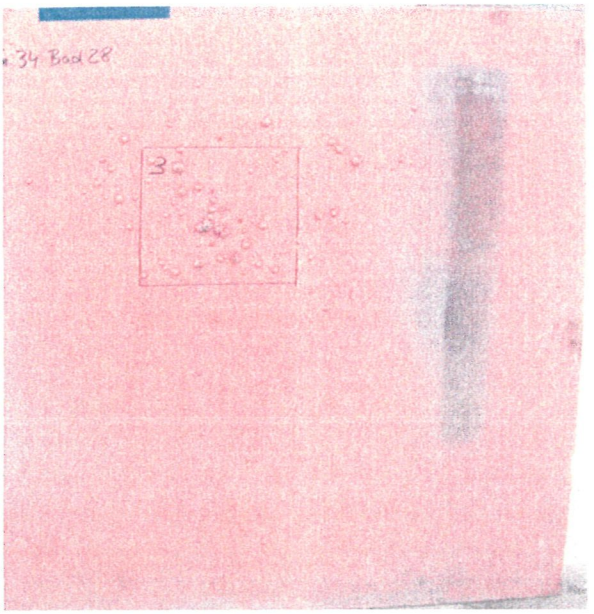

(b) Cathode E 2

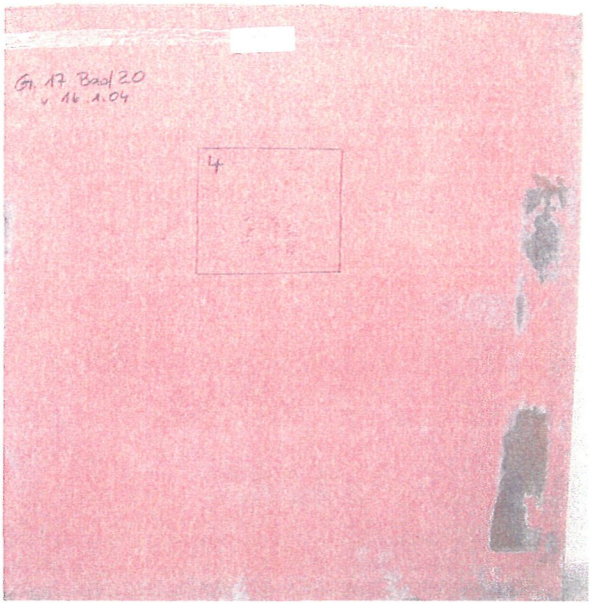

(c) Cathode E 3

Figure 4-9: NA cathodes with the selected dendrites samples

Included in Figure 4-9 are photographs of the location of the nodules on the cathode surface, as well as the sample pieces used for the metallography study. The current density, anode composition, inhibitor composition and other parameters at the NA refining plant were obtained from questionnaire results and detailed in Table 4-1. Microstructures of the samples are presented, which include the microstructure in the whole spot of the deposit and in the area "suspected" as the root of the nodule or inside it.

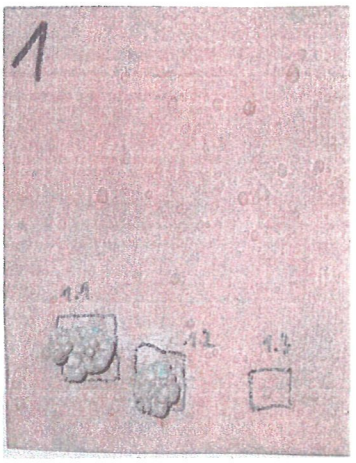

(a) Samlpe E 1

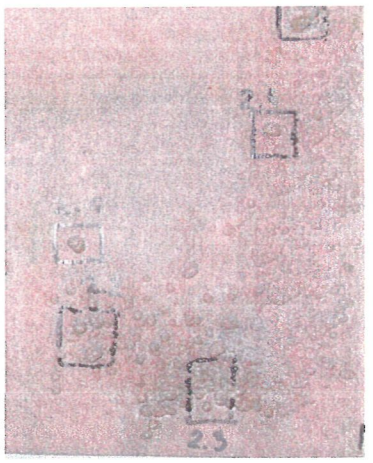

(b) Sample E 2

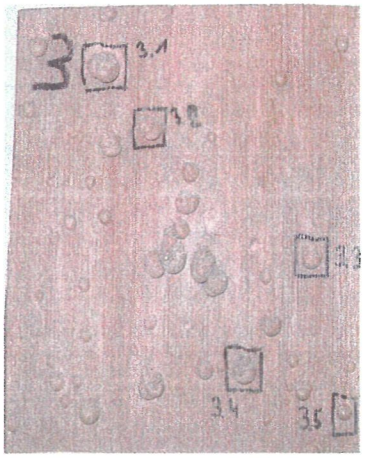

(c) Sample E 3

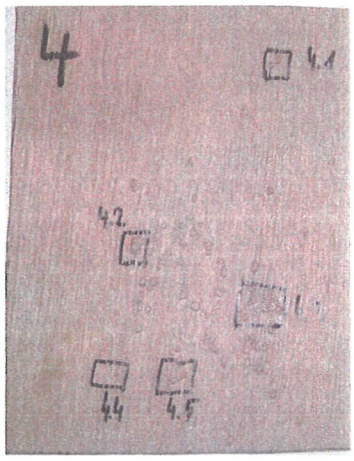

(d) Sample E 4

Figure 4-10: Cathode samples from E

In Figure 4-10 (a) two big dendrites of the bottom of the cathode are shown. At (b) a dendrite nest is demonstrated. There many small dendrites are concentrated in a special area. At (c) and (d) some bigger globular dendrites are picked out. At all four sample stripes are recognizable and they are all vertically.

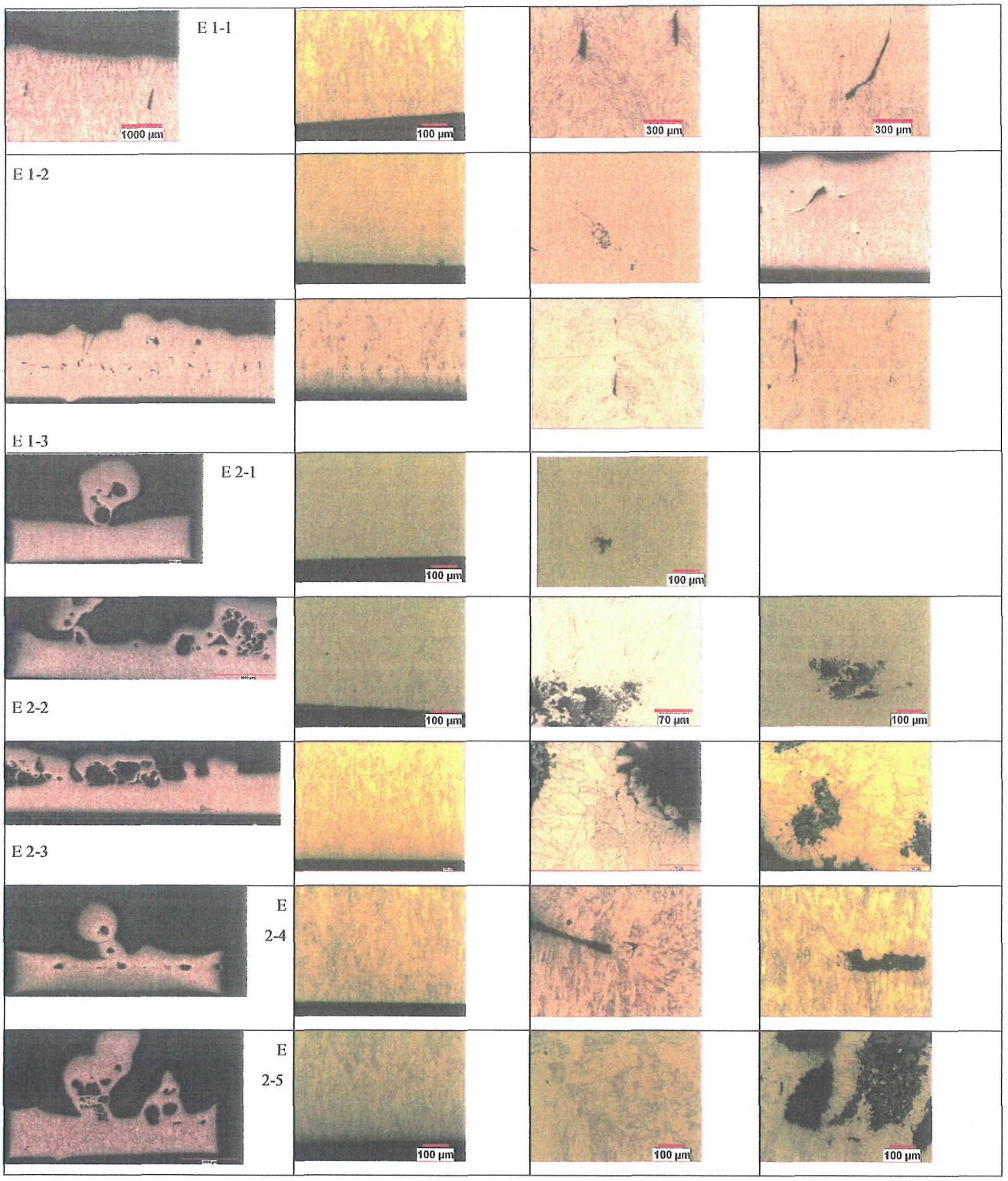

Figure 4-11: Metallographical samples from cathode 1, sample 1 and 2, bottom-part

At samples E 1-1 to E 1-2 the copper precipitation has very fine clefts. This phenomenon does not start at the stainless steel cathode without any irregularities, but after a small layer of FT type many clefts are recognizable at the total area of the cathode sample. By analysing the clefts with EDX no impurities could be found. At this location in the dendrites much anodic slime could be found. The main inclusions are Ag, Pb and Se, Figure 4-12 (a).

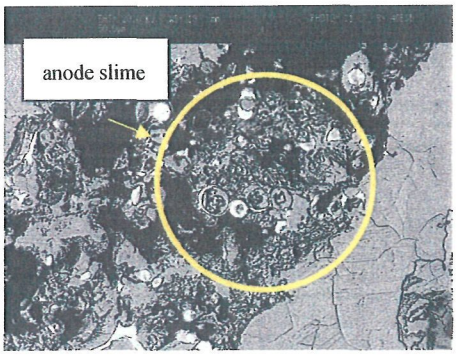

(a) Sample 1-1, spot 1

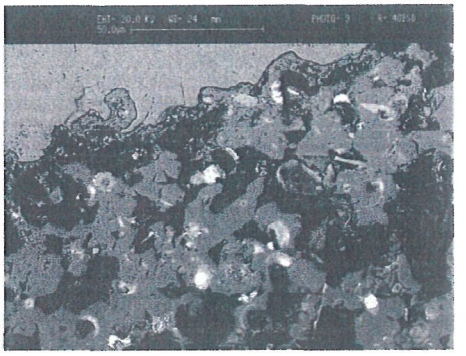

(b) Sample 1-2, spot 1

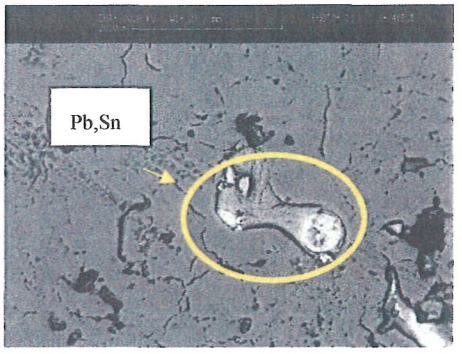

(c) Sample 1-2, spot 2

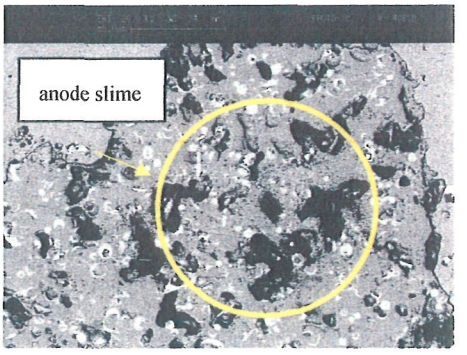

(d) Sample 2-2, spot 1

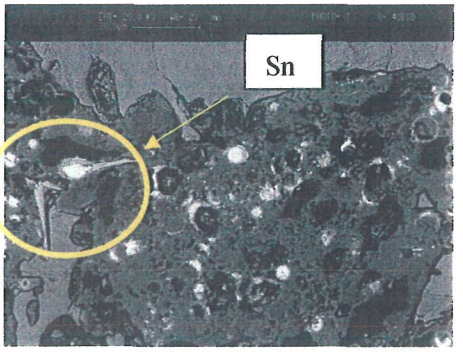

(e) Sample 2-5, spot 1

Figure 4-12: SEM analysis of cathode sample 1 and 2

At the second big dendrite the impurities are also anodic slime. The globular grey cycles are Zn and Ni inclusions. The big inclusion at (c) is mainly Pb with Sn. In (e) typical Sn needles can be seen. The Se and Ag combinations are shown as rings. Also here much Pb with Ag and Sn inclusions could be found. In (d) an overview of the big amount of all impurities is shown.

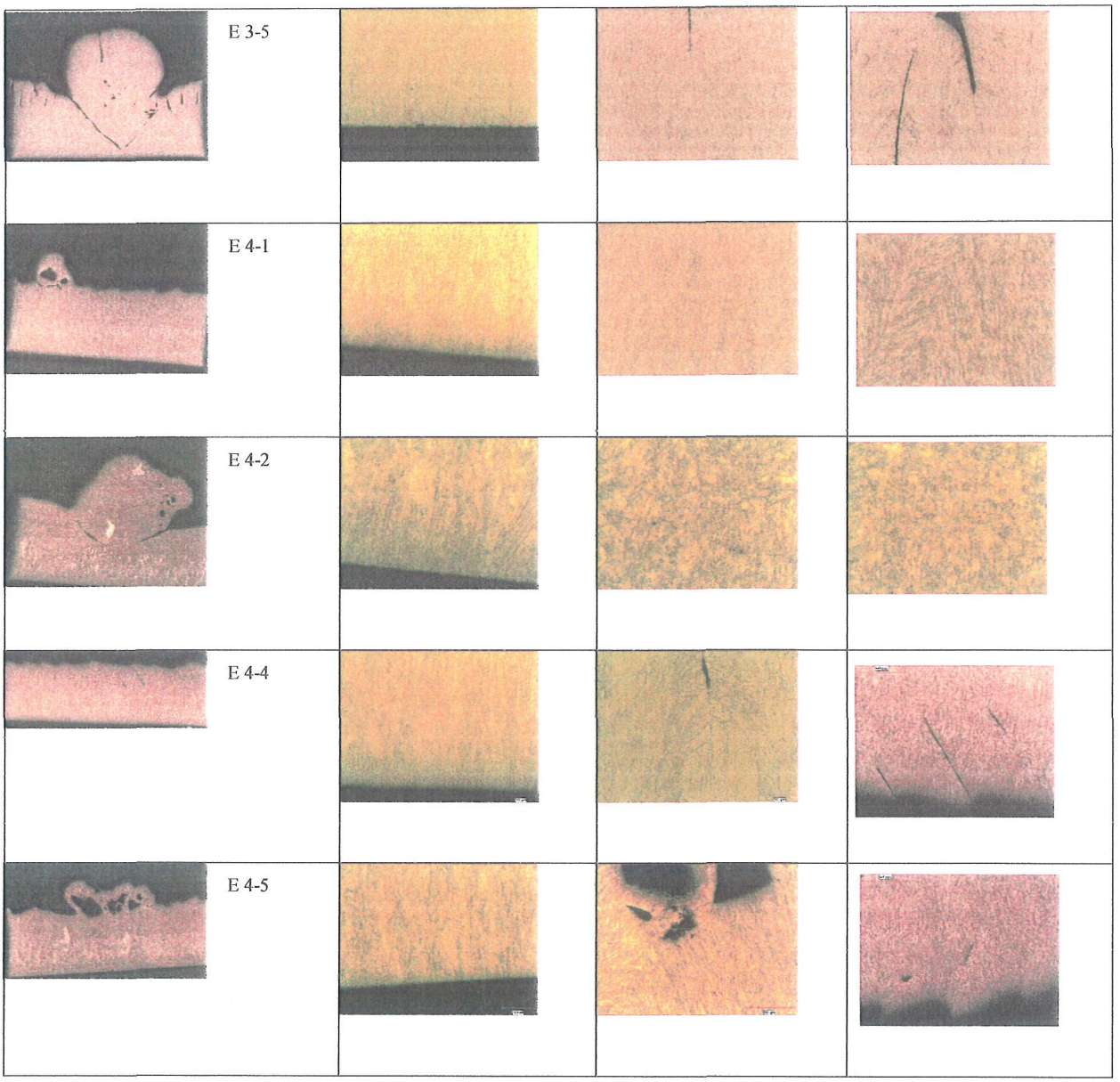

Figure 4-13: Metallographical samples from cathode 2 and 3, middle-part

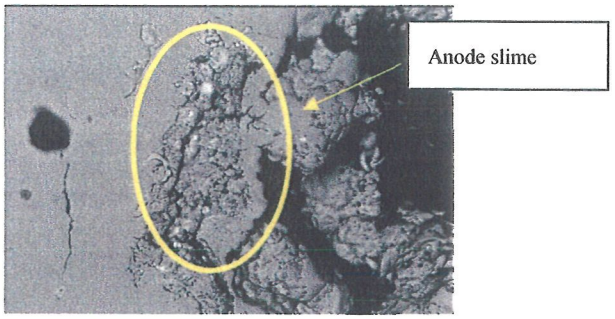

Figure 4-14: SEM analysis of cathode sample 3-2

Inclusions of 3-2 consist of a big amount of Pb, with many small white spots of Ag. Also As and Sb are in these dendrites. The typical form of Se and Te is there, too. At all samples clefts are detected. Inside these clefts no impurities are found.

4.3.3 Company B

In Figure 4-15 the five cathodes from B are shown. Samples from the bottom-part 1 and 2, from the mid-part, 3 and 4 and finally from the top-part, 5 are chosen.

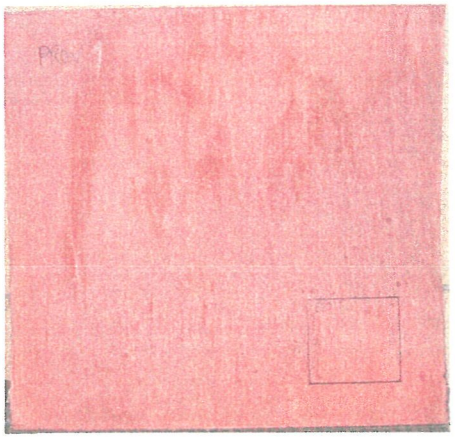

(a) Cathode B 1

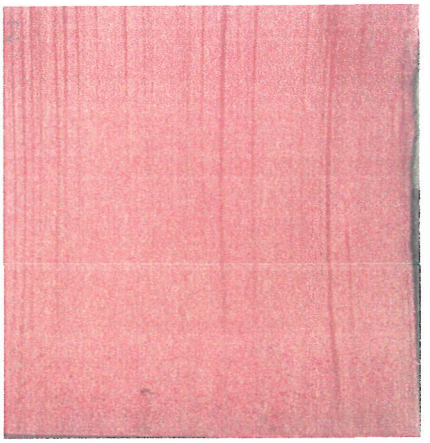

(b) Cathode B 2

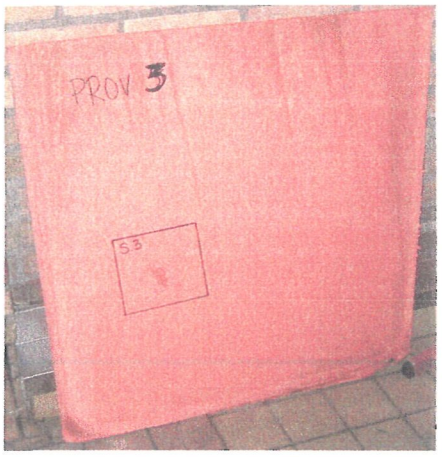

(c) Cathode B 3

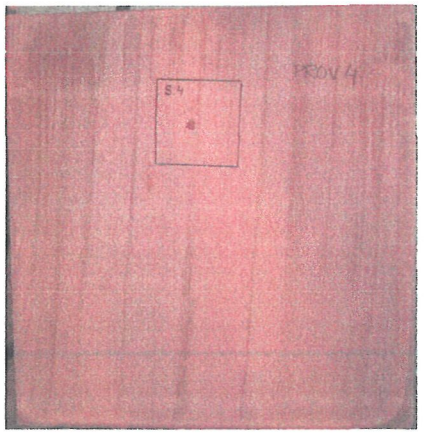

(d) Cathode B 4

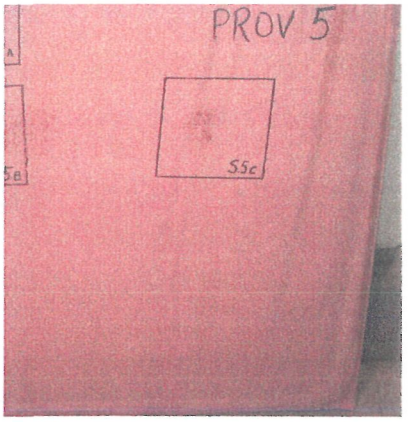

(e) Cathode B 5

Figure 4-15: B cathodes with the selected dendrites samples

Included in the Figure 4-15 are photographs of the location of the nodules on the cathode surface, as well as the sample pieces used for the metallography study. The current density, anode composition, inhibitor composition and other parameters at the B refining plant were obtained from questionnaire results and detailed in Table 4-1.

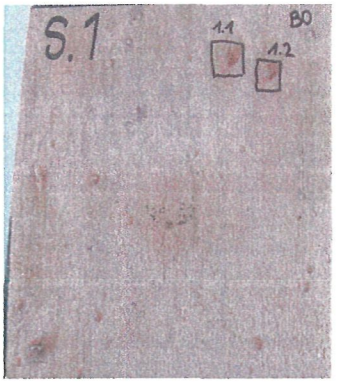

(a) Sample B 1

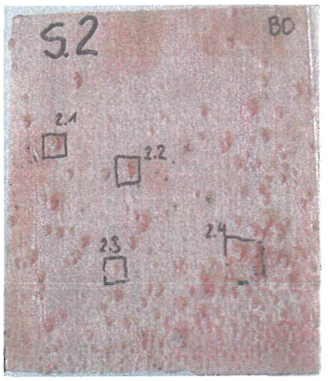

(b)Sample B 2

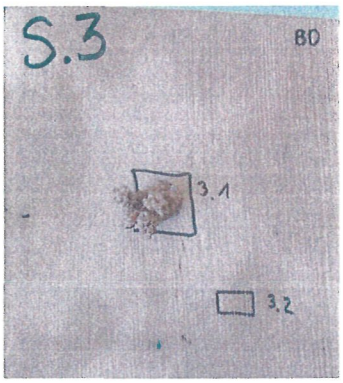

(c) Sample B 3

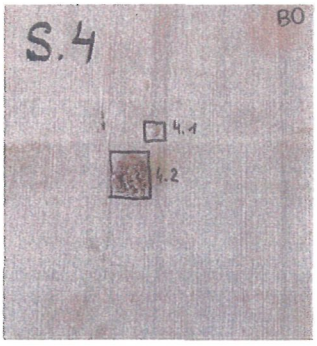

(d) Sample B 4

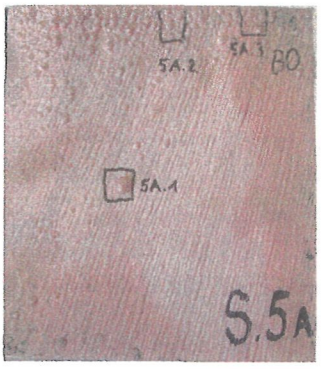

(e) Sample B 5A

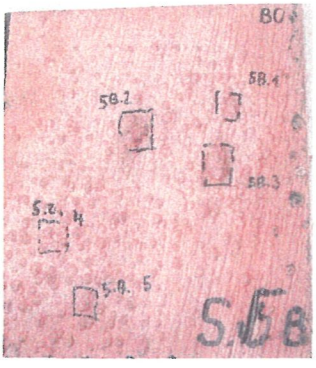

(f) Sample B 5B

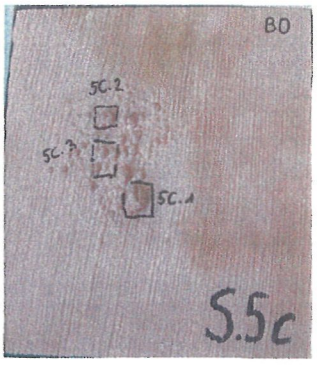

(g) Sample B 5C

Figure 4-16: Cathode samples B

Dendrite growing started soon after the beginning of the process. Some samples, B 1-1 and B 2-2 showed dendrite growing quite at the stainless steel sheet.

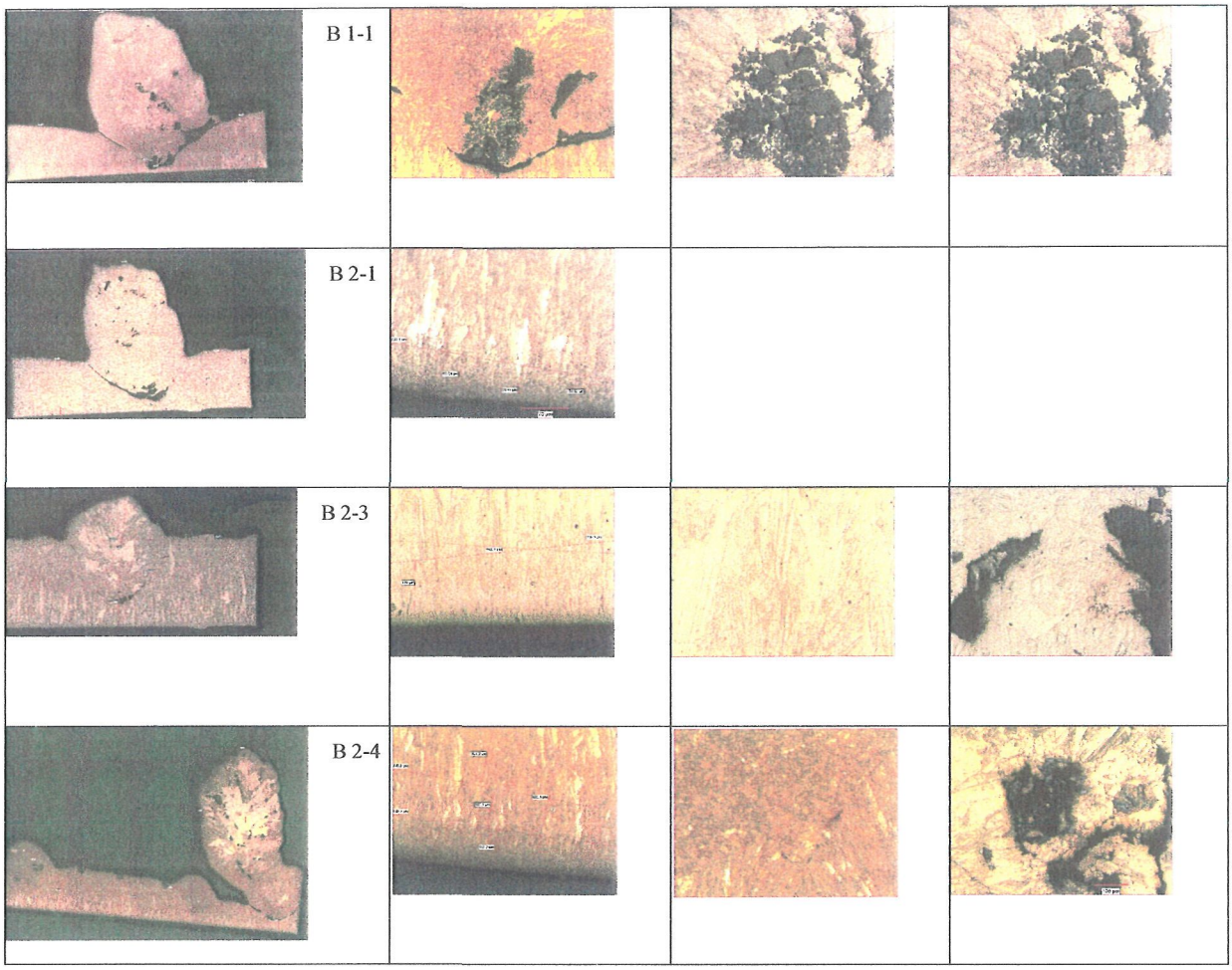

Figure 4-17: Metallographical samples from cathode 1 and 2, bottom-part

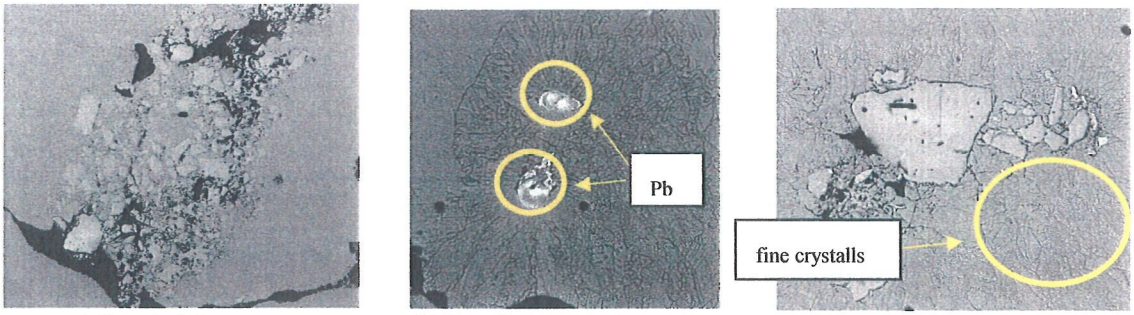

a) Sample 1-1 (b) Sample 2-1, spot 1 (c) Sample 2-1, spot 2

Figure 4-18: SEM analysis of cathode sample 1 and 2

The SEM analysis showed a big amount of Ba inclusions. In Figure 4-18 (a) and (c) the big bright particles demonstrated the Ba inclusions, at (b) much Pb particles combined with a little amount of Ag. Surrounding the impurities the copper precipitation was very fine crystallized.

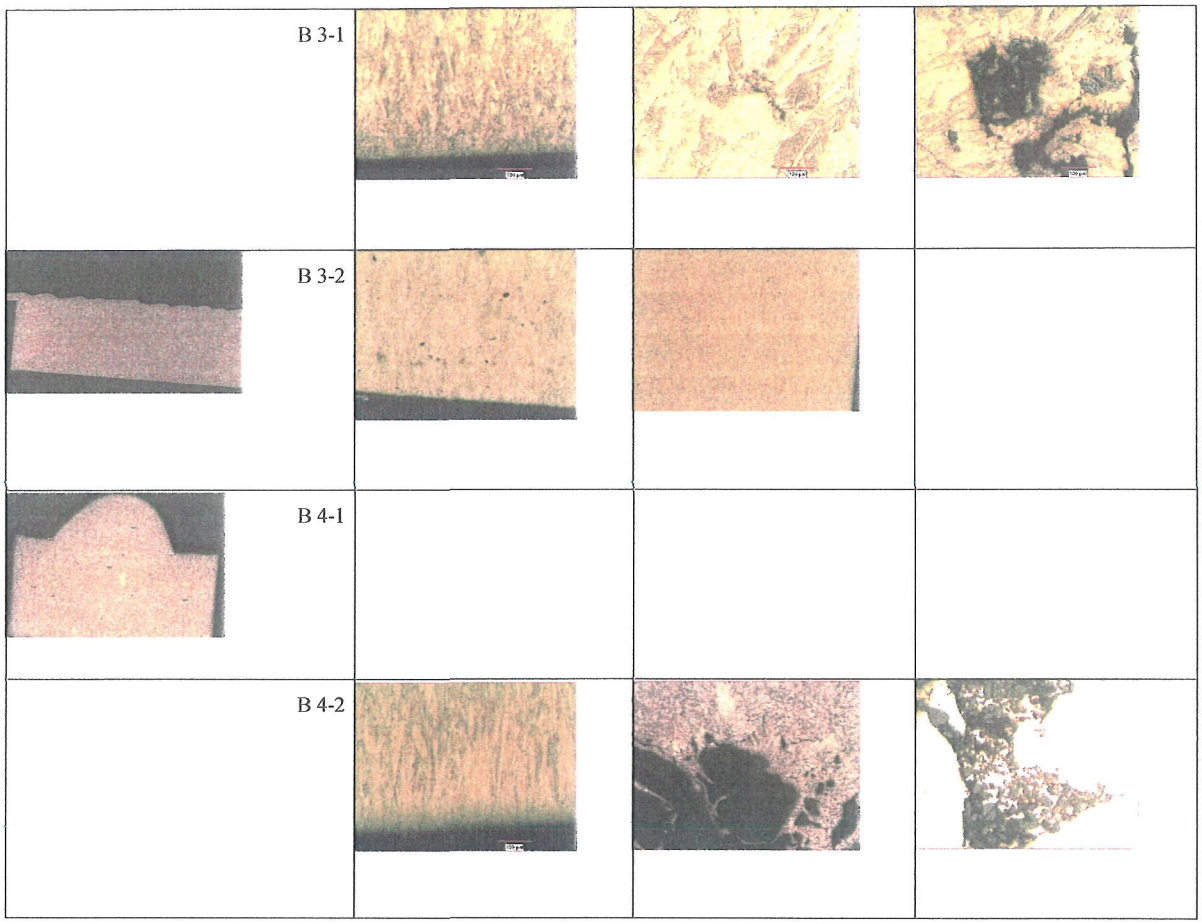

Figure 4-19: Metallographical samples from cathode 3 and 4, mid-part

At the ground of the cathodic precipitation there were no inclusions and holes. In the dendrites many holes and inclusions were analysed by EDX. In Figure 4-20 the big bright inclusion were Bi and As.
The bright round particles were Ag, Se and Te inclusions and the matrix is copper oxide. The big elongated particles were As, Bi and Sb.

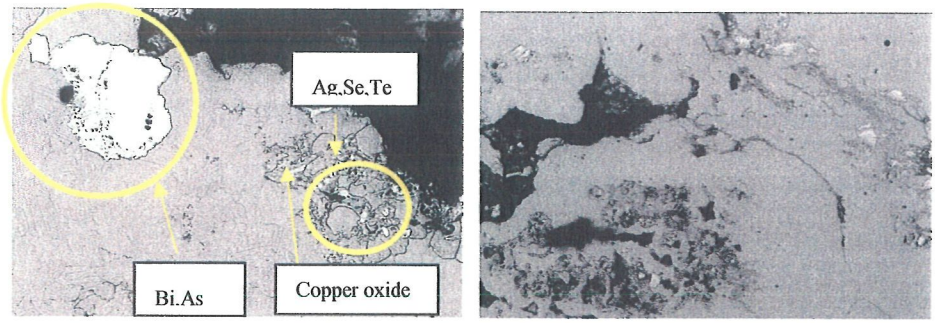

(a) Sample 3-2 (b) Sample 4-2

Figure 4-20: SEM analysis of cathode sample 3 and 4

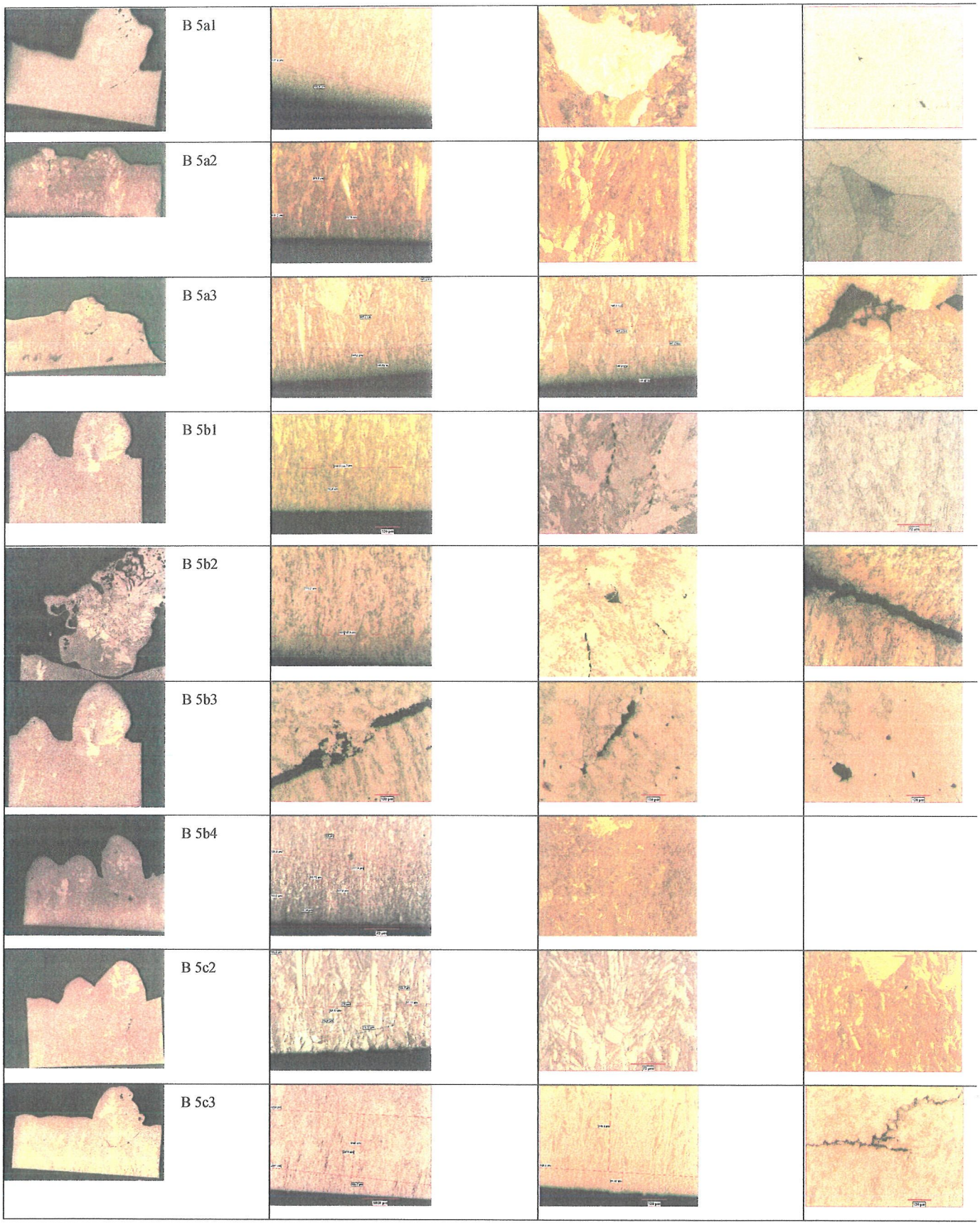

Figure 4-21: Metallographical samples from cathode 5, top located

At the very first copper layer no holes were detected. The dendrites started to grow at the later part of the cathode crop. Many inclusions had the same sponge-like consistence. The analysis, shown in Figure 4-22, demonstrated mainly Ag inclusions combined with Pb, Se and Te.

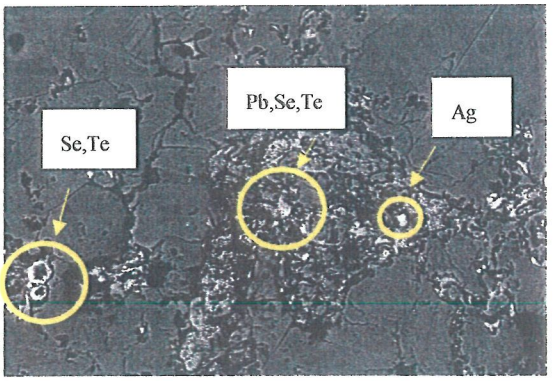

Figure 4-22: SEM analysis of cathode sample 5c3

4.3.4 Company F

The two samples sent by F are from the bottom of the cathode (a) and the middle of it (b). The dendrite samples were picked out and shown in Figure 4-23. Strips are seen in sample 1.

(a) Sample F 1

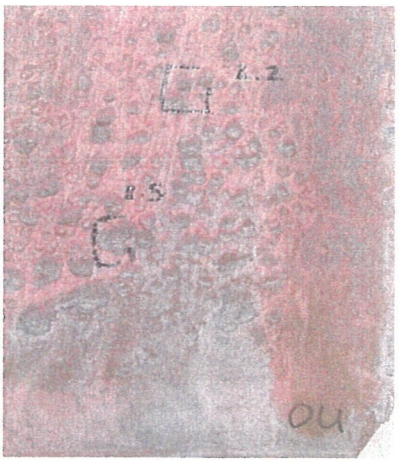

(b) Sample F 2

Figure 4-23: Cathode samples F

The ground sections showed all the similar change in copper precipitation after some hours. This seemed to indicate some discontinuities with the inhibitor transportation. It gave no answer about where this effect was coming from, either some problems at the inhibitor dosage or flow transportation problems. After changing of the fine regular FT type in a coarse-grained copper precipitation it rechanged again into the normal sized FT type.

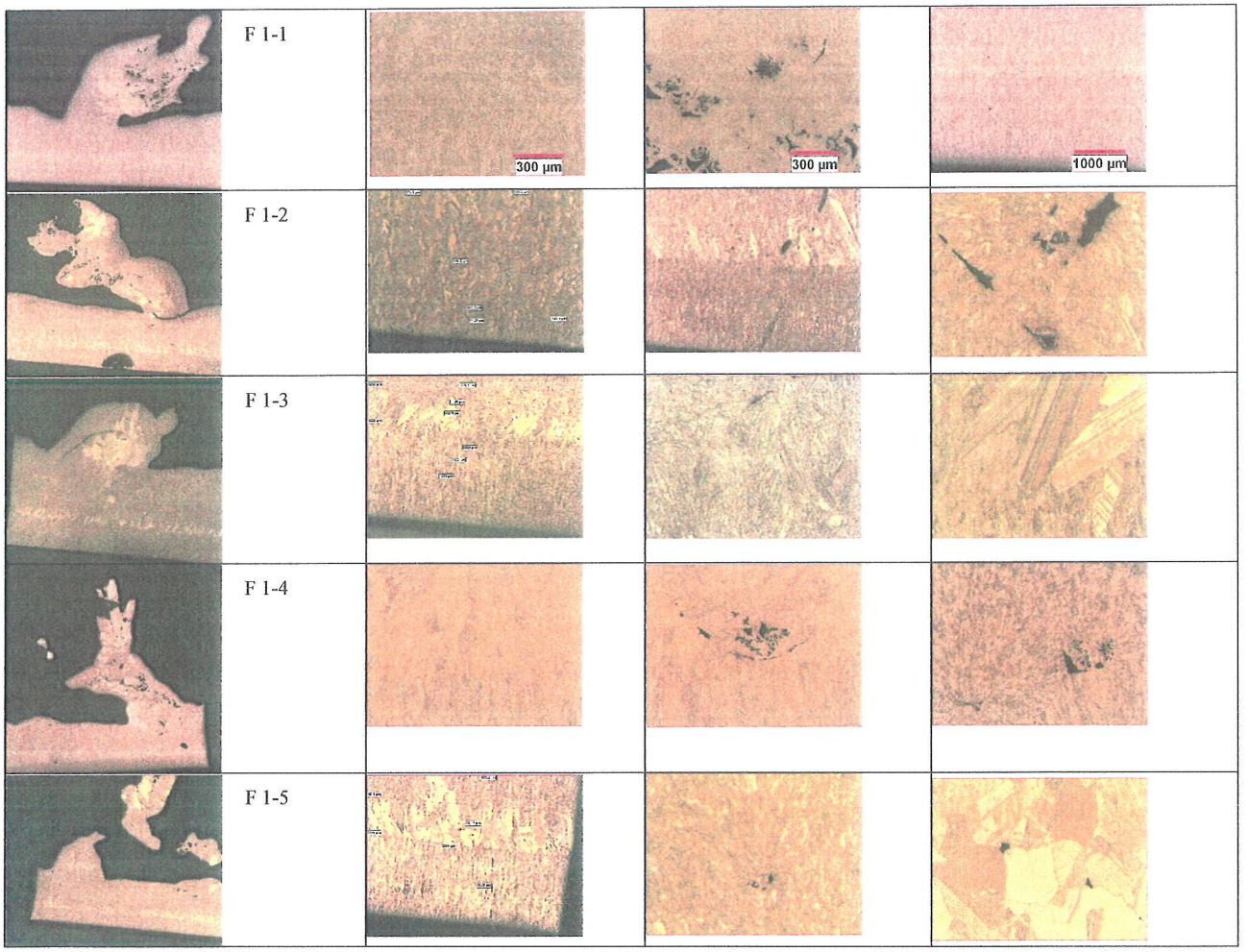

Figure 4-24: Metallographical samples from cathode 1, located at the bottom-part

The impurities in sample 1-6 were mainly Bi, As, Te, Ag and Se. All particles were embedded in copper oxide. In sample 1-5 Fe and Ni was dominating near by Bi. In all ground sections of sample 1 particles of Bi, Fe, Ni were found and less particles of As, Te, Pb were located there.

The ground layer was without inclusions at these samples, too. The analyses of these samples showed no significant differences in impurities in comparison to the samples from cathode one. The dominating impurity is Fe in combination with fewer amounts of Bi, Ni, Se, Te, Ag.

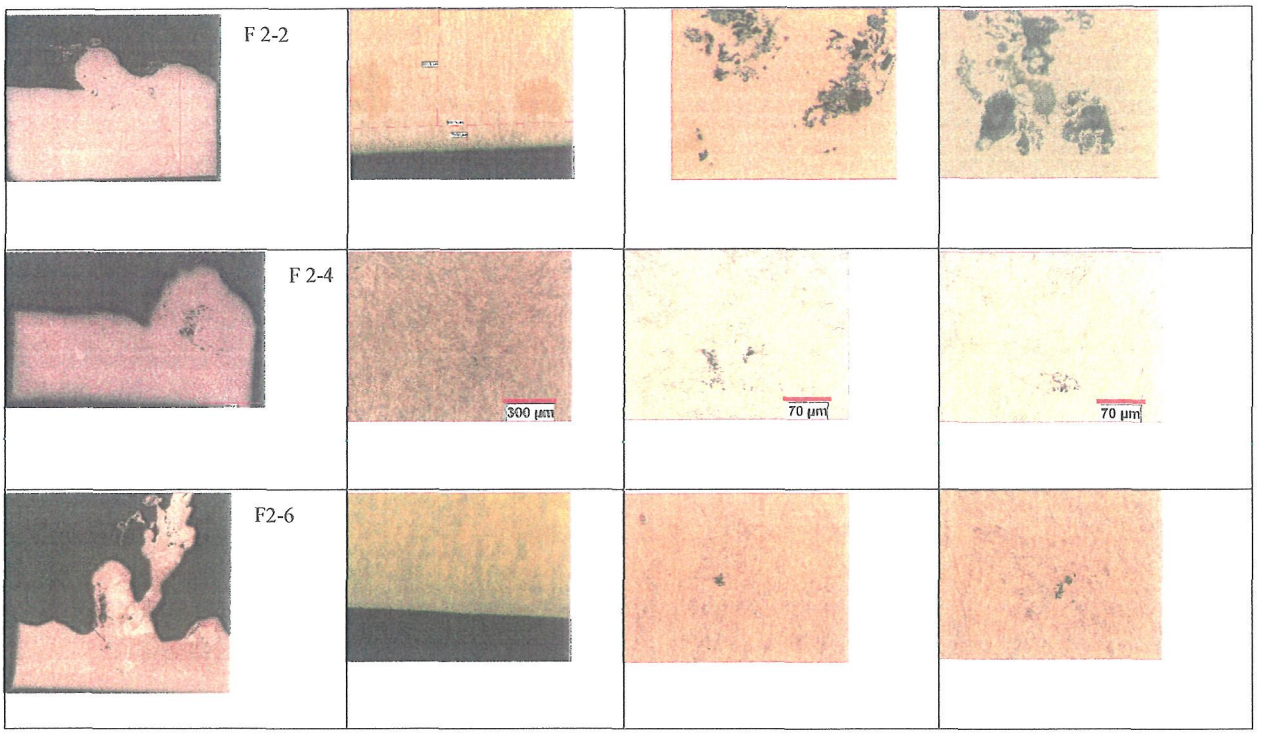

Figure 4-25: Metallographical samples from cathode 2, located at the mid-part

4.3.5 Company G

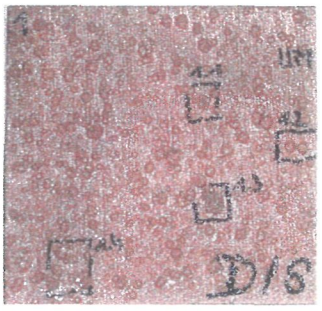

(a) Sample G 1

(b) Sample G 2

(c) Sample G 3

(d) Sample G 4

Figure 4-26: Cathode samples G

Company G, Figure 4-26, sent four different cathode samples, each of them are from different copper cathode producers. The cathode (a) had a lot of small globular dendrites all over the surface, (b) had a few amount of big dendrites and many smaller ones, (c) had also some big dendrites and some few small ones and (d) had many small dendrites with one big dendrite.

In Figure 4-27 the ground sections are shown. None of the samples have inclusions or holes near by the stainless steel starting sheet. The dendrite growing starts only after a significant first copper layer. After this the precipitation is disturbed and a dendrite started to grow.

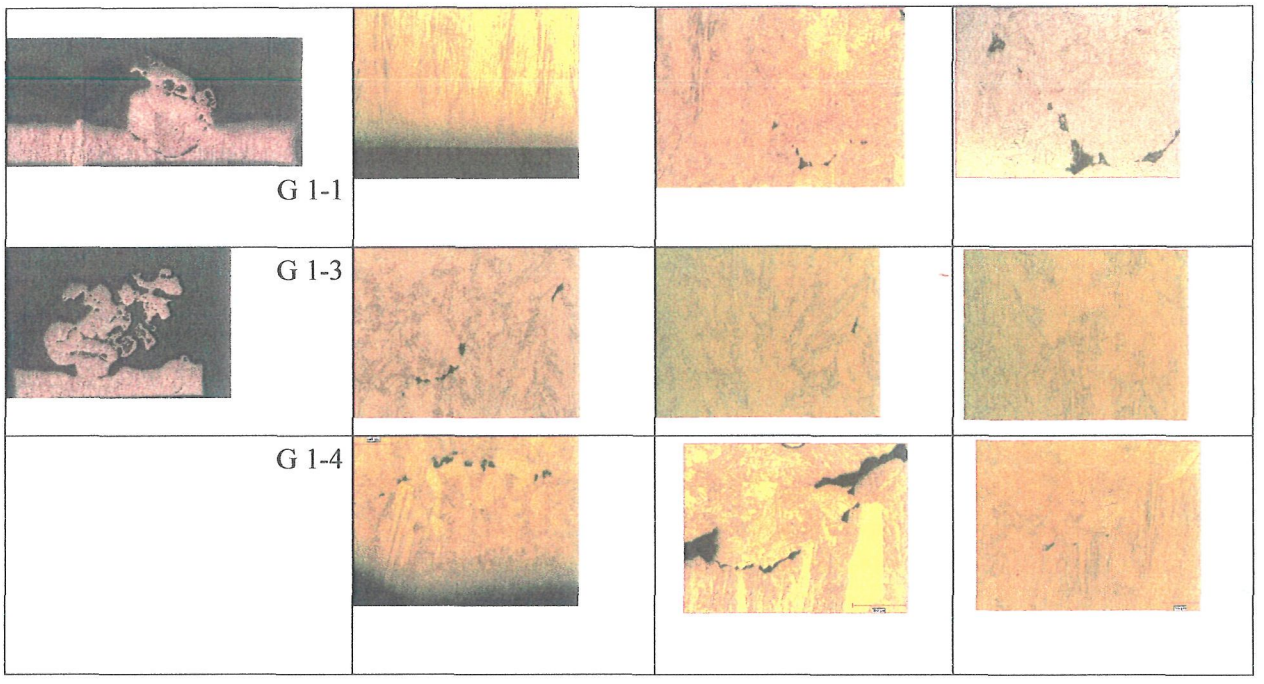

Figure 4-27: Metallographical samples from cathode 1

In Figure 4-28 the dendrites have many holes and no inclusions at the starting layer. The most significant difference compared to the other companies was the copper crystal size, which was much smaller than all the other samples, Figure 4-29(a). At the root of the dendrite no impurities were detected and inside the dendrite a lot of Pb was detected with a little Sb, Figure 4-31 (b).

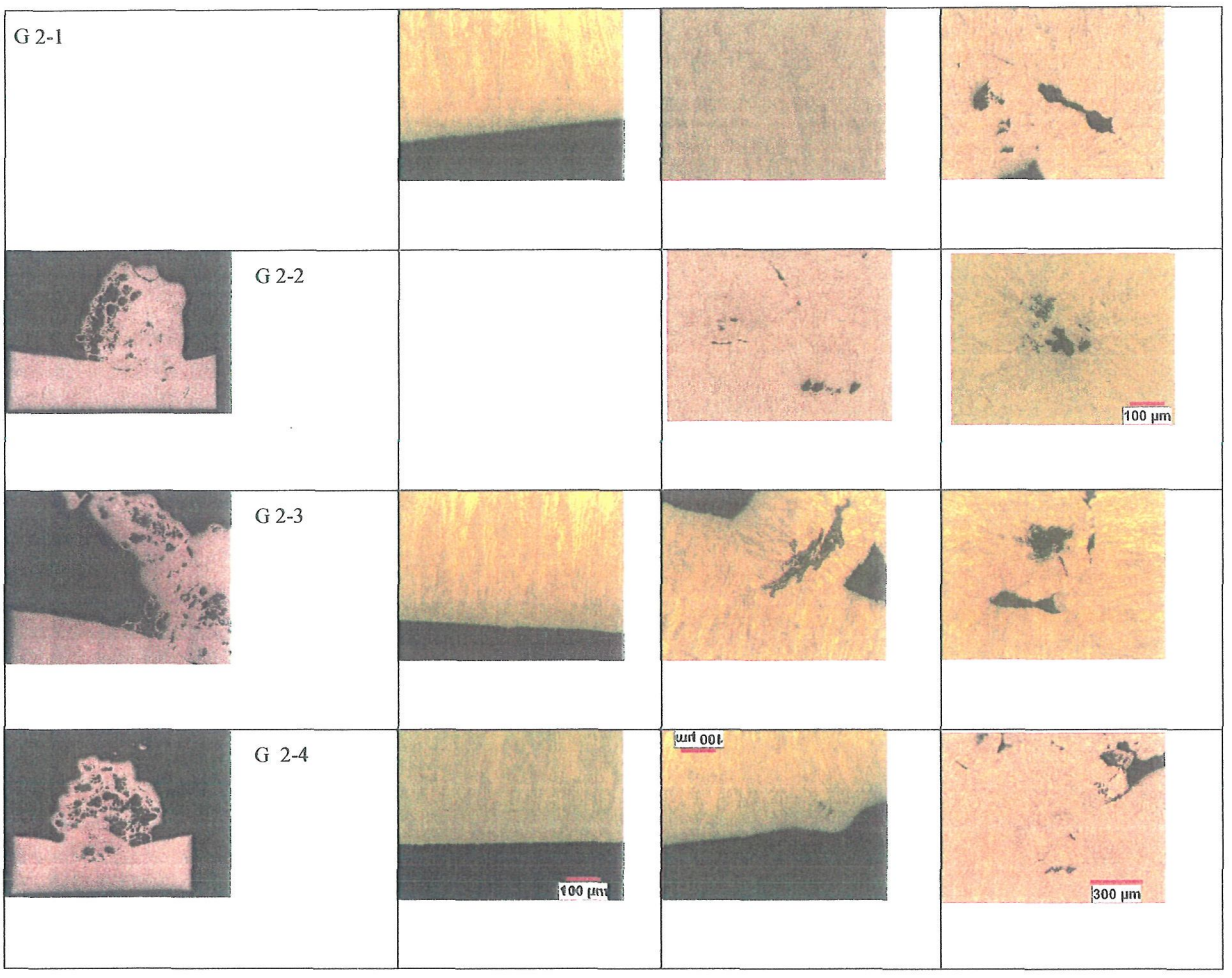

Figure 4-28: Metallographical samples from cathode 2

In Figure 4-29 (a) the special copper crystallization of these samples is illustrated. Many globular and very fine copper crystals were present. Inside the holes no impurities were identified and this area of the cathode was very porous.

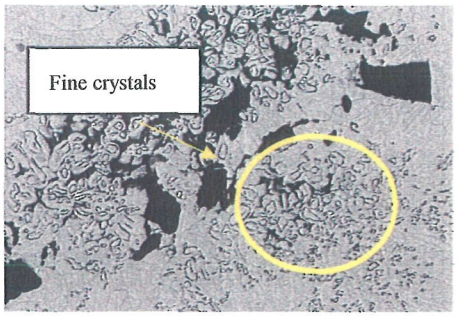

(a) Sample 2-3, spot 1

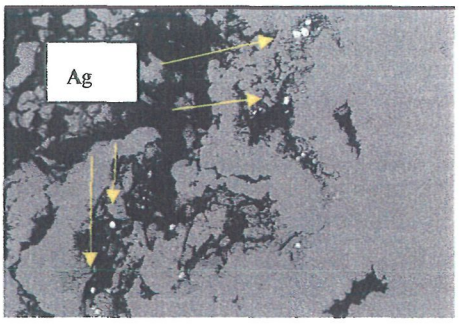

(b) Sample 2-3, spot 2

Figure 4-29: SEM analysis of cathode sample

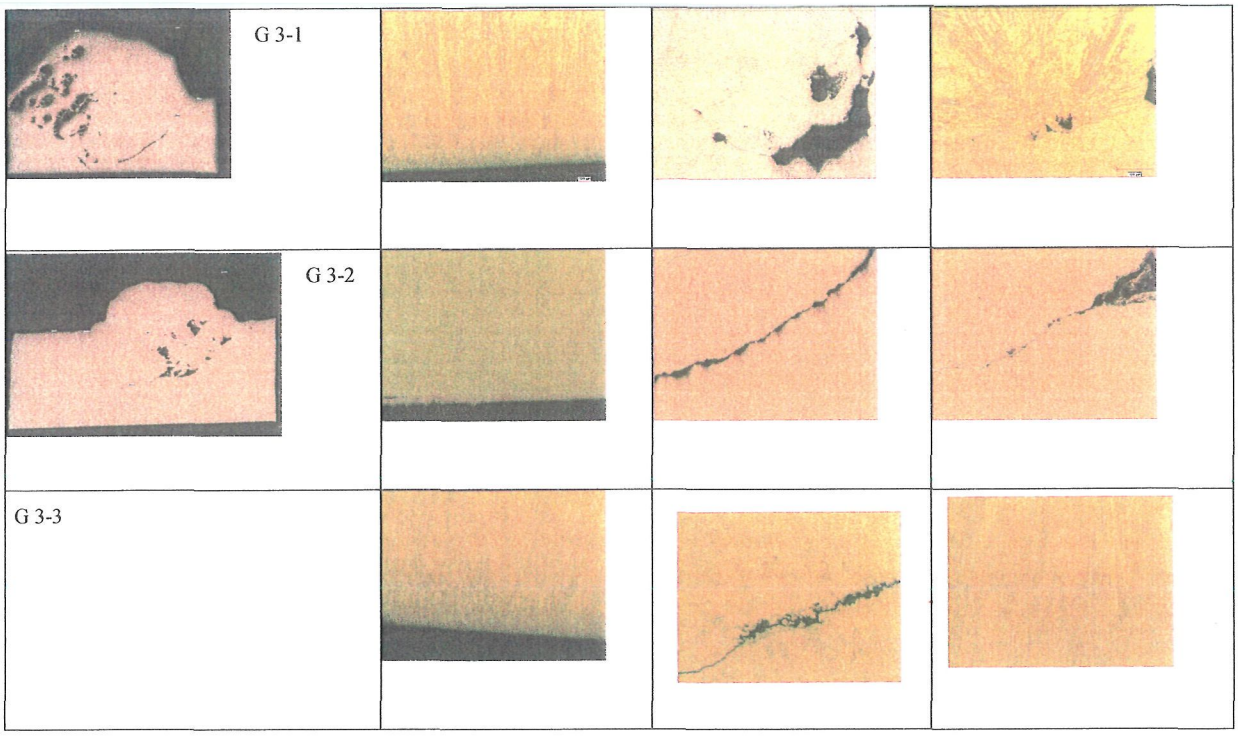

Figure 4-30: Metallographical samples from cathode 3

A characteristic of all these dendrites was the small grain size of the copper matrix. Inside a low level of impurities could be detected, mainly Pb with some Se.

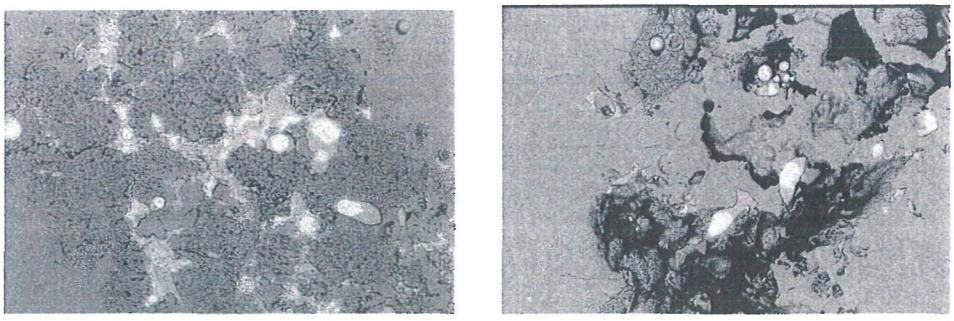

(a) Sample 3-2 (b) Sample 3-3

Figure 4-31: SEM analysis of cathode sample 3

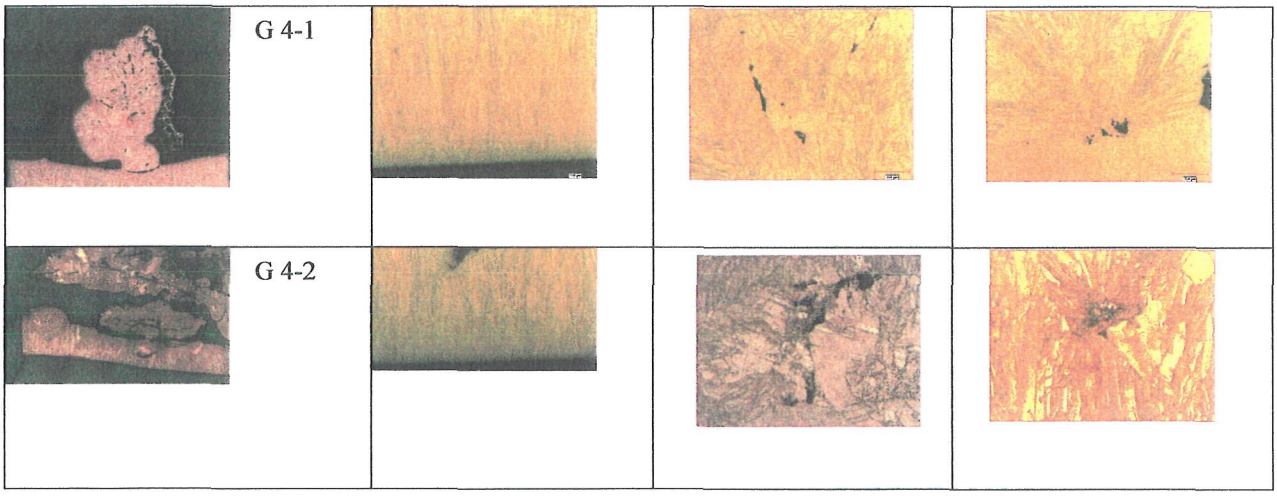

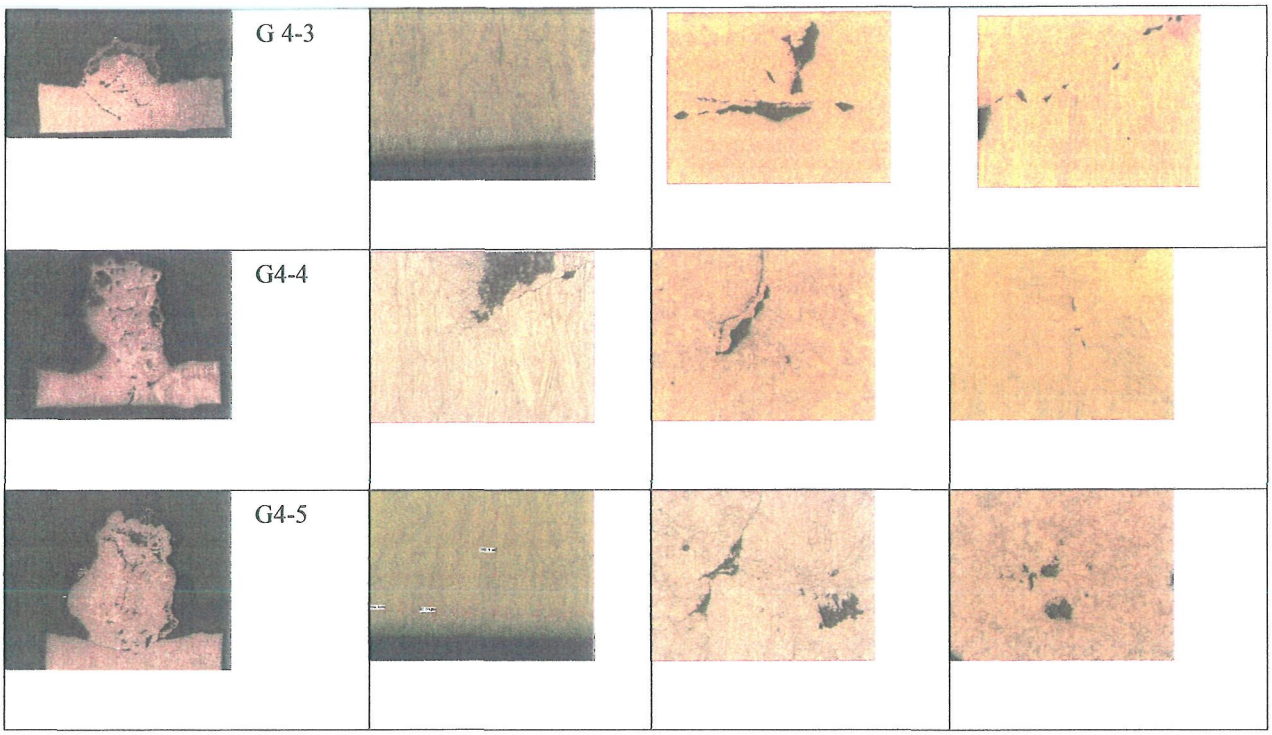

Figure 4-32: Metallographical samples from cathode 4, MC I

The dendrites in Figure 4-32 started to grow after some hours and had no inclusions at the root.

4.4 Summary

4.4.1 Company A

The A anodes have the highest Fe content and the lowest Sb content. The MFR I is much higher than 1. Cathode sample 4 had the lowest oxygen content of all samples. When the electrolyte composition is examined the MFR I was also found to be quite high. The ratio of glue to thiourea was 1.5, and thereby one of the highest values.

Samples 3 and 5 were taken from the top-region of the cathode. The dendrites in this area were globular and distributed very densely over the total cathode "day/night border". All the dendrites in this area had the same appearance. The metallographic investigations of the first layer, near the stainless steel cathode, revealed many impurities and holes in sample 5.

Inclusions in the first layer:	$BaSO_4$.
Inclusions in the dendrites:	Se, Te and significant levels of Ag
	As, Sb, Bi and a small amount of Pb

Sample 1 was from the mid-region of the cathode. The dendrite form was a mixture between globular and dendritic crystals. The dendrites were isolated over the sample area. All the dendrites had holes and many inclusions. Furthermore, strips could easily be identified.

Inclusions in the first layer:	No holes and no impurities
Inclusions in the dendrites:	Se, Te, Sn (very low levels of Ag)
	$BaSO_4$ as a matrix for the inclusions

The dendrites in sample 4 and 2 were distributed over the whole cathode surface. The samples were from the bottom-region of the cathode. The size and the form of the dendrites were similar in both samples and appeared in dendritic form. No strips were detectable on this cathode sample.

In both cases the ground layer did not have any inclusions. After this layer the dendrite growth started and many big dendrites with quite a high number of holes were present. SEM provided the same results for all samples: Significant $BaSO_4$ inclusions and very ferw anodic slime particles were detected. In (a) to (d) single examples were picked out to examine the type of impurities. Big bright particles were mounted in the copper matrix of each sample. The analysis indicated that these inclusions were mainly $BaSO_4$.

Inclusions in the first layer:	No holes and no impurities
Inclusions in the dendrites:	$BaSO_4$
	Very low levels of anodic slime

4.4.2 Company E

No samples from the top-region of the cathode were supplied.

Two cathode pieces were provided from the middle of cathode 3 and 4. In all the samples clefts were detected. Inside these clefts no impurities were found. Furthermore, the inclusions in the dendrites were analysed.

Inclusions in the first layer:	No holes and no impurities
Inclusions in the dendrites:	Clefts without inclusions
	Dendrites with Pb, Ag, Sn, Zn and Ni

In samples 1 and 2 the copper precipitation also had very fine clefts. However, no impurities were detected when the clefts were analysed with EDX.

Inclusions in the first layer:	No holes and no impurities
Inclusions in the dendrites:	Ag, Pb, and Se

4.4.3 Company B

Five samples were supplied by B.

Cathode samples 5 are from the top-region. The dendrites were analysed and the consistence of the inclusions was frequently similar with a sponge-like appearance.

Inclusions in the first layer:	No holes and no impurities

Inclusions in the dendrites: Ag, Pb, and Se

Samples 2 and 4 were from the mid-region. One single big dendrite had grown.

Inclusions in the first layer: No holes and no impurities
Inclusions in the dendrites: Bi, As, Ag, Se, Te, and Sb

Samples 1 and 2 showed dendrite growth from the stainless steel sheet.

Inclusions in the first layer: Holes and impurities
Inclusions in the dendrites: $BaSO_4$, significant levels of Pb with low amounts of Ag

4.4.4 Company F

No samples from the top-region were supplied.

The impurities in sample 1, which was from mid-region, were embedded in copper oxide.

Inclusions in the first layer: No holes and no impurities
Inclusions in the dendrites: Bi, As, Te, Ag, Se, and significant amounts of Fe, Ni, and Pb

Sample 2 was from the bottom-region. The ground layer of these samples also did not have any inclusions. The analyses of these samples showed no significant differences in impurities when compared to the samples from cathode 1.

Inclusions in the first layer: No holes and no impurities
Inclusions in the dendrites: Fe, Bi, Se, Te, and Ag

The ground sections showed a similar change in copper precipitation after some hours. This appears to indicate some discontinuities with the inhibitor transportation. However, it provided no answer about where this effect was coming from, either some problems with the inhibitor dosage or flow transportation problems. After the change of the fine regular FT type to a coarse-grained copper precipitation it changed back again into the normal sized FT type.

4.4.5 Company G

G supplied four different cathode samples: G4, G2, G3, and G1. The cathode G4 had a lot of small globular dendrites all over the surface, G2 had a low amount of big dendrites and many smaller ones, G3 had also some big dendrites and some small ones, and G1 had many small dendrites with one big dendrite.

Inclusions in the first layer: No holes and no impurities
Inclusions in the dendrites: Pb with lower levels of Sb and Se

The most significant difference between the G cathodes and the cathodes from other companies was the size of the copper crystals that were much smaller than on all the other samples.

After processing the current data and the supplied cathodes an investigation of the anodes provided by the companies was performed. For a collective summary of the effects of various parameters on dendrite formation the chemical and physical quality of the anode was also important.

- The grain size of the G cathode precipitation was very fine. When the ratio of glue/thiourea at G was examined it had the highest value at 1.7. This indicates that the higher relative glue content increased the cathodic polarization. With a higher cathodic polarization the formation of nuclei occurred; therefore, a high number of new nuclei resulted in a fine grain size of the cathodic precipitation.

- In complete contrast to the observed effects at G, at E all the cathodes had fine clefts between the copper precipitations. E had the lowest ratio of glue/thiourea with a value of 0.7. Furthermore, the number of new nuclei was lower than the crystal growth.

- If the stainless steel starter cathodes are examined no significant connection can be found between the levels of SiO_2 and $BaSO_4$. Both of these compounds were in the majority of cases not at present at the cathode surface.
- Amount of $BaSO_4$ in the copper precipitation:
  - much $BaSO_4$ at A and B
  - less $BaSO_4$ at E, G and F

- The cathodes from F had a layer with very big crystals. The reason for this phenomenon could not be unequivocally explained. There are three possibilities:
  - irregular inhibitor dosage
  - transportation of the active inhibitor to the cathode
  - current fluctuation

- The size and shape of the dendrites could be classified according to the location of their appearance along the length of the cathode.
  - top-region: globular and round dendrites
  - mid-region: a mixture of globular and dendritic
  - bottom-region: dendritic

In total 150 cross-sections (150 cathode samples with one or more dendrites) were examined. A clear allocation of the cross-sections to the conditions in the tankhouse was evident. Therefore, the occurrence of the dendrites at the cathodes could be attributed to the operating conditions in the cells. In the following conclusion the details obtained from the questionnaire and the metallographical investigations are examined to provide an explanation for the dendrite formation.

4.5 Conclusion

The influences on cathodic precipitation determined from the analysed cross sections can be summarized as follows:

Impurities on the cathode starting sheets
Impurities including anode slime particles, mould coating particles, and particles on the cathode surface from outside caused a polarization modification at the cathode surface and formed the nuclei initiating an irregular crystal growth. Thereby, the BR type in the first copper layer did not form or was disturbed, and holes or leaks were formed. The analysis of the ground sections clearly revealed that dendrites started to grow from these holes or leaks.

Mould coating
The residual anode mould coating influenced the electrolysis as follows:

- The mould coating did not dissolve in the electrolyte and these particles were transported to the cathode. By adhering to the cathode surface they provide nuclei for dendrite growth.
- If a dendrite has already formed, the insoluble mould coating can be incorporated into the copper precipitation. Thereby, the mould coating decreases the copper quality.

In the metallographical investigations two situations were observed. Either no mould wash particles were detected in all the ground sections from a particular company or alternatively mould wash particles were present in all the samples from a certain company.

Inhibitor effects
The experimentally determined inhibitor influence on cathode precipitation was in good agreement with the observations described in the literature.

- A relative high glue/thiourea ratio resulted in copper crystals with a fine grain size due to the polarization increase.
- A relative low glue/thiourea ratio caused fine clefts to form over the entire copper precipitation due to the lower polarization and decrease in the number of nuclei.
- If the inhibitor dosage varied during the cathode crop, crystallization layers with different copper crystal sizes were detected on the entire copper cathode.

Anode slime
The analysis indicated that the anode slime influenced the cathodic precipitation in the following ways:

- Anode slime particles formed a nucleus for irregular crystal growth.
- Anode slime particles influenced the cathodic polarization and furthermore the crystallization behaviour
- After precipitation at the cathode the anode slime particles decreased the cathode quality.

5 ANODE QUALITY AND DISSOLUTION

The anode quality is a decisive factor for the effectiveness of a refining electrolysis. A high current yield, low energy consumption, few anode remnants, low specific manpower requirement, in addition to an excellent cathode quality depend to a great extent on the anode quality. Thereby, it is obvious that the anode quality has a decisive influence on copper refining electrolysis. The anode criteria are:

- Always same thickness
- Equal surface properties on both sides
- Regular distribution of the impurities over the thickness
- No negatively influencing spray chemicals
- No bends and undulations
- No craters
- Perfect plugs preparation (milling) for good electrical contacts
- Content of unnoble impurities as low as possible

It has been highlighted several times that one problematic variable in the total refining and electrocrystallization process is the anode quality /38/. The type and amount of impurities in the anode influence the passivation behaviour. Especially higher current densities can accentuate passivation. Passivation time is a function of the electrolyte, current density, slime amounts, and oxygen levels in the anode.

A problem with the casting process is the incompatibility of the goal of combining a high casting rate and a long mould durability with good physical anode characteristics. All the investigated anodes were cast on conventional casting wheels. Anode preparation machines were used, for example the Wenmec type /39/, where the anodes are weighed and pressed (sometimes the thickness is also measured). The lugs are milled, often bottom milling is employed, and side milling is used if the thickness of the lugs exceeds a certain dimension.

5.1 Anode physical quality

The physical quality of the anodes has a significant effect on the refining process. Thereby the weight, the roughness and the form is important.

5.1.1 Anodes weight

The anode weights must be optimally selected because the anode weight directly influences the electrolysis system. It not only dictates the anode – cathode distance but also the final anode scrap is dependent on the starting weight. The anode must be thick enough so that when it is lifted out of the electrolysis bath the anode scrap does not break. Furthermore the anode weights must not vary to greatly resulting in an increased thickness and a reduced electrode distance, which particularly at the beginning of the anode crop can cause an increased current density. This can cause anode-lateral passivation,

cathode-lateral nodulation, and as a further consequence shorts. The greater the anode weight variation, the more challenging the operating conditions. Establishing the balance between fragile thin anode scraps and too heavy anode scraps which have to be remelted is problematic if the anode weight variation is too high. The anodes supplied varied in their dimension: The heights varied between 800 mm and 950 mm and the widths between 35 mm and 55 mm. Furthermore, the weight tolerance was between $\pm$ 1 kg and $\pm$ 10 kg.

5.1.2 Anode roughness

When the anodes are examined it is quite easy to see the two different physical qualities of the two surfaces. The surface that was in contact with the casting mould ("mould side - MS") and the surface that was in contact with the air ("air side - AS").

Figure 5-1 and Figure 5-2 show the two different sides.

To achieve smooth and equal surfaces on both sides should be the task of the casting shop. The reasons for a certain anode roughness are:

- *On the mould side*
  - mould quality and age
  - smoothing procedure – type and amount of used material, ratio water to smoothing material
  - mould temperature

- *On the air side*
  - oxygen content
  - minor elements content – mainly sulphur
  - cooling procedure
  - velocity and movement of the casting wheel

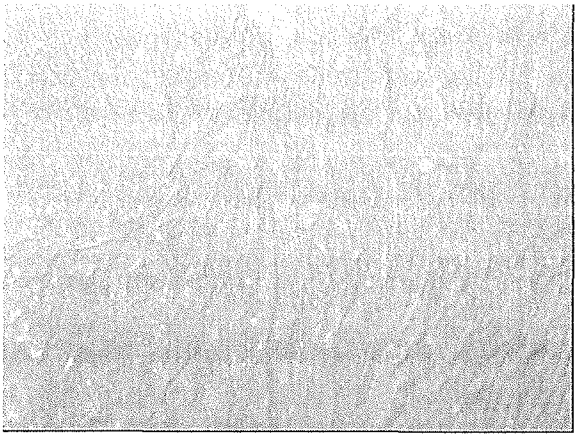

Figure 5-1: Air side

In Figure 5-1 the reflief of the air side is illustrated. This surface is quite smooth without recognizable adherences.

Figure 5-2: Mould side

In Figure 5-2 the mould side is shown with recognizable optical structures on the surface. The coating materials and bumps are easily visible. The smoothing layers, which work like isolators, can cause inactive surfaces and the anodes will not dissolve as regularly as they should. This can influence the current density distribution on the cathode and the resulting copper deposit. In addition particles of smoothing material go into the electrolyte. Subsequently, these particles will go to the cathode and negatively influence the copper deposit, especially as a nucleus for dendrites and buds formations.

To compare the various anode brands and surfaces, the roughness of the anodes was measured. The decisive value is the mean roughness R_z, defined (following DIN 4768) as the average of the roughness values of five reference paths within an evaluation length.

The anode stripes were measured at five different points over the width and in distances of 1 cm over the length.

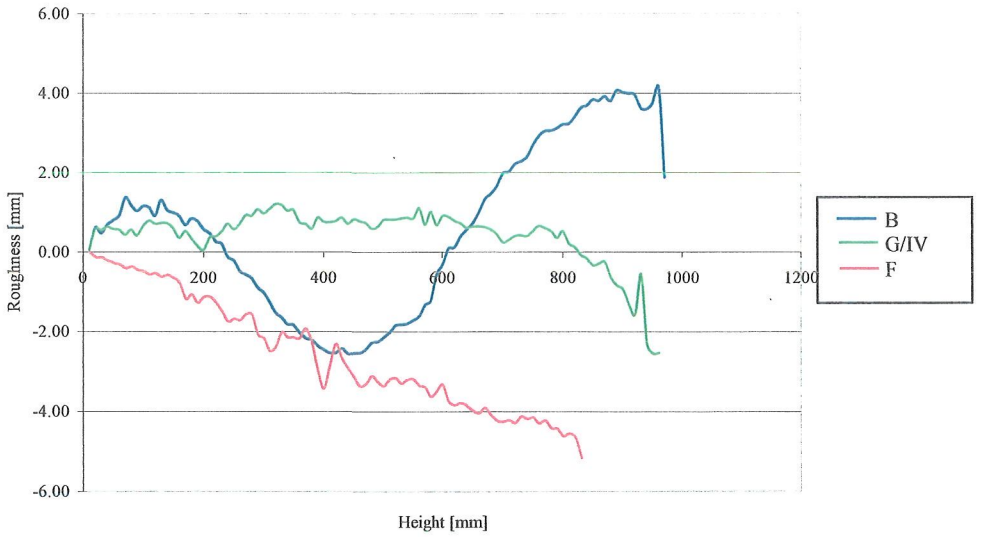

Figure 5-3: Roughness of anodes B, G/IV and F

If the surface roughness values measured in Figure 5-3 are compared, a variation of the anode thickness of up to 5 mm can be identified, however a different anode form is also recognizable. Anodes from F exhibit a slight conical form, while anodes from B have a bent form. The anodes of G are the most regular ones. If the anode roughness is examined with the anode-cathode distance, the influence on the current density distribution is immediately evident. With a variation of only 5mm and a distance of 20 mm a 20 % variation in the current density distribution resulted. This can cause a massive disturbance of the electrocrystallization. The anode roughness measurements were performed on the mould and air sides of the anodes. Table 5-1 details the measured results.

Anodes	side	Min.[mm]	Max.[mm]	R_z [mm]
E/005	AS	-1.87	1.17	3.04
	MS	-5.13	1.26	6.39
E/006	AS	-1.06	1.43	2.49
	MS	-3.62	0.73	4.35
H/003	AS	-2.21	1.91	4.12
	MS	-0.81	1.08	1.89
H/004	AS	-1.53	3.81	5.34
	MS	-2.61	2.60	5.21
B/008	AS	-2.87	1.09	3.96
	MS	-3.46	0.69	4.15
B/010	AS	-2.02	0.86	2.88
	MS	-1.29	2.30	3.59
G/I/005	AS	-3.37	2.32	5.69
	MS	-1.60	0.40	2.00
G/I/006	AS	-2.45	1.60	4.05
	MS	-2.25	0.44	2.69
G/III/006	AS	-2.33	2.21	5.54
	MS	-4.09	1.08	5.17
G/III/007	AS	-2.20	1.75	3.95
	MS	-1.73	2.15	3.88
G/IV/007	AS	-0.78	1.49	2.27
	MS	-1.53	2.00	3.53
G/IV/008	AS	-0.98	1.20	2.18
	MS	-1.68	1.25	2.93
F/001	AS	-1.21	1.86	3.07
	MS	-2.36	3.12	5.48
F/002	AS	-1.19	1.39	2.58
	MS	-2.46	1.75	4.21
A/001	AS	-1.55	1.46	3.01
	MS	-1.90	0.44	2.34

Table 5-1: Anode roughness measurements

The measurements revealed a minimum of – 5.13 mm and a maximum of 1.26 mm. This means that the anode surface had a distance difference up to 6.39 mm from the cathode, which has an influence on the current density. The Table 5-1 illustrates the remarkable roughness differences

In the Figure 5-4 and Figure 5-5 anodes from D and C are compared.

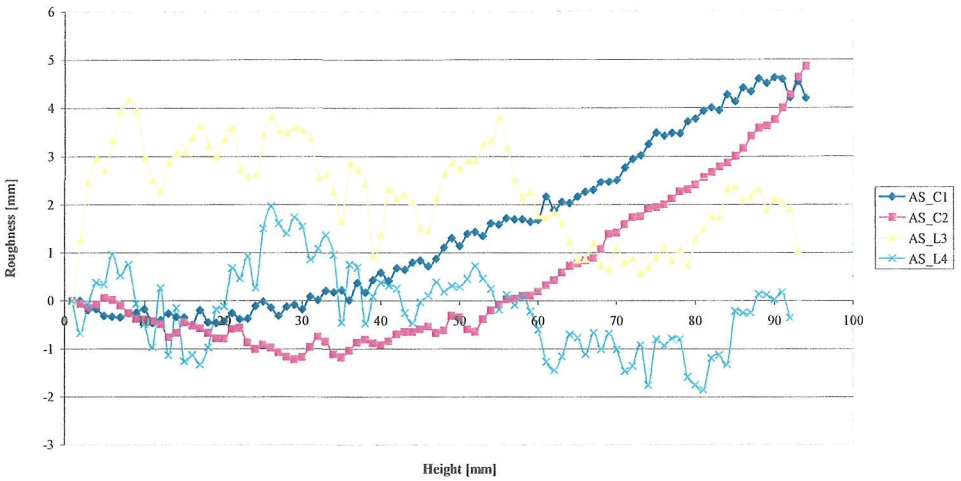

Figure 5-4: Roughness of D and C anodes, on the AS

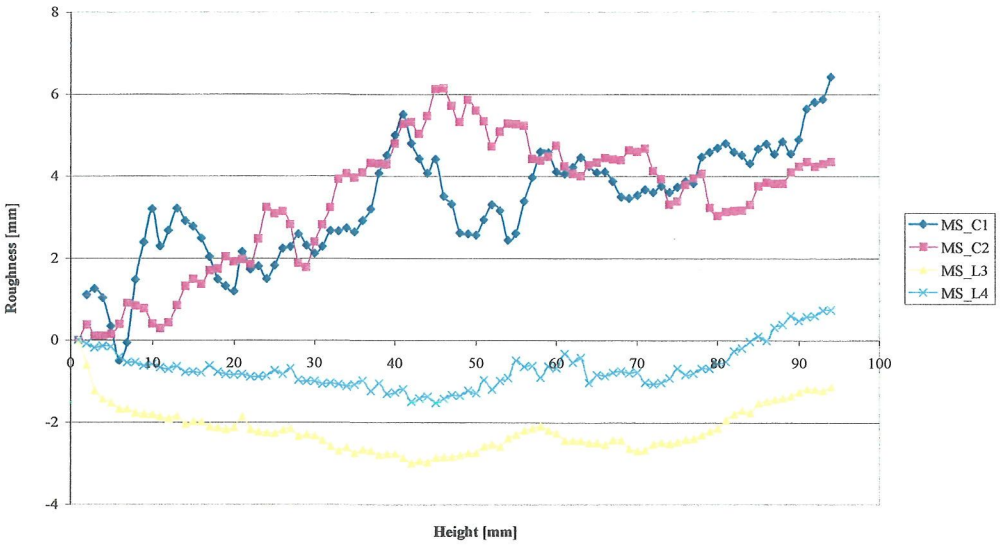

Figure 5-5: Roughness of D and C anodes, on the MS

The measurements of anodes from C revealed a roughness of less than 1 mm; therefore the anodes are very smooth. However, the anode thickness varied from top to bottom. The anode was 6 mm thinner at the bottom than at the top. This resulted in an unequal current density distribution from the top to the bottom of the anode and the cathode. The d anodes were very rough. The difference in roughness was about 6 mm. This resulted in a strange current density distribution over the entire cathode height. The

roughness measurements of the air and mould side of the anode were very similar. This indicated that the roughness significantly influences the distance between the anode-cathode.

It was recognizable that the AS and the MS did not have regular surfaces. The skin was wavelike. The MS also exhibited very irregular structures. The remainder of mould washes as well as dents and holes, which are due to different mould temperatures or damp form lubricants in the copper, were highly visible. The reasons for these irregularities could be:

- Rocking vibration boundary can be due to jerky operation of the casting machine, an incomplete mould lubrication, incorrect casting temperature or uneven pouring.

- Buckling can be due to the incorrect mould temperature, the cooling conditions, and unfavourably high sulphur content in the copper.

- Water bubbles usually indicate a too early use of direct anode cooling.

An unevenness on the MS of the anode is in most cases the effect of worn anode moulds. The features of the AS unevenness are among other things due to dents, burrs, points, scoring, and other effects. In addition, the MS surface disturbances may be due to adhering lubrication material such as barium sulphate. Furthermore, an insufficient cathode overlap results in an increased current density at the cathode edges and the problem of the copper precipitate bulging. This can have particularly unfavourable effects on copper quality at the lower surface of the cathode.

To influence the physical anode quality the following casting parameters have to be taken in consideration:

- Slag carry over
- S/O_2 relationship
- Water quantity
- Mould life span
- Mould material
- Quantity of coatings
- Mould temperature

The target is a smooth anode surface that is as evenly and as freely of impurities as possible. Finally, the following anode preparation can be performed

- True up the anodes
- Press the anodes
- Wash the anodes
- Grind the anode ears

5.2 *Anode chemical quality*

A generally applicable fact is that the grain size on the mould side is finer than on the air side, which is due to the higher solidification and cooling rate. The finer grain results in more grain boundaries and this mean better dissolution in the electrolyte.

The anodic dissolution is characterized by the anode reaction and the secondary reaction in electrolytes in the anode-near layers. In addition to the electrochemical behaviour the specific form of the compounds also effects the solubility of the anode impurities. If they form only one mixed crystal or connecting phase with the refining metal, then the primary electrochemical dissolution reaction takes place with the noble elements, this is unavoidable for example with silver. If they are distributed over several independent phases, with low polarization, only the base metal elements are selectively dissolved. According to their electrochemical characteristics the accompanying copper elements in the anode can be divided into different groups /40, 41/.

5.2.1 Distribution coefficient

A further important fact is the distribution of minor elements over the anode thickness. The most important characteristic to understand the procedures as well as for the purposeful controlling of its refining effect is the distribution coefficient. The distribution coefficient possesses a character material-specific to the available matrix and the minor elements in its physicochemical definition. It is affected by the conditions existing during the crystallization and makes a description possible of the macro distribution of impurities. However, the crystallization from melts is a complex procedure, and the description of which can be done from different points of view. On the one hand structural changes occur with the phase transition liquid-solid. At the same time fundamental changes of the characteristics result including viscosity, density, conductivity etc. The liquid and crystal also differ with respect to their thermodynamic parameters.

An easily observable effect is for example that the latent heat of crystallization is released with solidification. On the other hand the crystallization is also connected with a material and/or heat transport. The different solubility of the admixtures in melt and crystal leads in connection with the material transfer to a local rearrangement of the matrix.
The term "distribution coefficient" is used in science and technology with different meaning. Generally the distribution coefficient indicates the concentration relationship between phases in a thermodynamic sense. The phases can both resemble different states of aggregation. Here, the distribution coefficient is used exclusively for the description of concentration conditions with the crystallization from the liquid phase.

K = concentration in the solid phase c_S/concentration in the liquid phase c_L

The liquid phase (melt) and the solid phase (crystal) are in principle regarded as merged phases. With higher concentrations the merged phase is also designated as an alloy. The numeric value of the distribution coefficient is calculated from the concentrations, whose numerical values differ depending upon the definition.
During crystallization the distribution coefficient is dependent on:

- The thermodynamic characteristics of the main component and admixture in the two corresponding phases (liquid-solid)
- The kinetics at the liquid-solid boundary surface (phase boundary, and crystallization front)
- The completeness of the material changes at the phase boundary due to diffusion and convection
- The form of the phase boundary-liquid

The equilibrium distribution coefficients of the minor elements in copper are the following /42/:

$K_{Cu} > 1$:	V, Fe, Co, Ni, Nb, Rh, Pd, Pt
$K_{Cu} < 1$:	Li, Be, B, Mg, Al, Si, P, Ti, Cr, Mn, Zn, Ga, Ge, As, Y, Zr, Ag, Cd, In, Sn, Sb, Ce, Ho, Au, Th
$K_{Cu} << 1$:	O, S, Ca, Se, Te, Ba, La, Pr, Yb, Tl, Pb, U, Bi, Pu

5.2.2 Minor element distribution over the thickness of the anode

Table 5-2 details results of the elements' distribution over the anode thickness. Thin disks cut from the anodes and analysed by spectrometry in three different zones, see Figure 5-6.

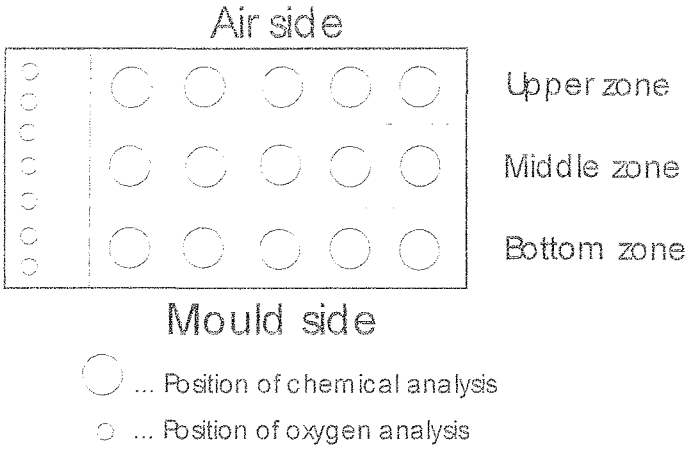

Figure 5-6: Anode disk with spectrometry positions

	Ni [%]	Pb [%]	As [%]	Sb [%]	Sn [%]	Ag [ppm]	Si [ppm]	Bi [ppm]	Zn [ppm]	S [ppm]	Te [ppm]	Se [ppm]
upper zone	0.014	0.019	0.065	0.011	0.004	263	29	71	68	45	23	336
middle zone	0.014	0.017	0.059	0.010	0.004	246	6	67	59	43	22	321
bottom zone	0.014	0.016	0.055	0.009	0.004	227	3	60	57	41	19	298

Table 5-2: Chemical analysis of A/003

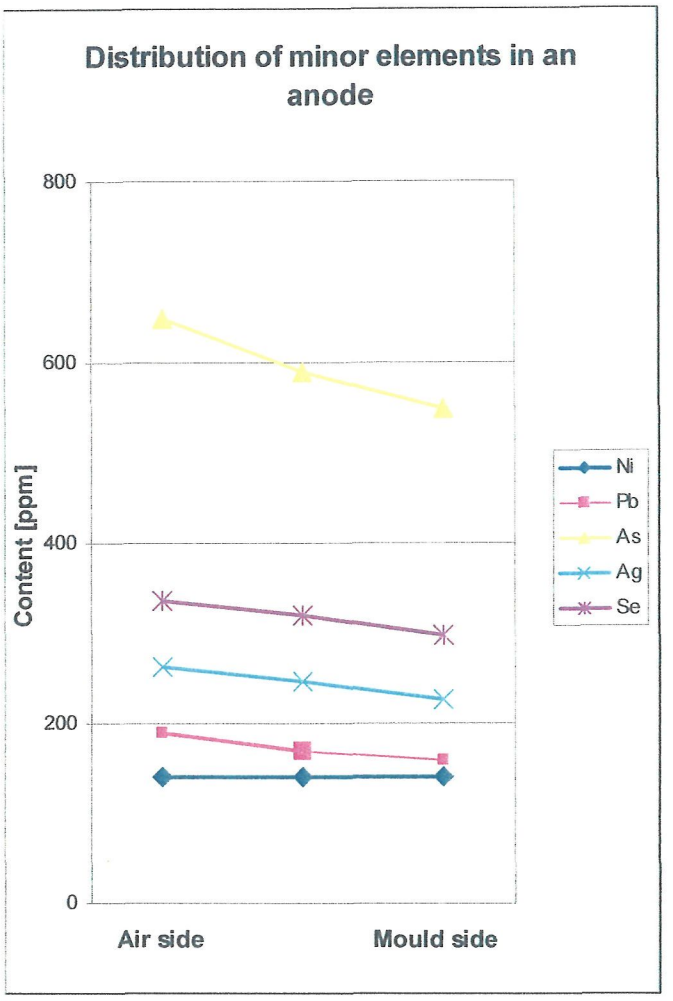

Figure 5-7: Distribution of minor elements in A anode

By comparing the results of the analyses of the anode and the equilibrium distribution coefficient with respect to copper, the significant correspondence was remarkable. For example, for lead the equilibrium distribution coefficient is less than 1, this means lead has a tendency to move out of copper and go to the air side. In Figure 5-7 the distribution of the minor elements in an anode is detailed.

The accumulation layers in direction of the air side can clearly be seen. In case of generally higher impurities' contents (anode A) these accumulations, however, can hardly be detected (only for As, Ag).

F	1	2	3	4	5	6	7
O_2 %	0.234	0.225	0.212	0.212	0.227	0.219	0.192

Table 5-3: O_2 content in the F anode

In Table 5-3 and Figure 5-8 the oxygen distribution in the analysed F anode is detailed. The positions where the analysis was performed are represented by 1 to 7. 1 is near to the air side and 7 is the nearest position to the mould side. The oxygen content was analysed using inductively coupled plasma atomic emission spectrometry (ICP-AES).

In general it was possible to see the tendency with regard to the oxygen and minor elements distribution. Therefore, the influence of these differences on the anodic dissolution could also be possible. Frequently differences in characteristics between the third and second cathode crops were recognizable.

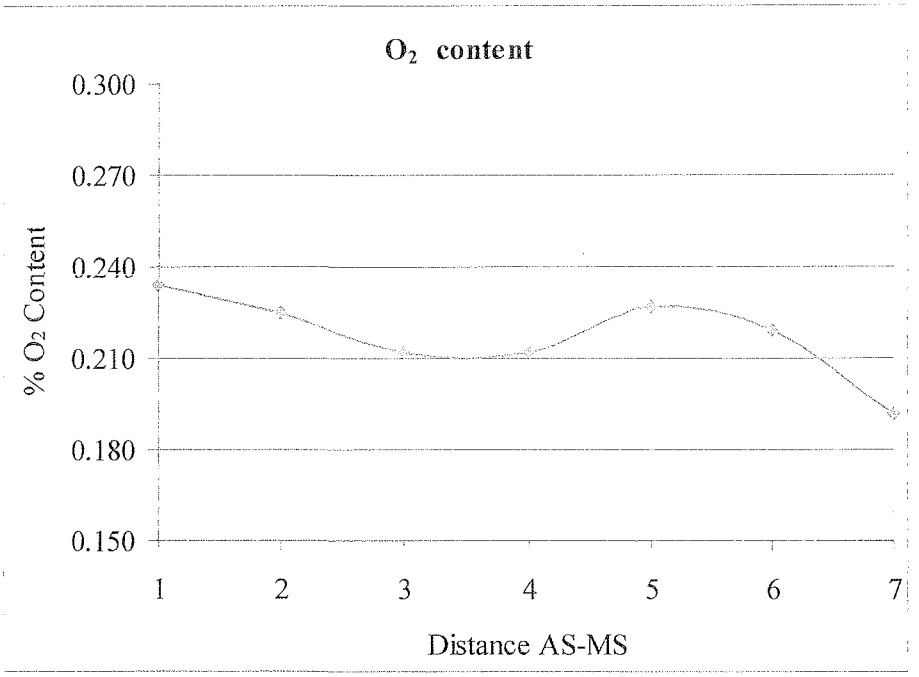

Figure 5-8: Oxygen distribution in a F anode

5.3 Anodic Dissolution

In general the chemical anode composition is dependent on the type of ores and other materials including scrap. If it is a primary plant the chemical composition will be totally different from a secondary plant.

5.3.1 Behaviour of the elements under electrolysis conditions

Generally nickel is one of the main anode impurities. In the form of dissolved metallic nickel (concentrations < 0.3 %) and depending on the oxygen content which can form NiO during solidification and in the presence of antimony it can be combined as Kupferglimmer (Cu_3Ni_{2-x} SbO_{6-x} with x = 0.1 to 0.3 or $3Cu_2O*3.55NiO*Sb_2O_5$) /43/.

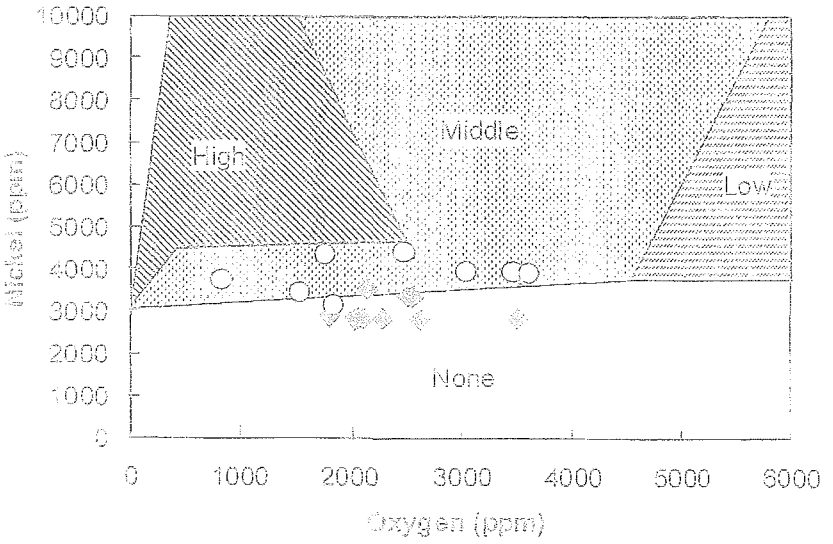

Figure 5-9: Cu-Ni-O phase diagram with schematic indications of the amount of Kupferglimmer /44/.

A reactivation of the anode by reduced passivation occurs when slimes detach from the anode surface. The reasons for a more or less sudden detachment are unknown. It is possible that the slime´s adhesion decreases with increasing levels of arsenic.

Nickel from the Ni-Cu-mixed crystal goes into solution as a bivalent ion with anodic polarization. NiO, which could be proven according to investigations of /45, 46, and 47/ is dissolved in the electrolysis neither chemically nor electrochemically and therefore goes completely into the anode mud /48/. Furthermore, the relationship between the nickel and oxygen content in the anode, for example the presence of nickel oxide was established. Thus determined /45/ a strong rise in the anode slime nickel content occurred with a rising anode oxygen content. This feature is due to stable NiO phases and /49/ experimentally confirmed that the behaviour of nickel in the system anode - electrolyte - anode slime could be summarized /47/ as follows:

Anode	Electrolyte	Anode slime
Cu-Ni-mixed crystal	Dissolved as Ni^{2+}	Partly precipitated $NiSO_4.nH_2O$ $(Cu,Ni)SO_4.5H_2O$ Cu-Ag-Se-As-Ni-S-O-complexes
Kupferglimmer $Cu_3Ni_{2-x}SbO_{6-x}$	Partly dissolved as Ni^{2+} Unconverted	Kupferglimmer
NiO	Unconverted	NiO
$NiFe_2O_4$ Cu-Fe-Ni-Oxide Cu-Fe-Oxide Cu-Sn-Fe-Ni-Zn-Oxide Cu-(Sn,Sb)-(Ni,Fe)-Oxide Cu-Ni-Silicate	Unconverted	$NiFe_2O_4$ Cu-Fe-Ni-Oxide Cu-Fe-Oxide Cu-Sn-Fe-Ni-Zn-Oxide Cu-(Sn,Sb)-(Ni,Fe)-Oxide Cu-Ni-Silicate

Table 5-4: Behaviour of Ni in the system anode – electrolyte – anode slime /50/

In the observations of /51/ up to approximately 50 % of the "Kupferglimmer" that could be detected in the anode mud is chemically redissolved. Through a protective layer of CuAgSe or $PbSO_4$ and by the constant supply from the dissolving anode "Kupferglimmer" is always in the anode mud. During the electrolysis process an enrichment of nickel ions in the electrolyte can occur, whereby the resistivity and thus the energy consumption rise. Nickel ions are transported preferentially by migration to the cathode and adsorb ionically at the cathode surface, without any further reaction. The effective cathode surface is decreased and the marginal current density causes the copper problems. With the rise in the nickel ions concentration the electrolyte shifts its electrode potential to more positive values, and the danger of an electrochemical codeposition increases. A further aspect is the passivation susceptibility of the anodes in relation to the nickel and oxygen content /52, 39/.

During the electrolysis process, iron and zinc enrich themselves as ions in the electrolytes. The dissolution of compounds present in the anode (as for example Fe_3O_4 or $CuFe_2O_5$) was confirmed by /53/. These elements do not cause anode mud. These elements are typically no precious elements. Iron and zinc form mixed crystals with copper in their typical concentration range. The unnoble elements together form mixed crystals as well as intermetallic compounds.

Arsenic forms with copper α-mixed crystals at arsenic concentrations < 6 %, as illustrated in the phase equilibrium diagrams. Investigations by /54/ indicated that Cu_3As is already an intermetallic phase at 3 % arsenic. At the grain boundary arsenic is in combination with other impurities and oxygen complexes, including As-Pb-O-complexes
Antimony is in the anode at concentrations < 1.25 % under optimal cooling conditions as a α-mixed crystal, whereas under poor cooling conditions a β–mixed crystal can exist. /55/ detected intermetallic combinations like Cu_2Sb and Cu_3Sb and also "Kupferglimmer" and complex compounds with lead and oxygen. The behaviour of arsenic, antimony and bismuth can vary considerably during the anodic dissolution. These compounds can be present dissolved in electrolytes; in addition, they can be involved in the formation of the anode mud. As under the copper refining conditions becomes a trivalent ion forming $HAsO_2$.

As	+	$2H_2O$	$\leftrightarrow$	$HAsO_2 + 3e^- + 3H^+$	($E^0 = +0.34$ V)	Equation 5-1
Cu_3As	+	H_2O	$\leftrightarrow$	$3Cu^{2+} + AsO^+ + 9e^- + 2H^+$	($E^0 = +0.44$ V)	Equation 5-2
Cu_3Sb	+	H_2O	$\leftrightarrow$	$3Cu^{2+} + SbO^+ + 9e^- + 2H^+$	($E^0 = +0.31$ V)	Equation 5-3

In the presence of dissolved oxygen in the electrolytes, As can be oxidized to As(V). This reaction occurs prior to the antimony oxidation /6/. The analysis by /56/ showed that As(V) - as well as Sb(V) ions developed by second reactions with dissolved components of the electrolyte (heavy soluble lead antimoniate or arsenate as well as arsenates and/or antimoniates with Cu and Ag). With anodic polarization bismuth is solved and goes as a trivalent ion into solution. Furthermore, Bi, As and basic bismuth salts can also form. Bismuth arsenate can form when Bi reacts with certain electrolyte components (AsO_4^{3-} - ions). In anode dredging, Pb-Cu-Bi-oxides were also detected, which became insolvable due to a Cu_2Se-surface coat. Bi present as an oxide (Bi_2O_3) in the anode is chemically reactive in acid electrolytes according to /56/.

$Bi_2O_3 + 3H_2SO_4 \leftrightarrow Bi_2(SO_4)_3 + 3\ H_2O$ Equation 5-4

/57/ measured a copper and silver mixed crystal potential in relation to pure copper of 3 mV. Therefore, with sufficient anodic polarization the copper and silver go together in solution. The following reaction can be formulated:

$Ag \leftrightarrow Ag^+ + e^- \quad (E_0 = +0.779\ V)$ Equation 5-5

In the following equations silver ions in the anode-near area enrich themselves, whereby a secondary reaction can occur resulting in the formation of silver:

$Cu + 2\ Ag^+ \leftrightarrow Cu^{2+} + 2Ag$ (A) Equation 5-6

$Cu + Ag^+ \leftrightarrow Cu^+ + Ag$ (B) Equation 5-7

$Cu^+ + Ag^+ \leftrightarrow Cu^{2+} + Ag$ (C) Equation 5-8

The reactions (A and B) can occur both at the anode surface and in the dust-cupreous anode mud. In contrast, reaction C takes place in the area with a high Cu^{2+} concentration. The silver can change into the anode mud or deposit itself on the anode surface. According to /58/ and /59/ and 60/ a high silver level forces anode passivation.

The silver content in the anode, of course, is decisive. Silver can react with various selenides. If silver reacts with selenides before passivation, it does not dissolve. Anodes with a higher molar ratio of Ag/(Se+Te) react under the passivation potential.

$x\ Ag^+ + Cu_2Se \rightarrow (Cu_{2-x}Ag_x)Se + x\ Cu^+$ Equation 5-9

Lead forms heavy soluble lead sulphate which changes almost completely to the anode slime.

$Pb^{2+} + SO_4^{2-} \leftrightarrow PbSO_4$ Equation 5-10

If lead is present in the form of PbO in the anode, it sinks down with high reaction rate after the following equation /$Cu + Ag^+ \leftrightarrow Cu^+ + Ag$ (B) Equation 5-7/

$PbO + H_2SO_4 \leftrightarrow PbSO_4 + H_2O$ Equation 5-11

As a mixed crystal it can also react electrochemically according to the following reaction mechanism:

$Cu_xPb_{1-x} + H_2SO_4 \leftrightarrow (1-x)PbSO_4 + xCuSO_4 + 2H^+ + 2e^-$ Equation 5-12

The different behaviour of lead in comparison to antimony, arsenic, and bismuth, was determined by /8/ using Cu-Pb-As-synthetic-anodes. In the anode slime antimony was present in the form of $PbOSb_2O_5$ in addition to lead sulphate. These observation was confirmed by /61/ using x-ray phase analysis. /55/ observed passivation features with lead concentrations (> 0.15 %) in the anodes and a low As/(Sb+Bi) ratio (< 0.5). The behaviour of tin is described as follows by /62/. Tin separates as a bivalent ion however also preferentially as a tetravalent ion. As a possible reaction the following equation is possible as proposed by /63/:

$$Sn^{4+} + 3H_2O \quad \leftrightarrow \quad SnO_2 + H_2O + 4H^+ \qquad \text{Equation 5-13}$$

The significant grain fineness of the hydrolysis product is a characteristic. /64/ and /62/ reported the formation of tin acid (H_2SnO_3). For anodes with low oxygen amounts (0.02 %) and a tin content of 0.8-1 % an electrolyte turbidity was detected. Therefore, the electrolyte turbidity depends on the anodic oxygen content. Over 0.4 % Sn no turbidity was detected, which is explained by the presence of tin(IV) oxide in the anode. Simultaneously, the decrease of soluble copper(I) oxide was measured.

The highest level precious metal is silver and 99 % is present as a solid β phase in the copper. Furthermore, silver telluride and silver selenide can exist. However, gold is always present as a metallic phase in the anode.

5.3.2 Different anode compositions in comparison with minor elements

As previously detailed, the companies sent anodes of different qualities; these analyses do not correspond with the questionnaire data. Furthermore, they had different impurity levels as listed in Table 5-5.

	A	B	C	D	E	F	G/I	G/III	G/IV	H
Pb	131	1200	61	2300	1390	65	200	460	260	1522
Bi	55	100	37	100	138	216	100	100	50	123
As	625	900	1366	1100	1401	2698	550	940	330	1016
Sb	49	500	168	1300	1185	102	1100	220	100	178
Se	331	400	434	100	434	428	20	450	450	1352
Te		110	31		157	166	60	130	30	629
Sn			0.97	800	442		100	50	20	
Ni	133	3500	25	6200	1405	3100	4100	1040	100	2182
Ag	256	2000	389	800	1008	304	280	780	200	5047
Au	90	60	2.08		60					
O	1200	2000	1411	1700	1800	1700	1600	2100	2900	2924
Zn	35		33	100						
MFR	6.424	1.746	9.030	1.320	1.799	9.229	0.508	3.176	2.423	0.972

Table 5-5: Chemical composition of different anodes [ppm]

The anodes from D contained considerably more lead than those from C. This could result in an anode mud with a much higher lead content. This slime would be heavier and fall to the bottom rapidly.

Therefore, the probability of anode slime particles being incorporated in the cathode would be lower than for anode slimes with a low lead content.

A publication /43/ from Montanwerke Brixlegg, the Austrian secondary copper smelter, describes the special effects and phenomena that result from the chemical and structural differences of the mould and air side. The cathodes produced exhibit definite double-sided characteristics. The cathode side opposite to the mould side of an anode is much smoother and the cathode side opposite to the air side of an anode is much rougher with buds and dendrites, and from a chemical perspective has a higher nickel, lead, arsenic, antimony and sulphur content.

Furthermore, the cathodic deposits opposite the air side are lower in thickness and weight, especially in the first cathode crop. This difference amounted to up to 12 %. From the second crop onwards the difference becomes negligible. Obviously the "irregular" thickness zone at the air side of an anode is about one third of the total thickness and, therefore, has dissolved after the first cathode crop.

The chemical analysis shows the total oxygen content in the copper on the air side (not taking the outer casting skin into consideration), is up to 200 % higher than on the mould side. In addition, the surface area of oxidized phases can be six times higher and nickel is more often present as nickel oxide.

The nickel behaviour is very characteristic for the physical, chemical, and electrochemical differences of the two anode sides. At Ni contents below 0.25 to 0.30 % the nickel is nearly completely dissolved in the copper matrix and goes into the electrolyte during electrolysis. However, a higher Ni content in combination with oxygen, results in the formation of nickel oxide octahedrons in the anode, with significantly more at the air side (because of the higher nickel concentration). These octahedrons go into the anode slime during electrolysis. Separately analyzing the anode slimes from the air and mould side of the anode revealed that the anode slimes from the air side contained a higher level of nickel.

With a higher anodic oxygen content the mass differences of the cathodes were increased, even a constant nickel percentage. However, with a higher nickel content these mass differences rise further.

Nickel oxide aggregates can cause passive layers on the anode surface with the effect of a worse dissolution..

Many investigations have been performed to focus on the impurities in the anode and find the behaviour in the electrolysis system. A main point is to determine the level of influence due to the electrolysis system. Is the chemical anode composition a main factor or is it possible to evaluate some of the most important influences, including impurities, current density, and concentrations?
To investigate different influences it is necessary to evaluate experiments in electrolysis cell systems with exactly defined conditions. Thereby, the calculation and design of near technical cell systems was performed. Subsequently, the cell construction was done and the optimal control and adjustment systems were implemented. In the following chapter the cell arrangements employed are described.

5.4 Conclusion

To evaluate the anode quality and dissolution two different characteristics were assessed.

Physical quality

- Anode weight
  The anodes from the different companies varied in weight by ± 1 kg to ± 10 kg. These different anode weights resulted in an irregular anode thickness that directly influenced the electrode distance and furthermore effected the current density distribution.
- Anode roughness
  After measuring the anode roughness variations up to approximately 7 mm could be detected. By comparing these roughness values with the individual electrode distances (minimum of 18 mm between cathode and anode) the significant influence on the electrolysis system was evident.
- Anode form
  The variation in the thickness of an individual anode could be up to 6 mm. This also influenced the distance between the anode and cathode and furthermore the current density distribution.

The variation in the current density distribution that is caused by the above mentioned phenomena is discussed on page 87.

Chemical quality

The investigated elements could be divided into the following two groups:

- Oxygen content
  By measuring the oxygen content through the entire anode thickness the variation between the airside with a content of 0.234 % and mould side with a content of 0.192 % was analysed
- Impurities, including Pb, As, Ag, and Se
  The analysis revealed that between the airside and the mould side the measured impurities varied by up to 100 ppm.

6 CELL DESIGN FOR NEAR TECHNICAL SCALE INVESTIGATIONS

To handle the large number of investigations different cell systems have been employed. The electrolysis parameters were fixed so that an exact description of the electrolysis system was possible.

6.1 Beaker cells

A small electrolysis system was important because

- To have active cathode surfaces of 1 cm^2 (polarization measurements)
- To dope the electrolyte with solids
- To evaluate a detrimental influence of a special parameter in the near technical scale cells
- To have a system which is easy and fast to handle

Only one anode and one cathode were used which were isolated on the back by a macrolon plate. The electrolysis "cell" was a 5-l-beaker, maintained at constant temperature on a regulated heater plate. After charging with the solids (e.g. anode slime etc.) a magnetic stirrer provided continuous mixing. A Marriot bottle balanced out evaporation losses. A continuous measuring and control system was installed for recording the temperature and voltage. Polarization measurements were performed at defined time intervals. The experimental duration was 24 or 48 hours. Figure 6 -1 illustrates the cell set-up.

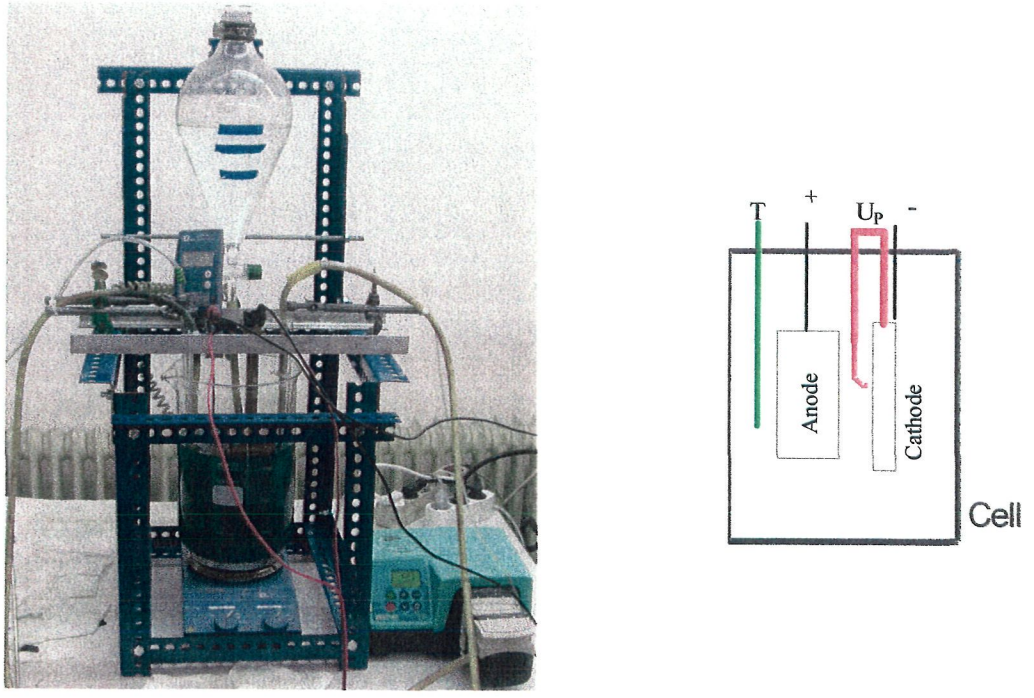

Figure 6 -1: Cell arrangement; left: photography; right: sketch

For the investigations standard electrolysis conditions were employed:

- Standard electrolyte
  Cu^{2+}-concentration = 45 g/l
  H_2SO_4-concentration = 175 g/l
  Ni-concentration = 10 g/l

- Experimental conditions
  Temperature = 65 °C
  Bath exchanges per hour = 3 BW/h
  Distance cathode-anode = 20 mm
  Cathodic current density = 350 A/m^2

- Inhibitor dosage
  Glue: 53 g/t Cu
  Thiorea: 55 g/t Cu
  Cl^-: 50 mg/l

Cathodic copper (CC) was used as the anodes, Table 6-1. This guaranteed the same chemical and physical anode surface at the start of each experiment.

Anode	Pb	Ag	As	Se	Sn	Bi	Sb	Te	Ni	Au	O
CC	1.4	9.3	1.3	0.4	1.2	0.9	0.5	0.1	2.9		6

Table 6-1: Anode composition in ppm

The cathodes were brushed, washed and degreased prior to each test. The isolating plate on the back was clamped under the isolating side ribs and the bottom edge was dipped into hot wax. After hanging-in of the anode and cathode into the electrolyte cell, the respective solid material was added and stirred for 24 hours. After this 24 hours preparation period, the electrolysis was started.

6.2 Laboratory cells

To carry out experimental investigations it was necessary to construct, build up, and start up suitable electrolysis cells. Figure 6-3 depicts the lab scale cells that were produced from macrolon with the following dimensions: length = 230 mm, width = 170 mm, height = 200 mm, and holding capacity = 6 l. Both cells had an inlet box at their right hand side with a bottom slit over the total width to ensure a uniform electrolyte flow into the cell, Figure 6-2. The inhibitor was also pumped into the inlet box. The cells each have three thermocouples: one at the electrolyte inlet, one in the middle of the cell, and one at the outlet. The temperatures are registered by measured data logging. Thirty litres of standard electrolyte were prepared and fed into the tank; within the cell there were 3.9 l. The glue had a soaking time of 24 hours and was then mixed with thiourea and distilled water, heated up to 70 °C, and cooked.

Subsequently, the mixture was filled into a measuring flask and added to the cells continuously within 24 hours with the already mentioned pump.

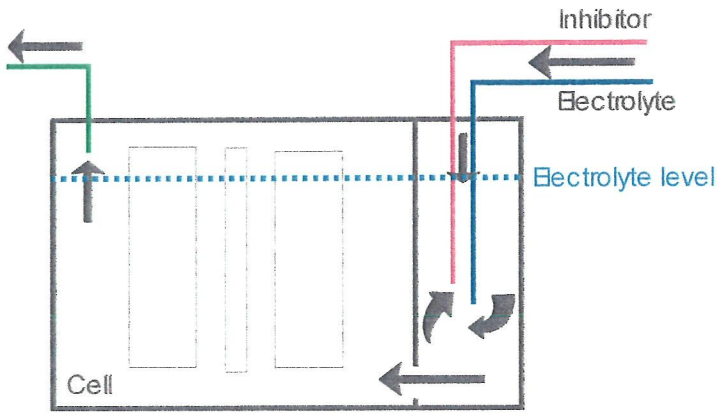

Figure 6-2: Supply of electrolyte and inhibitors to the cell

The electrolyte inlet channel ensures that the warmer and lighter fresh electrolyte from the tank flows directly from the surface to the outlet. It has to enter into the cell at the bottom and to mix there with the heavier and enriched electrolyte. Furthermore, the inhibitors and the fresh electrolyte already mix in the inlet channel before they enter into the cell. To compensate for evaporation losses and to keep the liquid level constant both tanks were equipped with Boyle-Marriott bottles and were covered with Macrolon plates.

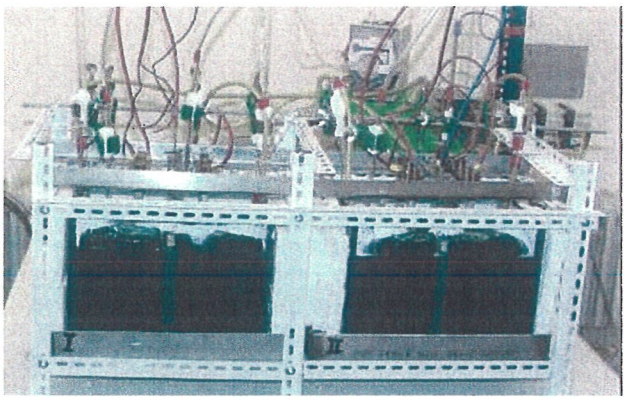

Figure 6-3: Cell Type A

Dasy-Lab 5.6 recorded the temperature, bath voltage, and polarization voltage with suitable measuring modules. In these cells, investigations were performed to determine the different precipitations. The various geometry parameters are described on page 87. The function of the measuring and control system was to guarantee an undisturbed and continuous operation within the limits of the preset parameters and at the same time to supply and store the experimental data for evaluation and interpretation. Furthermore, important data could be immediately sent to correct running faults or breakdowns. The points measured during the experiments were the temperature, bath voltage, and polarization voltage in each cell. Schematically this is illustrated in Figure 6-4.

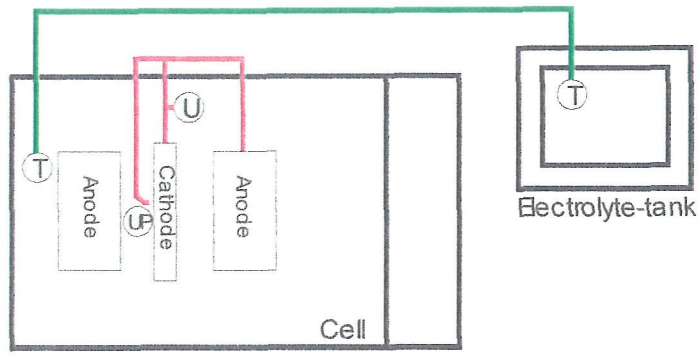

Figure 6-4: Diagram of the measuring points

The temperature in the tank was adjusted automatically so that a constant temperature in the whole process was guaranteed. The heating rod was turned on and down by the automation system. In both cells the cell voltage was measured between the left anode and cathode and also continuously recorded. For the polarization voltage measurement a Luggin capillary with a copper wire was positioned with its opening at a distance of less than 1 mm from the cathode surface.

The direct current was provided by a power supply (EA-PS 9018-100 Ampere) with a current stability of < 0.05 %, non linear < 20 mV. The electric circuit can be seen in Figure 6-5.

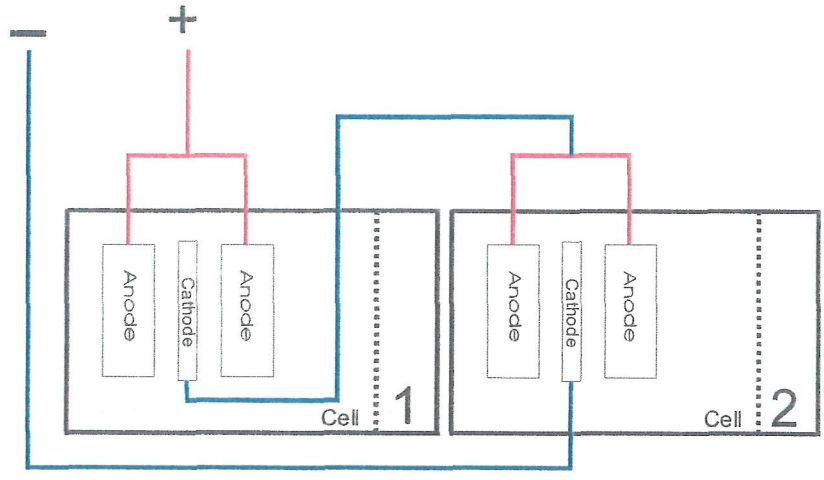

Figure 6-5: Electric circuit of the electrolysis cells

The electrical contacts were made by plugs or by screwjoints. Great importance was set on clean contacts to keep losses and resistance as low as possible. All current-carrying parts were made of copper to keep losses low.

In the following paragraphs the experimental conditions in these cells are described. The cathode plates were cut into pieces of 160 x 100 mm. To ensure uniform surfaces these cathode pieces were brushed with a stainless steel brush and then polished. This was necessary to guarantee, especially for repeated application, a surface free from copper rests or other impurities. Thereafter, the lateral edges were insulated with a cut open plastic pipe and the lower end with a wax layer, about 10 mm high. Then the cathode piece was fitted on the suspension and cleaned with distilled water and alcohol. For each

experimental series 30 l of standard electrolyte had to be prepared. This electrolyte was filled into the electrolyte reservoir tanks and doped with HCl. Copper and sulphuric acid concentrations were always controlled prior to the experiments by titration. Anodes and cathodes were hung into the cell following the geometrical guidelines. Finally all measuring and control units were assembled. After that the cells could be filled. The heating-up of the electrolyte in the tank (continuously, 10 to 15 °C/h) was started. Figure 6-6 illustrates the total arrangement.

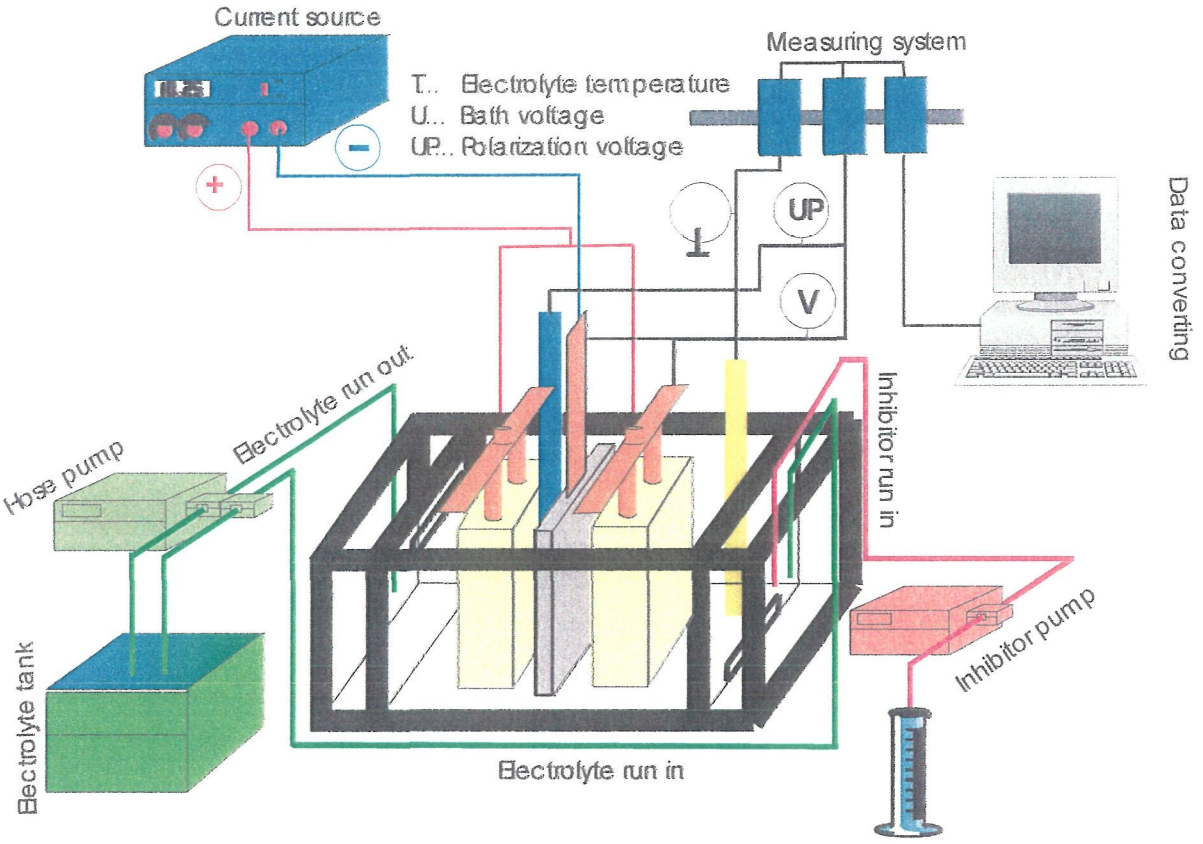

Figure 6-6: Total arrangement

One hour before the experimental start-up, addition of the inhibitor was started to guarantee an even distribution in the cell and at the anode and cathode surfaces.

6.3 Near technical scale cells

In order to carry out near industrial tests a semi-technical experimental plant was built. In this installation the height of the test electrodes corresponded to that of industrial ones. The width was chosen to be 10 cm for the anodes and 11 cm for the cathodes.

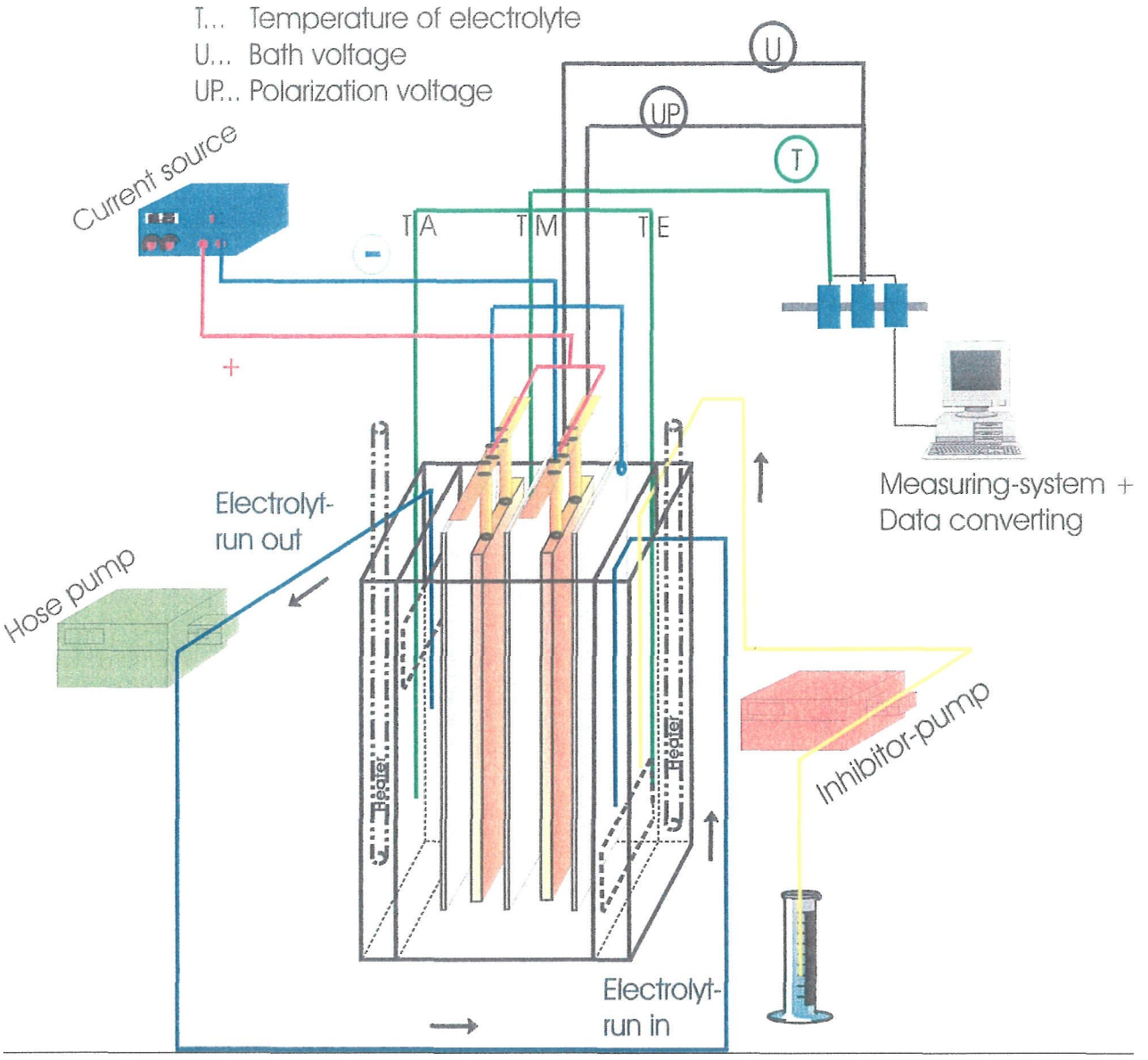

Figure 6-7: Cell arrangement

The cell was built from 1 cm thick Macrolon® and had the following dimensions: length 40 cm, width 16 cm, height 100 cm, all inside measures. The whole cell was stuck with glue. It can be seen in Figure 6-7 that the cell consisted of three parts: An inlet box (right), the electrolysis cell (middle), and an outlet box (left). The electrolyte stream entered the cell by an opening between inlet box and cell, 4 cm above the bottom and 2 cm wide over the total width. The same opening existed for the outlet 4 cm under the upper surface, so that the electrolyte had to flow through the cell diagonally.

Figure 6-8: Near technical scale cell

During the experiments, all cell walls are insulated against heat losses with styropor plates at their outer side. The heating rods are positioned in the inlet and outlet box. The dipping depth was 90 cm. The temperature control switched on/off automatically with the aid of a Dasy Lab programme. The electrolyte circulation was performed with two hose pumps with variable rotational speed rpm. With two hoses an electrolyte circulation of 0.3 to 3 bath exchanges per hour could be achieved. A good mixing of the electrolyte was provided by pumping the lighter electrolyte from the surface of the outlet box (where distilled water was also added) into the bottom of the inlet box. The opposite happened to the heavier electrolyte from the bottom part of the outlet box to the upper part of the inlet box. The inhibitor pump was a hose pump, too. The inflow into the cell came from a 1000 ml measuring cylinder. The control was performed volumetrically. Current supply: Power Supply EA-PS 8068-250A. The current supply to the cell was using copper busbars (□ 3 x 0.8 cm) and flexible cables with Ø 1.4 cm. Connections were made only with brass or copper screws. The contacting of the two anodes was performed in parallel with a copper busbar with three cores for exact symmetrical current supply. The three current streams from the cathodes were conducted over an equilateral copper triangle. A control resistor guaranteed the precise current symmetry. The two cells were connected in series. The PC had the operating system Windows NT and the programme DasyLab 5.6 for data control and memory. Temperature measuring was performed at three positions in each cell: In the lower part of the cell between anode and cathode and in the bottom zone of inlet and outlet box. These temperature measurements regulated the heating. There were four voltage measuring points per cell: Between the two anodes and the cathode in the middle and the polarization voltage on each side of the cathode. Both, temperature and voltage were measured each

second and then stored as a minute average on the fixed disc. The monitor always showed the moment data and the respective time dependent curve. To maintain a constant electrolyte level in the cell two separating funnels were installed with 2 l volume and the corresponding plugs.

The standard experimental parameters were:

- Temperature: 65°C ±1°C
- Current density: 350 A/m²
- Inhibitor: Glue: 53 g/t of copper
  Thiourea: 31 g/t of copper
  Cl^-: 50 mg/l
- Electrolyte: Cu: 45 g/l
- H_2SO_4: 175 g/l
- Duration: 6 days = 144 hours

The electrolyte analysis was performed at least once a day /65/. The copper concentration increased during the test time. However, whenever the cathodes were changed, a small loss of electrolyte occurred and, in addition the volume of the deposited copper was refilled with distilled water, so, the copper concentration over the total duration did not have to be adjusted. Sulphuric acid and chlorine concentrations decreased during the experiments. At each cathode change they were again standardized. It was imperative to maintain the electrolyte copper concentration between 44 and 52 g/l. Therefore, a liberator cell for a winning electrolysis was constructed, Figure 6-9. After each cathode crop the copper content was analysed. If the concentration was too high (more than 52 g/l) the electrolyte was decopperized in a winning cell. This winning copper electrolysis cell could be used in parallel with the refining cell. Four Prengaman anodes and three stainless steel cathodes were installed in the winning cell which enabled rapid decopperization of the electrolyte. This equipment worked effectively during the project.

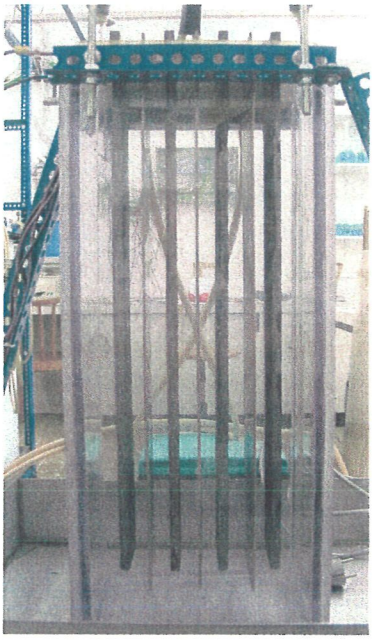

Figure 6-9: Winning cell

Figure 6-10: Total cell arrangement

In Figure 6-6 the total cell built-up is presented. It was possible to work with four independent simultaneously.

In this chapter the cells are described which were used in the following investigations. The four near technical scale cells with the combined winning cell, the two laboratory cells and the beaker systems could be operated at the same time or one after the other with different conditions. A control and/or a regulation were guaranteed during the whole working crop. That was the reason that the electrolysis cell could be established with all parameters that had to be fixed, and that constant electrolysis conditions could be guaranteed (concentration $H_2SO_4 \pm 2$ g/l, Cu ± 2 g/l).

7 EXPERIMENTAL INVESTIGATIONS

As previously described the target of this work was to evaluate the different influences on copper refining electrolysis. Therefore, the following experimental studies were performed:

- Investigations with different geometrical conditions
- Electrolysis with different current densities
- Electrolysis with anodes from various companies
- Influence of solids' distribution in the electrolyte to the cathodic copper precipitation

7.1 Current density

The thickness of the precipitated copper is often not equal over the cathode and depends on the current density distribution. The current density is defined as current per surface. At a small range, which has the form of a cube of the edge length a, then the current divided by the cross-section area of the cube a^2 is defined as the current density. In Equation 7-1 the current density j is represented as mathematical formula, whereby i_w describes the amperage by the cube /66/.

$$j = \frac{i_W}{a^2} \qquad [A/m^2]$$

Equation 7-1

The current density distribution can be differentiated on the one hand into a macroscopic and on the other hand into a microscopic one. The macroscopic distribution represents a relatively slow change of the local current density over the electrode; it shows larger areas of the electrode, e.g. thicker separation in the area of the edge of electrode. The microscopic current density distribution results show that the change of the local current density extends only over small areas. This results in the formation of buds and dendrites or an increase in the surface roughness.

With an uneven surface the points for charge transportation are more accessible to the solution than the recesses, which disturb the uniformity of the current density distribution and cause an increase of the current density at the protruding parts. Figure 7-1 shows schematically the uneven surface of a cathode and preferential mass transport at the managing points (active places) /40/. δ_N describes the final copper deposition layer thickness.

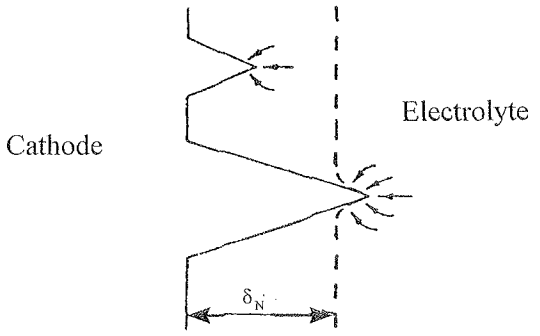

Figure 7-1: Current density distribution

Inhibitors predominantly adsorb in the most active places of the electrode surface whereby these managing points of the surface are blocked and the unloaded ions are forced to separate due to the formation of numerous new nuclei on the crystal faces. An inhibitor (surface-active material) is a material that lowers the speed of an electrochemical reaction due to its adsorption at an electrode surface, without participating in the final result directly in the reaction. Thus inhibitors cause a regular and even growing of the copper layer on the cathode.

The conductivity of the electrolyte, namely the transport of the electrical charges by the electrical field in the solution, has a large influence on the current density distribution in an electrolysis cell. The conductivity depends, irrespective of the electrolyte type and temperature, on the electrolyte concentration. Equation 7-2 describes the specific electrical conductivity of the electrolyte, and from this equation it is possible to recognize how important the electrode distance is.

$$\kappa = \frac{1}{\rho} = \frac{L}{R \cdot A}$$

Equation 7-2

κ is the specific electrical conductivity in 1/Ωm, ρ the specific electrical resistance in Ωm, R the electrical resistance of the electrolyte in Ω, L the electrode distance in m and A the effective electrode surface in m^2. The electrolyte conductivity depends essentially on the $CuSO_4$, H_2SO_4, $NiSO_4$, $ZnSO_4$ and $FeSO_4$ concentration and their electrolytic dissociation. The arsenic and antimony content have only a small influence on the electrical conductivity.

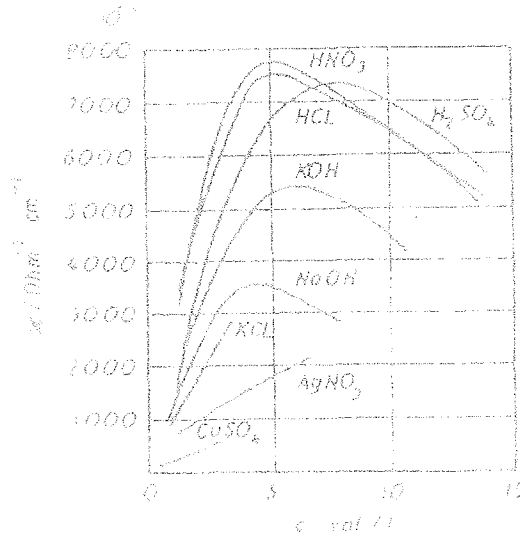

Figure 7-2: Electrical conductivity

In Figure 7-2 the electrical conductivity is presented in relation to the concentration (in val/l) of different electrolytic solutions.

Thereby the influence of the main components on the specific electrical resistance becomes particularly clearly. The dependence of the specific electrical resistance on the electrolyte temperature shows that the resistance in the temperature range between 50 °C and 60 °C changes around 0.7 % per degree Celsius /67/.

The causes which lead to concentration differences between the fluid nearby the electrode and the electrolyte inside are the electrochemical processes in the phase boundary layer electrolyte and electrode. Since the cathodic metal deposition leads to a depletion of the metal ion concentration, the specific density of the cathode near the electrolyte layer is reduced. Due to this fact the specifically lighter volume elements that develop in such a manner ascend in cathode proximity. However, at the anode the metal ions enrich themselves during the anodic dissolution of the raw metal within the near anode fluid range. The specific density in the phase boundary layer differs dramatically from the specific density in the electrolyte, which results in convection. Due to the developing concentration differences in electrolytes the specific electrical resistance of the electrolyte changes locally, whereby the current density at the electrodes is affected /68/.

A crucial factor was the distance between the electrodes. Distance changes of only a few millimetres, caused by inaccurate hanging up of the electrodes into the electrolysis bath or by surface defects in the electrodes (e.g. blisters or crater), can result in large shifts of the current density distribution in the tankhouse.

7.2 *Investigations with different current densities and three different anode qualities*

Many investigations have been performed to investigate the effects of current densities and anode qualities. The influence of current density on the electrolysis is already well established. However, the evaluation of this influence compared with all other parameters cannot be found in literature. It is the question whether the current density is the limiting factor or the anode composition or other significantly influencing parameters.
To provide answers to these interesting questions investigations under electrolysis conditions like in practice have been performed. The varying parameters are in the range of the variations in industrial practice..

Three different anodes were selected for the first investigation series. The guideline for the anode selection were their MFR I (As/Sb+Bi) and MFR II (Ag/Te+Se) and using these rates, the following anodes were selected:

F:	Highest MFR I (9.23) and second lowest MFR II (0.42)
G:	Lowest MFR II (0.312)
B:	Second highest MFR II

For all the anodes the MFR I was between 0.51 and 9.23 (Table 7-1). The anodes from E, H, B and G all had a MFR under 2. During the electrolysis no problems with antimony and the creation of floating slimes were encountered. All the other anodes, detailed in Table 7-1, had a MFR I higher than 2.

A high ratio of the MFR I in the anode is an advantage in the refining plant because a higher level of As means a reduced level of Sb^{5+} will be formed from Sb^{3+}. An increased level of Sb^{5+} is deleterious to the cell because it forms floating slimes. All MFR I <1 are problematic because there is too little As and the presence of Sb^{5+} is very probable.

An increased content of As, Sb, and Bi in the cathodes can be produced by increased Sb and Bi concentrations in the electrolyte. An increased Sb^{+5} concentration in the electrolyte resulted in an increase in the As, Sb, and Bi concentrations in the anode slime and floating slimes. A Sb-Bi-As precipitation layer can form on the cell walls and in the pipes if certain Sb saturation concentrations are exceeded. The precipitates on the cell walls and in the pipes may act as crystallization nuclei and influence the value of the Sb equilibrium concentration in the electrolyte.
The As^{+3} concentration in the electrolyte can be increased by increasing the As content in the anodes and minimizing the oxygen level in the electrolyte by nitrogen purging.

	A/I	A/II	A/III	A/IV	A/V	B	E	F	G/I	G/III	G/IV	H
Pb	131	139	135	120	139	1200	1390	65	200	460	260	1522
Bi	55	58	54	51	54	100	138	216	100	100	50	123
As	625	653	594	623	594	900	1401	2698	550	940	330	1016
Sb	49	64	55	49	58	500	1185	102	1100	220	100	178
Se	331	346	311	328	311	400	434	428	20	450	450	1352
Te						110	157	166	60	130	30	629
Sn							442		100	50	20	
Ni	133	135	139	132	139	3500	1405	3100	4100	1040	100	2182
Ag	256	268	241	254	243	2000	1008	304	280	780	200	5047
Au	90.3	92	88.8	89.8	88.9	60	60					
O	1200	1200	1200	1200	1200	2000	1800	1700	1600	2100	2900	2924
Zn	35	42	47	36	51							
MFR I	6.42	5.67	5.74	6.53	5.53	1.75	1.80	9.23	0.51	2.42	3.18	0.97
MFR II	0.57	0.57	0.57	0.57		3.13	1.39	0.42	3.59	1.08	0.312	2.12

Table 7-1: Chemical composition of the anodes in ppm

If Se and Te are in excess in the anode there will normally be insufficient Ag present in the anode to combine with the Se and Te. This subsequently results in the formation of Cu_2Se and Cu_2Te. Alternatively, the Ag will migrate directly to the cathode if there is too little Se and Te in the anode. Se and Te form precipitation complexes in the anode slime. The anode slime, with all it components, is then whirled up by convection and adheres to the cathode where it presents problems.

These electrolysis experiments were performed at two different current densities (350 and 500 A/m^2); with two anode cycles (six cathode crops) and with three different anode qualities (anodes from B, F and, G).
The decision was made to start with the high current density of 500 A/m^2, and to evaluate the lower current density in the following test series. The lifetime of the three cathode cycles was always calculated such, that the anode scrap at the end of the anode cycle was < 20 % of the original weight. The inhibitor concentrations, Table 7-2, were used in the electrolyte. Conditions and parameters were chosen as in the industrial tankhouses.

	B	F	G
Glue	75	120	100
Thiourea	78	70	60

Table 7-2: Inhibitor concentration (g/t_{Cu})

The electrolyte was doped with arsenic, nickel and chlorine, Ni = 10 – 15 g/l, As = 5 – 10 g/l, c_{Cl} = 50 mg/l. The temperature was fixed at 65 °C and three bath exchanges were used in the cells.

The anodes were weighed before and after the electrolysis to determine the remnant anode weight. The remnant of the anodes from G was higher than 20 %. In all three cells the electrolyte level had the same height. Furthermore, the distance between cell bottom and the lower edge of the anode was fixed. Therefore, the ratio of the anode length that was not in the electrolyte and not active, was different between anodes and the percentage of anode rest cannot be compared (anodes from G were the highest). The surface and form of the remaining anode from all the investigations appeared very similar, with no holes present and an even surface remaining. After the cathode periods the cathode planks were removed from the cell, washed and stripped. The copper cathode was then weighed /69/.

		Cu [%]	Ni [%]	As [%]	Sb [ppm]	Bi [ppm]
500 A/m²	G/IV	4.63	0.82	0.41	175	< 10
	F	4.87	1.23	0.71	330	97
	B	4.86	1.08	0.40	855	< 10
350 A/m²	G/IV	4.98	0.75	0.27	115	60
	F	4.80	1.52	0.95	380	102
	B	4.60	1.12	0.20	340	70

Table 7-3: Electrolyte composition

Current density [A/m²]	Company	Mass [g]
500	G/IV	166
500	F	234
500	B	360
350	G/IV	164
350	F	209
350	B	301

Table 7-4: Anode slime amount

The analysis revealed that the electrolyte composition was quite similar to industrial electrolytes. In these experiments the cathode yield was also in the range of industrial practice. After pumping the anode slime out of the cell, sedimentation investigations were performed on it.

The variation in the weight of anode slime from different investigations is presented in Table 7-4. When the mass produced using the same company anode, run either 350 A/m² or 500 A/m² was compared, only a very small difference in weight was detected between the different current densities. However, between the different company anodes a variation in the anode slime weight production was detected, with the G anode producing less slime than the F and B anodes. During these investigations the composition of the anode slime was also analysed.

	G/IV	F	B
Ag	4.5	5.2	21.8
As	1.9	4.2	1.9
Bi	0.06	1.20	0.70
Cu	31.7	32.5	12.4
Ni	0.91	2.98	1.71
Pb	3.3	1.9	10.2
Sb	0.22	0.66	3.60
Se	11.7	7.6	3.6
Sn	0.34	1.40	1.30
Te	0.63	2.80	1.60
H_2O	0.11	0.08	0.18

Table 7-5: Anode slime composition (weight %)

Table 7-5 details the analysis of the final anode slime after the three cathode crops. The anode slime composition is similar to anode slime analyses of the companies.

From the investigations at 500 A/m² cathodes were produced with no dendrites or buds. Individual sparse fine grains where detected at the cathode surface. From the investigations at 350 A/m² the cathodes produced from anodes of the above mentioned companies were very smooth with no dendrites or buds. During these investigations no short circuiting occurred.

The main results of these investigations indicated that the influence of the cathodic precipitation is not dependent on

- Using current densities of 350 A/m² or 500 A/m²
- Using anodes with different chemical compositions

The conclusion of these investigations is that the influence of the different anode quality and the variation of the current density cause no problems if the electrolysis is run under exact controlled conditions, including the inhibitor transfer, equal anode-cathode distance, constant ion concentrations, and temperature. Due to the anode and cathode change, to the mechanical influences, and the anode slime disturbance it is not possible to control all these parameters in the tankhouse as good as in a laboratory cell.

7.3 Influence of different geometrical conditions

In the following investigations the current density distribution was investigated in relation to the variation in distance between the anode and cathode. Furthermore, anodes with different chemical composition were used. In order to perform these investigations two different types of cells were built.

In practice there are many reasons why variations in the distance between the anode and cathode pair can occur. A particular factor influencing the geometry (dimension) of the anodes and their arrangement is the

casting weight tolerance, which may vary between 4 and 15 kg. An alteration in the casting weight tolerance can result in up to a 4 mm variation in the thickness of any one anode. Furthermore, bubbles, so called casting edges, bent anodes, bent or canted cathodes and the different hanging of cathodes and anodes in the cell can cause a variation in the distance between the anode and cathode with the consequence of different current distributions at the electrodes, which was very important for the formation of irregular crystal growth.

In principle it is the distance between the anode and cathode that is the important value. However, because in these investigations it was not possible to change the anode geometry, the cathodic stainless steel plate was mechanically deformed. To produce different cathode geometries the cathodes had to be bent and canted. After the slope was measured in the horizontal and vertical directions the cathodes were hung into the cell.

The various parameters were different geometries between the anode and cathode and different anode qualities. Using these conditions the current distribution on the cathode was calculated. The anode dimensions for the laboratory cell are detailed in Figure 7-3 whilst the cathode dimensions are illustrated in Figure 7-4.

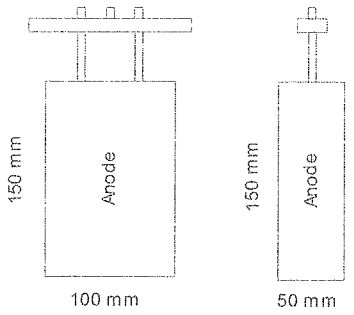

Figure 7-3: Anode size

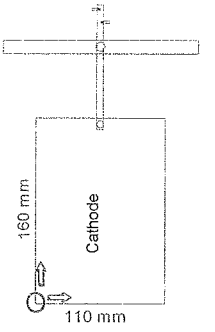

Figure 7-4: Cathode size

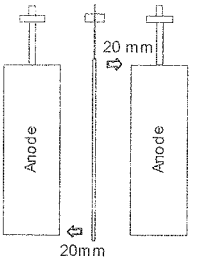

Figure 7-5: Anode-Cathode geometry PS

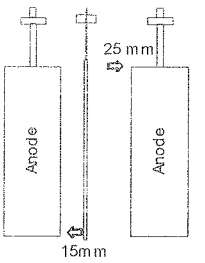

Figure 7-6: Anode-Cathode geometry PD

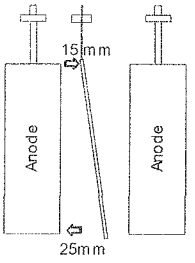

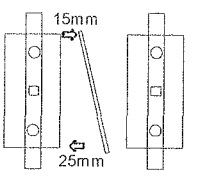

Figure 7-7: Anode-Cathode geometry CT

Figure 7-8: Anode-Cathode geometry CL

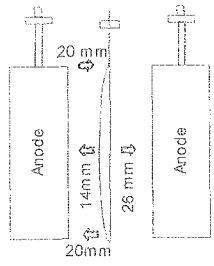

Figure 7-9: Anode-Cathode geometry BT

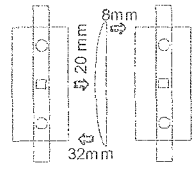

Figure 7-10: Anode-Cathode geometry BL

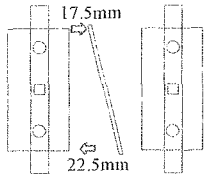

Figure 7-11: Anode-Cathode geometry CLD

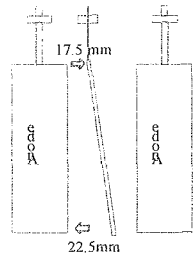

Figure 7-12: Anode-Cathode geometry CTD

PS: Parallel and same distance, Figure 7-5
PD: Parallel and different distance, Figure 7-6
CT: Canted top to bottom, Figure 7-7
CL: Canted left to right, Figure 7-8
BT: Bent top to bottom, Figure 7-9
BL: Bent left to right, Figure 7-10
CLD: Canted left to right different distance, Figure 7-11
CTD: Canted top to bottom different distance, Figure 7-12

In Table 7-6 the experimental parameters are listed. It is shown that different anode qualities and different geometrical conditions are used. Also the cathode crop varies. The first tests have been done in the laboratory cells. It was necessary to get an evaluation of the influence to the cathode current density distribution. Afterwards the investigations have been done in the near technical scale cell under different conditions.

Anode quality	Laboratory Cell	crops	Near technical scale cell	crops
E	PS/PD/CT/CL/BT/BL	1	PS/PD/CT/CL/BT/BL	1
G/I	PS/CT	1		
CC	PS/PD/CT/CL/BT/BL	1		
C			CT/CL	3
D			CT/CL	3

Table 7-6: Overview of the investigated anodes

With the anodes from E the investigations in both types of cells were performed. To get informations on the influence of the chemical quality of the anodes CC anodes have been taken too. These are anodes made of cathode copper. So they are very pure. Also anodes of D and C should show a dramatic different chemical composition and their influence.

Quality	Pb	Ag	As	Se	Sn	Bi	Sb	Te	Ni	Au	O	MFR I	MFR II
E	1390	1008	1401	434	442	138	1185	157	1405	60	1800	1.799	13.79
G/I	200	280	550	20	100	100	1100	60	4100		1600	0.772	3.59
CC	1.4	9.3	1.3	0.4	1.2	0.9	0.5	0.1	2.9		6	2.062	14.74
C	61	389	1366	434	0.97	37	168	31	25	2.08	1410	11.71	0.63
D	2300	800	1100	100	800	100	1300	-	6200	-	1700	1.316	5.86

Table 7-7: Chemical quality of the used anodes

In Table 7-7 the different chemical compositions of the anodes are shown. Therefore the resulting anode slime must have different compositions with various properties, like the weight, the amount and so on.

7.4 Results of the laboratory cells

At the end of the six days test time the electric current was shut off, the inhibitor supply was stopped. The cathodes were taken out of the cell, washed with distilled water, dried, and stripped. The copper deposited was weighed and the current yield could be calculated. As a next step 18 pieces of 10 x 10 mm were cut out from each cathode surface for determination of the current density distribution over the cathode surface. The cutting was done with a high pressure water jet/65/.

After the experimental work had been conducted the current density was calculated and the influence of the geometrical conditions on the current efficiency was determined. In these investigations three different anode qualities, E, G/I, and CC were used.
In Figure 7-13 the average of the calculated current density distributions for all the experiments is shown /70/.

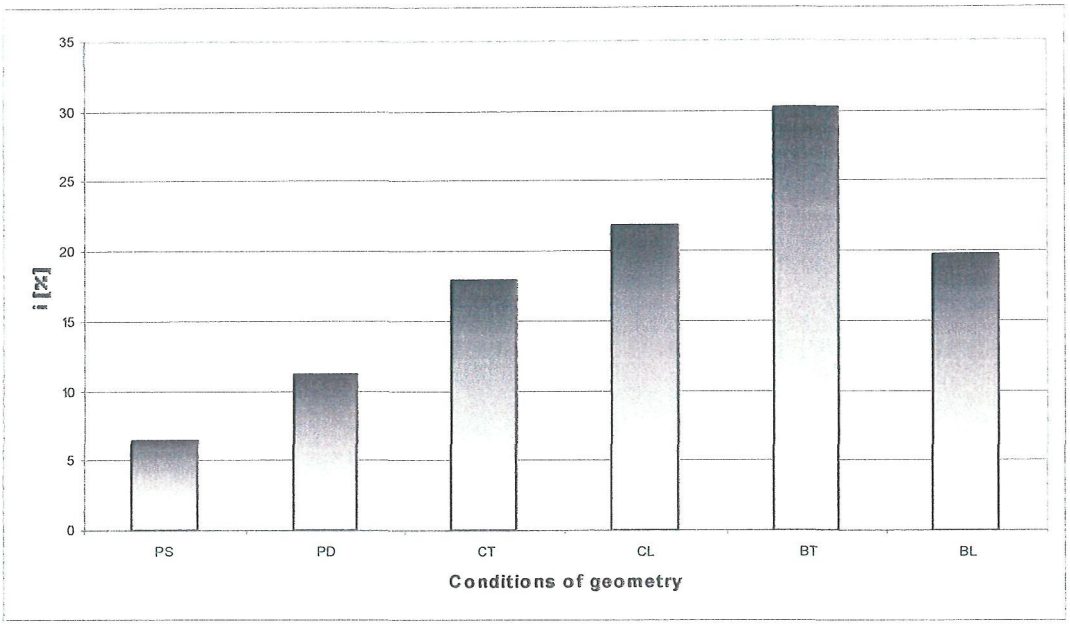

Figure 7-13: Current density distribution comparison

By changing the distance between the anode and cathode but not varying the parallelism of the electrodes the deviation in the current density was about 12 % of the standardized value. The basis for the standardization was 350 A/m².

Bent cathodes show the highest influence on current density. Here the current density distribution varied between 19 and 31 % of the standardized value.

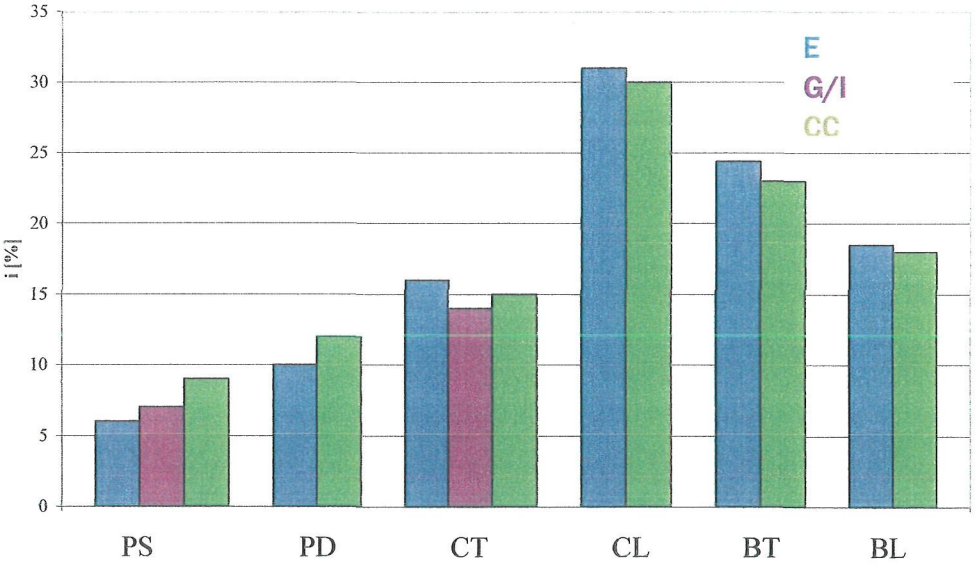

Figure 7-14: Current density variation due to anode quality and geometrical distance

The results of these experiments showed that the influence of the chemical anode quality on the cathodic precipitation and current efficiency was quite low even, if different electrode geometrical conditions were present in the electrolytic system. To produce smooth cathodes without dendrites it was necessary to have a regular current density distribution over the whole cathode. To reach this target, it was important to guarantee good geometrical conditions between the anode and cathode.

7.5 Investigations in the near technical cell

To produce technically comparable results it was necessary to make these investigations in a near technical scale cell. The various parameters were the geometry under the conditions described before. After the experimental work was conducted the current density was calculated using the weight of 24 samples cut out from each cathode.

Piece Nr.	Height [mm]	Weight [g]	Length [mm]	Width [mm]	A [mm²]	i [A/m²]	Stand. i [%]
1	820	5374	10.26	10.07	103.32	307	102
2	765	5883	10.20	10.05	102.51	339	113
3	615	5083	10.01	10.13	101.40	296	99
4	515	4915	10.16	10.06	102.21	284	95
5	415	4714	10.09	10.04	101.30	275	91
6	255	4550	10.12	10.06	101.81	264	88
7	85	4268	10.09	10.04	101.30	249	83
8	15	3043	10.05	10.00	100.50	179	60
9	820	5995	10.18	10.12	103.02	343	114
10	765	7257	10.27	10.12	103.93	412	137
11	615	6154	10.25	10.15	104.04	349	116
12	515	5750	10.19	10.16	103.53	328	109
13	415	5463	10.15	10.12	102.72	314	105
14	255	5320	10.15	10.11	102.62	306	102
15	85	5240	10.15	10.12	102.72	301	100
16	15	3707	10.09	10.08	101.71	215	72
17	820	5632	10.12	10.07	101.91	326	109
18	765	6294	10.15	10.04	101.91	365	121
19	615	5737	10.17	10.09	102.62	330	110
20	515	5533	10.16	10.09	102.51	319	106
21	415	5349	10.11	10.08	101.91	310	103
22	255	5228	10.14	10.09	102.31	302	100
23	85	5092	10.10	10.11	102.11	294	98
24	15	3452	10.06	10.03	100.90	202	67

Table 7-8: Current density calculation of experiment 3, AS cathode

These experiments were all performed at a current density of 350 A/m². At the end of the six days electrolysis the electric current was switched off and the inhibitor supply was stopped. The cathodes were taken out of the cell, washed with distilled water, dried, and stripped. During the investigations the

current was measured at periodic time points. It was necessary to control an equal current input to all anodes. It was very important to be able to guarantee ideal conditions because of the influence on the cathodic precipitation. The cathodic polarization was also measured.

The method used to calculate the current density distributions will be demonstrated using the CT example. After electrolysis 24 pieces of 10 x 10 mm were cut out from each cathode to determine the current density distribution over the cathode surface. The cutting was performed using a high pressure water jet at eight different heights, 15 mm, 85 mm, 255 mm, 415 mm, 515 mm , 615 mm, 765 mm, 820 mm from the cathode bottom and at three different widths, 23 mm, 53 mm and 93 mm measured from the left bottom corner of the cathode.

In Figure 7-15, the cathodic precipitations of the third investigation with canted cathodes from the top to the bottom are illustrated. The left cathode (AS) exhibited some small buds at the top and a smooth copper precipitation towards the bottom. Near to the bottom on the right cathode (MS) the precipitation was rough, with many dendrites. At this part of the cathode the current density must be higher, because the distance between the anode and cathode is smaller, the electrolytic resistance is smaller and therefore the local current density is higher. When examining the current density height distribution it was evident that at the top (about 10 mm under the electrolyte level) the current density distribution was nearly 100 %. At the subsequent measurement points the current density increased up to ~140 %. At the bottom of the cathode the current density decreased to ~ 60 %. Finally, a current density variation at this single cathode was up to 80 %. This indicates that at a standard current density of 350 A/m² a variation of 280 A/m² was detected. This large difference in current density forces dendritic growth as exhibited on the right hand cathode (MS).

The width current density distribution shows two effects. First, the current density decreases from electrolyte level to the bottom of the cathode. Secondly, the current density in the middle of the cathode is highest and near to the edges it is lower. Using the cathodes with an active width of 125 mm, the current density varied about 20 %, or at 350 A/m² it varied by 70 A/m². This effect will be seen at all width current density distributions independent of the geometrical conditions employed. In experiment 1 an anode and cathode with the same and parallel distance were used. The current density distribution of one of the produced cathodes is detailed in Figure 7-15. The decrease in the current density from top to bottom was about 128 A/m². The average current density varied between the left and right cathode by about 10 A/m². The cathode has parallel and different distances. The current density distribution at the right cathode (distance anode – cathode 15 mm) is similar but with higher variations of current density than at the cathode, at the left side (distance anode – cathode 25 mm). The difference between the current density average of the right and left side is about 50 A/m². This more irregular current density distribution also influences the current efficiency and in this experiment it was 86 %. Some small nodular precipitations were detected on these cathodes.

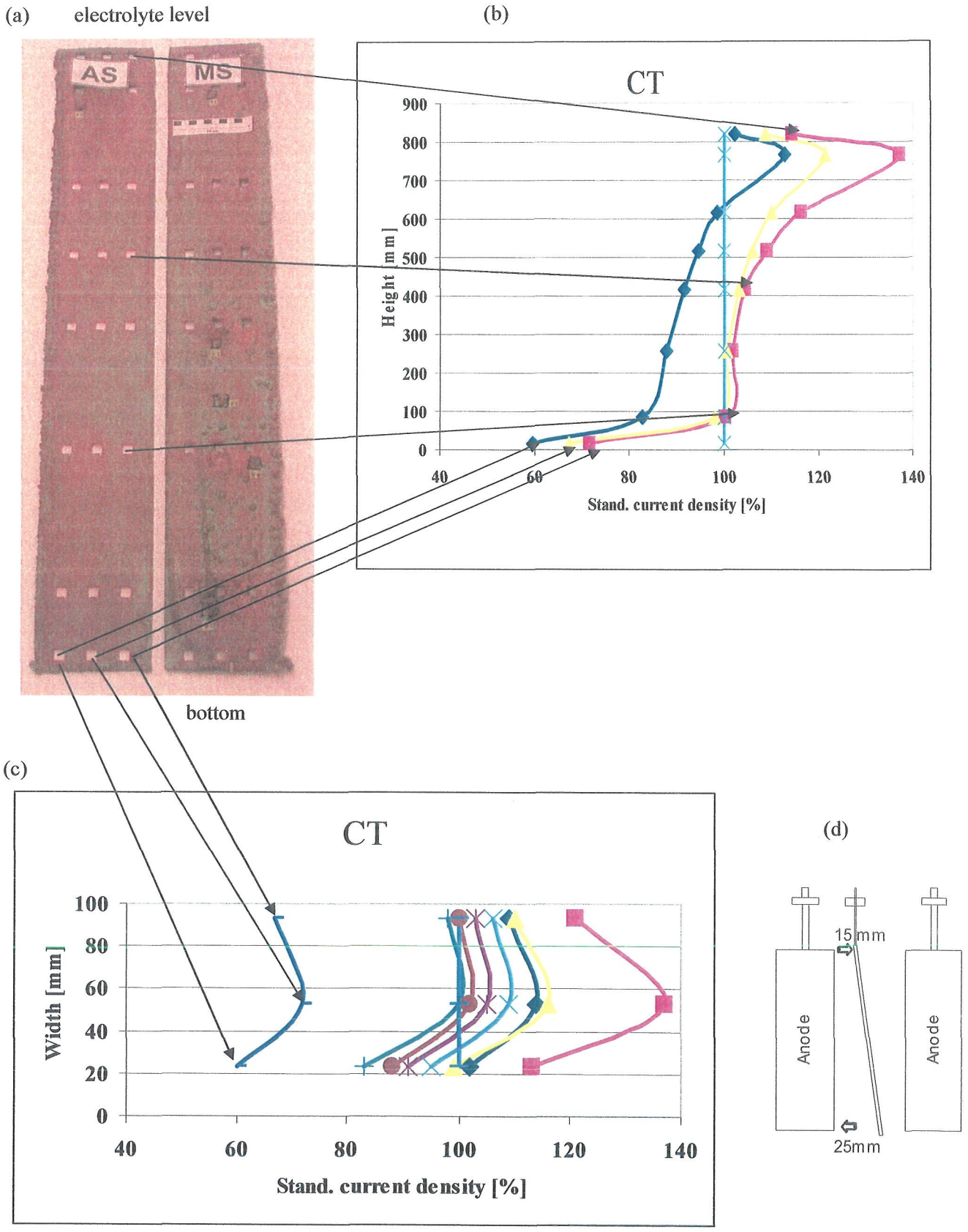

Figure 7-15: Cathode (a), current density height distribution (b), current density width distribution (c), geometry (d)

The value of the current density distribution of canted cathodes was between 60 and 140 %. The absolute current density difference was about 230 A/m². In both figures the variation of current density distribution over the complete cathode (height and width) is illustrated. This high current density variation forced dendrite growth over the entire cathode surface and some of the dendrites presented were very long.

In the BT experiments a current density distribution of about 130 % was detected. In the first days of electrolysis some small dendrites started to grow on the whole cathode area. After the second day, the dendrites became bigger and caused shorts. After removing the dendrites the electrolysis was continued but new dendrites started to grow.

All experiments using parallel electrode spacing revealed that the current density distribution across the cathode width was symmetrical. On both edges of the cathode the current density was lower than in the middle. The explanation for this is that the cathode width was 125 mm but the anode width was just 100 mm. Near the edges the cathodic current density is lower due to the larger cathodic area. The so called boundary effect can also be seen in the technical cells, however the ratio of the edge area to the whole electrode area is much smaller in the technical cells. Examining the cathodic precipitation revealed that the boundary effect causes smoother area near the edges and rougher precipitation in the middle of the cathode, due to the higher current densities in the middle.

In Table 7-9 the current density variation of these experiments are presented. The greatest difference between the minimum and maximum value of the current density was 395 A/m², the smallest difference was 113 A/m².

	1		2		3		4		5		6	
i	PS		PD		CT		CL		BT		BL	
[A/m²]	AS	MS	AS	MS	AS	MS	AS	MS	AS	MS	AS	MS
i_{max}	302	330	332	270	412	388	432	260	480	467	402	274
i_{min}	174	170	196	157	179	156	170	145	144	72	90	122
Δi	128	160	136	113	233	232	262	115	336	395	312	152
Δi [%]	37	46	39	32	67	66	75	33	96	113	89	43

Table 7-9: Current density distribution

After the electrolysis period of one anode crop and three cathode crops the remaining anode was removed.

To substantiate these resulted with one chemical anode quality some of the experiments had to be repeated at following conditions: The anode qualities were anodes from D and C. So, primary and secondary smelter anodes were used. These anodes had a total different chemical composition. They will have different dissolution characteristics as well they will have different amounts of anode slimes. In both anodes the MFR I was totally different. The anodes from C had a MFR I ratio < 2, which could cause problems in the electrolyses. The anode from D had a MFR I ratio higher than 10.

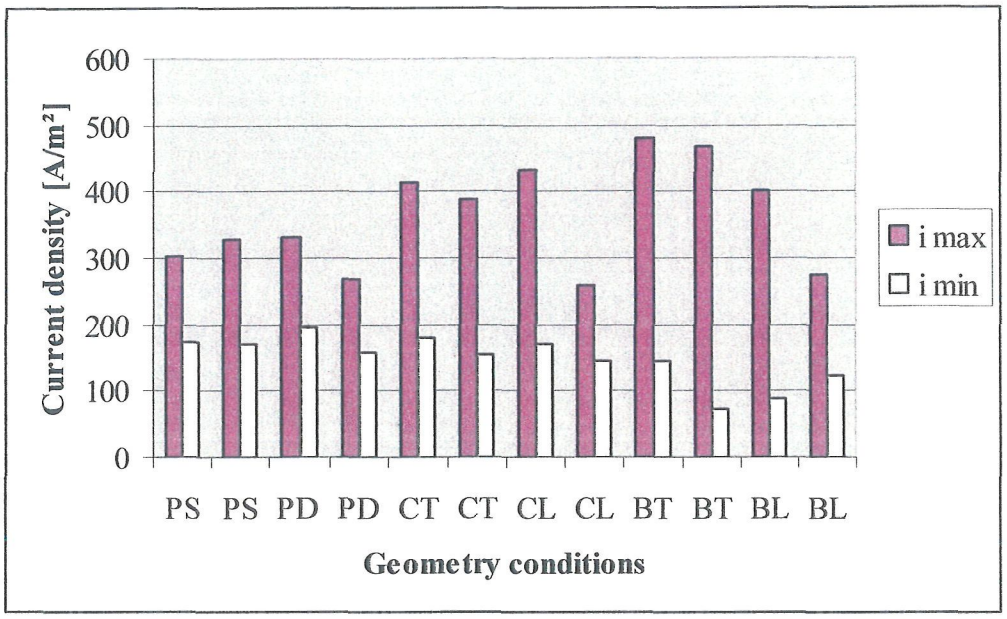

Figure 7-17: Current density variation at different geometrical conditions with anodes from E

The final investigations described in Table 7-10 were made with two significant different geometrical conditions. For each anode the duration was a crop with 18 days.

Experiment	Geometry	Number of crops
1	CT/ D	3
2	CT/ C	3
3	CL/ D	3
4	CL/ C	3

Table 7-10: Investigations parameter

The lowest current density at the electrolysis with canted cathodes left to right was about 145 A/m² and the highest was 381 A/m². This indicated a difference range of 236 A/m², which was a ~ 70 % variation in the standard current density.
At the investigations with canted cathodes top to bottom the lowest current density was 136 A/m² and the highest 402 A/m². This meant and difference range of 266 A/m², which was a ~ 75 % variation.
(At investigations with E anodes the results were: lowest current density: 170 A/m², highest: 412 A/m², difference 242 A/m², ~ 70 % variation).
The complete results of the current density of all investigations are presented in Figure 7-18.

The cathodic precipitations of the investigations, with canted cathodes from the top to the bottom and canted from left to right, were the same.
The current density distributions of canted cathodes from the top to the bottom showed two effects. Firstly, the current density decreased from electrolyte level to the bottom of the cathode. Secondly, the current density in the middle of the cathode was highest and near to the edges it was lower.

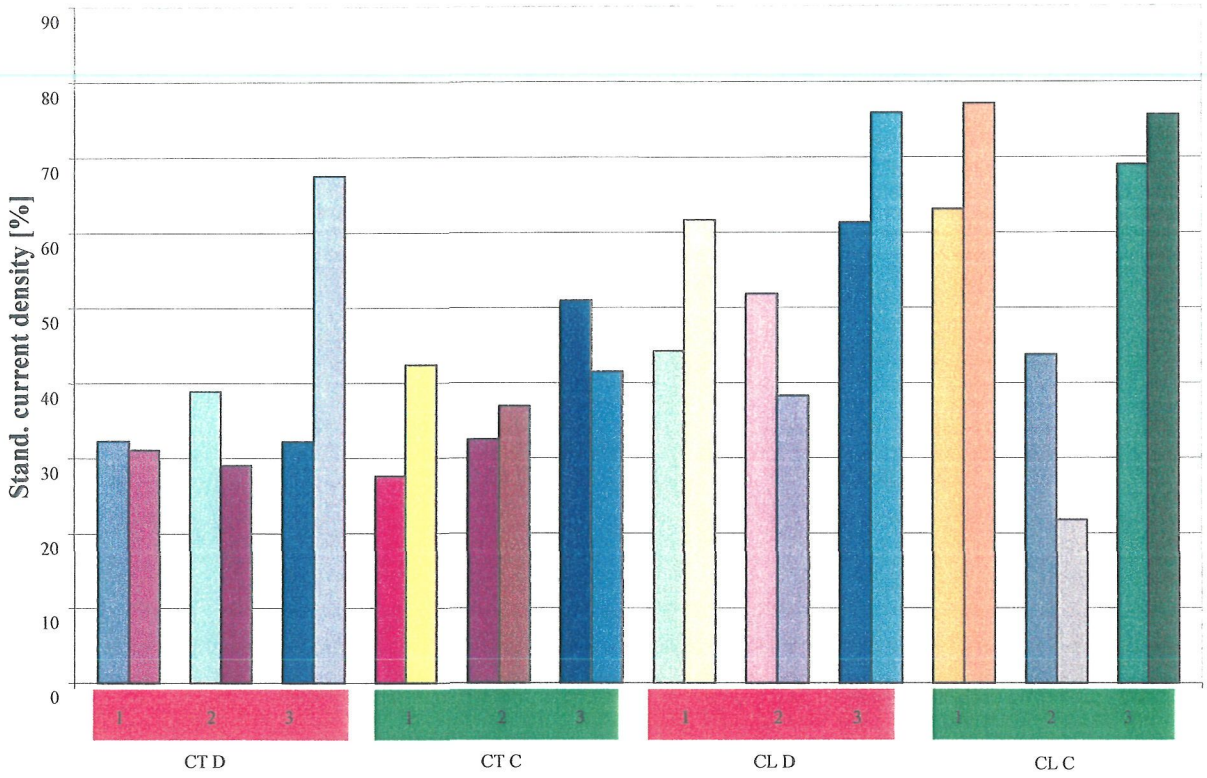

Figure 7-18: Standardized current density distribution for single cathodes

A similar nodular precipitation was detected on the cathodes produced from anodes of C as well as from anodes from D.
Boundary effects caused smoother area near the edges and rougher precipitation in the middle of the cathode, due to the higher current densities in the middle.

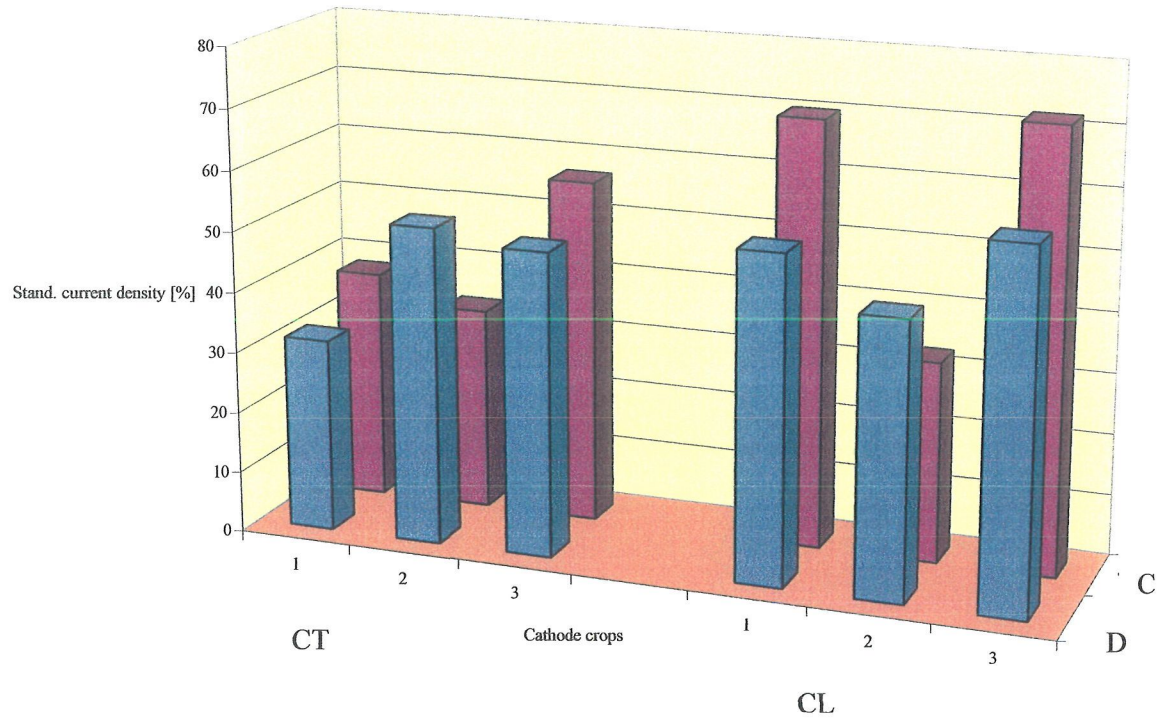

Figure 7-19: Average standard current density

The blue columns in Figure 7-19 show the current density distribution of the investigations with anodes from D and the red columns present the distribution with anodes from C. The current density distribution was nearly similar in all three crops with D anodes. The investigations with anodes from C had at CT geometry nearly the same range of current density variation than D.

After the electrolysis period of one anode crop and three cathode crops the remaining anode was removed and the anode slime was analysed, Table 7-11.

	Cu [%]	Ni [ppm]	Pb [ppm]	Ag [ppm]	Te [ppm]	Se [ppm]	As [ppm]	Sn [ppm]	Bi [ppm]
D	35.62	2200	4.40	23.46	1.61	12.360	5.050	0.20	0.08
C	4.80	15200	23.19	3.38	0.25	0.296	0.951	7.65	102.00

Table 7-11: Anode slime composition

The analyses showed a total different composition of both companies, D being a secondary smelter. Also the amount of anode slime of both companies was very different. In the cells with anodes from C a very low amount of anode slime was produced. The D anodes, however, produced a big amount of anode slime (three times of the amount of C).

In the near technical scale cell first all used different geometries were investigated. Afterwards the influence of electrode distances and geometries on the cathodic current density distribution as a function of anode slime was quantified. At these final investigations two different anode qualities have been used. Anodes from D have a very high amount of anodic slime and anodes from C have a very low amount of anode slime in the cell. So the range of solid particles in the electrolyte is total different. Under these conditions it can be shown that the influence of geometrical irregularities is quite high and independent of the amount of anodic slime.

In conclusion the results from these experiments indicate the factor of geometrical conditions in the cell. To produce smooth cathodes without dendrites it is necessary to have a regular current density distribution over the entire cathode. To attain this target it is important to guarantee good geometrical conditions between the anode and the cathode, and it also may be necessary to control these factors during all cathode crops and at regular time intervals.

7.6 The influence of solid particles in the electrolyte on the copper deposition

The presence of solid materials in the electrolyte has an important influence on the quality of the cathodic deposition. To quantitatively and qualitatively assess these effects it is necessary to determine the type and amount of solids present in the cells. In these experiments the following materials were selected:

- $BaSO_4$ (two different types)
- SiO_2
- $PbSO_4$
- Anode slime

$BaSO_4$ and SiO_2 are used as a mould coating.

$PbSO_4$ results from lead of the anodes. Lead is present in the anode at a concentration of up to 600 ppm, and also as PbO and Pb/As/Cu mixed oxides. The following processes can take place during anodic dissolution:

$PbSO_4$ (slightly soluble)			anode slime
$Pb^{2+} + SO_4^{2-}$	$\leftrightarrow$	$PbSO_4$	as ion
$PbO + H_2SO_4$	$\leftrightarrow$	$PbSO_4 + H_2O$	as an oxide
$Cu_xPb_{1-x} + H_2SO_4$	$\leftrightarrow$	$(1-x)PbSO_4 + xCuSO_4 + 2H^+ + 2e^-$	as mixed crystals
$PbOSb_2O_5$			

Anode slime was obtained from previous experiments. Decisive in the selection of anode slimes was the chemical analysis and the sedimentation behaviour. Heavy and light anode slimes could be included in the analysis. Table 7-12 details the chemical analyses of the selected slimes produced using a current density of 350 A/m^2 in the F and B anodes test series. The sedimentation behaviour of various slimes is illustrated in Figure 7-20.

	Cu [%]	Ni [%]	As [%]	Sb [ppm]	Bi [ppm]
F	4.8	1.52	0.951	380	102
B	5.0	1.2	0.366	830	105

Table 7-12: Chemical analysis of F and B anode slimes

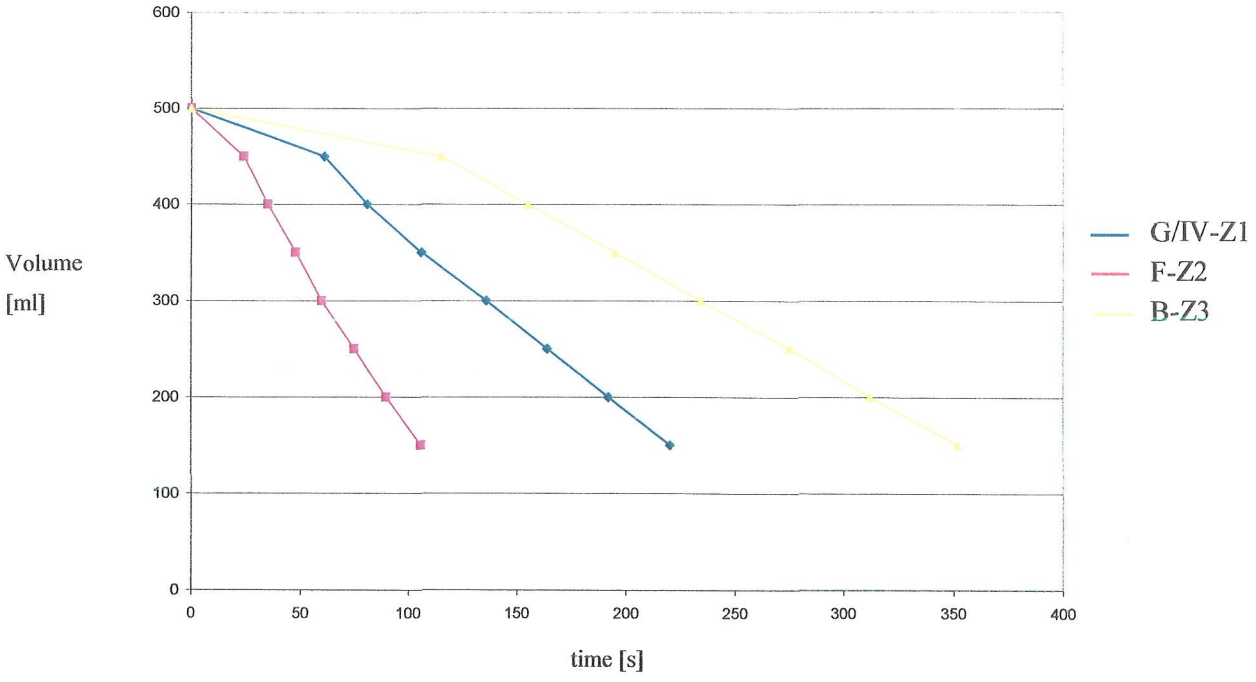

Figure 7-20: Sedimentation behaviour of various anode slimes

In Figure 7-20 the sedimentation behaviour of these three different anode slimes is shown. The slime of F falls down quicker than the slime of B. This may have to do with the size and the density of the particles and the chemical compounds in the anodic slime /56/.

Cathodic copper was used as anodes. This guaranteed the same chemical and physical anode surface at the start of each experiment.

Table 7-13 details the type and amount of solids and test duration. The decision of whether to run the cell for 24 or 48 hours was taken following the observed surface quality of the cathodic precipitate. At the end of the test the cathode was removed, washed, stripped and weighed and a photograph was taken. Each test started with a fresh anode to guarantee the same anodic conditions and same anode-cathode distance.

Examining the effect of various amounts and types of solids on the cathodic precipitation was performed. The cathodic surface differences in the roughness are tremendous /71/. Furthermore, no short-circuiting occurs due to dendritic formation.
In Table 7-14 the results of the cathodic mass deposit, specific energy consumption and current efficiency are presented. The measured current, bath voltage and the average of the cathodic polarization is also detected.

Investigation	Kind of solids	Amount	Duration
0	-	-	24
1	-	-	24
2	Barytmehl N	1 mg/l	48
3	Barytmehl N	10 mg/l	24
4	Barytmehl N	100 mg/l	48
5	Barytmehl N	1 g/l	24
6	Blanc Fixe	1 mg/l	48
7	Blanc Fixe	10 mg/l	24
8	Blanc Fixe	100 mg/l	48
9	Blanc Fixe	1 g/l	24
10	$PbSO_4$	1 mg/l	24
11	$PbSO_4$	10 mg/l	24
12	$PbSO_4$	100 mg/l	24
13	$PbSO_4$	1 g/l	24
14	SiO_2	1 mg/l	24
15	SiO_2	10 mg/l	24
16	SiO_2	100 mg/l	24
17	SiO_2	1 g/l	24
18	Anode slime F	1 mg/l	24
19	Anode slime F	10 mg/l	24
20	Anode slime F	100 mg/l	24
21	Anode slime B	1 mg/l	24
22	Anode slime B	10 mg/l	24
23	Anode slime B	100 mg/l	24

Table 7-13: Experimental parameters of the investigations

The current efficiency obtained during the investigations was between 98 and 107 % and the specific energy consumption between 130 and 300 kW/t_{Cu}.

To get further information on the influence of the solid materials the cathodic polarization voltage was measured during the electrolysis time with a Luggin capillary. The three measuring points were placed at various heights in the middle of the cathodes, Table 7-15.

Investigation	U [V]	m [g]	m theor. [g]	I [A]	Up [V]	$E_{spec.}$ [kWh/tCu]	η [%]
0	0.26	123.15	122.06	4.3	0.103	218	101
1	0.26	127.39	123.77	4.4	0.069	213	103
2	0.17	243.65	245.16	4.3	0.029	143	99
3	0.21	133.14	126.04	4.4	0.099	165	106
4	0.21	280.40	281.68	5.0	0.101	178	100
5	0.22	146.70	139.42	4.9	0.104	175	105
6	0.15	243.55	245.16	4.3	0.027	131	99
7	0.20	132.50	125.54	4.4	0.100	160	106
8	0.21	274.44	261.76	4.6	0.107	172	105
9	0.20	133.65	134.44	4.7	0.095	169	99
10	0.21	127.35	124.24	4.4	0.069	171	103
11	0.19	123.70	120.92	4.3	0.090	160	102
12	0.31	129.67	120.92	4.3	0.069	244	107
13	0.25	124.95	124.24	4.4	0.078	206	101
14	0.20	122.84	125.19	4.4	0.020	171	98
15	0.22	125.55	125.19	4.4	0.085	184	100
16	0.17	120.35	125.19	4.4	0.036	153	96
17	0.17	124.26	125.19	4.4	0.050	143	99
18	0.23	124.60	126.61	4.5	0.081	197	98
19	0.22	128.44	125.19	4.4	--	180	103
20	0.22	127.60	125.19	4.4	--	184	102
21	0.23	128.80	123.77	4.4	0.102	190	104
22	0.17	126.26	128.03	4.5	0.045	150	99
23	0.36	129.48	126.61	4.5	0.074	296	102

Table 7-14: Results of polarization measurements

	H1	H2	H3
mm top to measuring point	40	85	130

Table 7-15: Measurement points

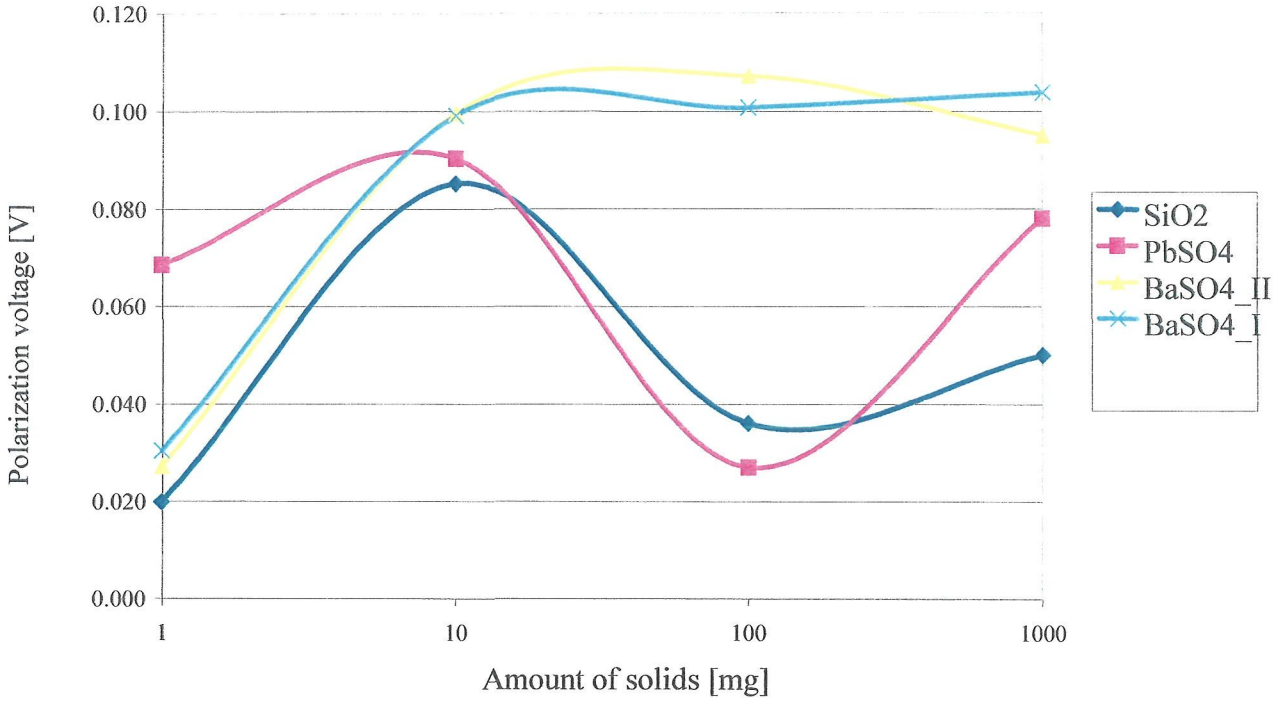

Figure 7-21: Polarization measurement of different amounts and types of added solid particles

Physical analysis of the cathodic precipitation

Experiment			
Nr.	Kind	Amount [mg/l]	
0			smooth, even deposit
1			smooth, even deposit
2	Barytmehl N	1 mg/l	smooth deposit, slight bud formation at the borders
3		10 mg/l	fine dendrites all over the face, no short circuits
4		100 mg/l	some bigger dendrites after 24 hours, short circuits after 40 h
5		1000 mg/l	dendrites over entire face, short circuits after 24 h
6	Blanc Fixe	1 mg/l	smooth deposit, dendrite formation on the borders
7		10 mg/l	fine dendrite formation at the lower part of the cathode
8		100 mg/l	fine dendrite formation over the entire face, no shorts
9		1000 mg/l	bigger dendrites over the entire face, break-off after 24 h
10	$PbSO_4$	1 mg/l	dense dendrite formation
11		10 mg/l	dense dendrite formation
12		100 mg/l	dense dendrite formation
13		1000 mg/l	big, coarse dendrites at the borders
14	SiO_2	1 mg/l	relatively smooth, even deposit
15		10 mg/l	slight dendrite formation at the borders
16		100 mg/l	total face rather coarse granular deposit, no dendrites
17		1000 mg/l	some single large dendrites
18	Anode slime F	1 mg/l	Rough cathode, with dendrites smaller than 2 mm
19		10 mg/l	Rough cathode with longer dendrites at the edges
20		100 mg/l	Rough cathode with dendrites > 5 mm, shorts will probably occur
21	Anode slime B	1 mg/l	High dendrite growth on the whole surface
22		10 mg/l	Dendrites longer than 5 mm, at the edges > 10 mm
23		100 mg/l	Dendrites > 10 mm, shorts will probably occur

Table 7-16: Visual characteristics of the cathodic precipitation

Anode slime [mg/l]	**I [A]**	**t [h]**	**$m_{theo.}$ [g]**	**$m_{prac.}$ [g]**	**η [%]**	**$U_{average*}$ [V]**	**$E_{spec.}$ kWh/t_{Cu}**
0.5	3.69	47.87	209.21	208.67	99.74	0.236	199.4
0.8	3.69	48.03	209.94	204.42	97.37	0.148	128.32
1.0	3.69	47.95	209.57	208.55	99.51	0.166	140.84
5.0	3.69	47.53	207.75	200.33	96.43	0.154	135.30
10.0	3.98	47.88	225.73	224.47	99.44	0.253	214.80

Table 7-17: Current efficiency, average bath voltage, and specific energy consumption

*bath voltage

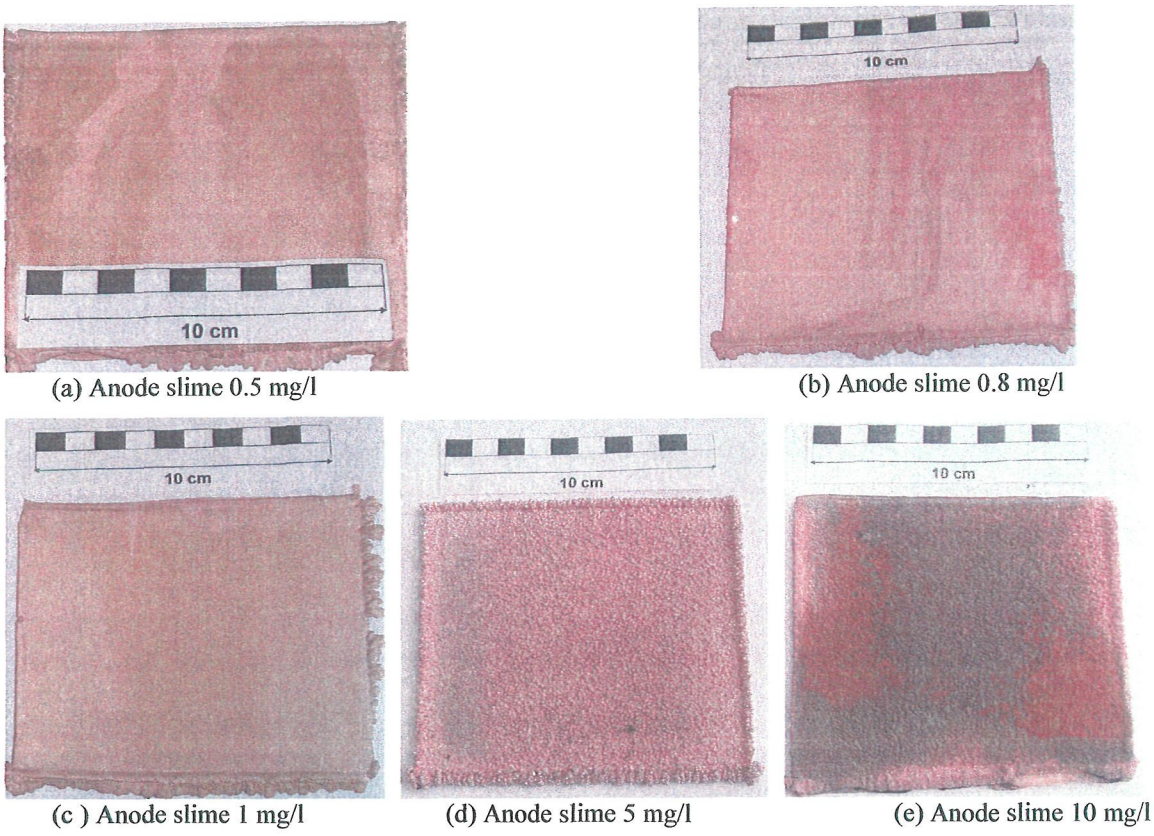

(a) Anode slime 0.5 mg/l (b) Anode slime 0.8 mg/l

(c) Anode slime 1 mg/l (d) Anode slime 5 mg/l (e) Anode slime 10 mg/l

Figure 7-22: The deposit appearances resulting from the experiments with various anode slime particles content

Addition of anode slime particles up to 1 mg/l did not affect the quality of copper deposit. Smooth deposits without dendrite growth are identified on the cathode surface resulting from the experiments with anode slime contents in the electrolyte from 0.5, 0.8 and 1 mg/l. Significant dendritic growth is identified from the experiment with the addition of 10 mg/l anode slime particles into the electrolyte. Rough deposits with smaller bud sizes were obtained from experiments with 5 mg/l anode slime in the electrolyte. The deposit appearances resulting from the experiments with various anode slime particles contents are presented in Figure 7-23. The dendrites after two days experiments with anode slime contents of 5 and 10 mg/l are shorter and less severe compared with those in the experiments without inhibitor addition /8/. Current efficiency, average bath voltage, and specific energy consumption from the experiments with various anode slime particles contents in the electrolyte are presented in Table 7-17.

A visual evaluation of the cathodes produced during the analysis was useful. In experiments 0 and 1, no solid particles were detected on the cathode, showing that by using a synthetic electrolyte the cathodic precipitation was smooth without any buds or dendrites.

In experiments 2 to 5 and 6 to 9 two different types $BaSO_4$ ($BaSO_4$ Type N and $BaSO_4$ Type Blanc Fix) were used. With 1 mg/l of either type of $BaSO_4$ no dendrites and buds were formed. However, in both cases an increase in the amount of $BaSO_4$ did cause a rougher precipitation and more dendrites and buds. The cathodic dendrites produced using $BaSO_4$ Type N were thicker and coarser-grained than the dendrites

produced using the $BaSO_4$ Type Blanc Fix. After 24 hours of electrolysis with $BaSO_4$ Type N shorts occurred.
The addition of SiO_2 to the electrolyte (experiments 14-17) did not influence the cathodic precipitation as significantly as $BaSO_4$. The cathode precipitation with 1 mg/l SiO_2 was smooth. However, with an increased amount of SiO_2 the precipitation became rougher, but no big dendrites grew and no shorts occurred.

In experiment 10 to 13 $PbSO_4$ was added to the electrolyte and the cathode precipitation became worse with increased amount. Many dendrites on the whole surface and the individual single dendrites were thicker than dendrites indicated by $BaSO_4$. If the electrolysis had continued shorts would have occurred.

In experiments 18 to 23 two different anode slimes were used. The two anode slimes were collected from experiments run using either an anode from F or an anode from B. The collected anode slime was weighed, balanced and dried but not washed. The decision to use slime from experiments F and B anodes was based on the sedimentation investigations. Both types of slime greatly influenced the cathodic precipitation. The whole cathode surface was very rough with many dendrites. Furthermore, by increasing the amount the dendrites got bigger and denser. After 24 hours shorts occurred.

In conclusion, the experiments revealed the following two issues:

- The cathodic precipitation was getting worse the more solid particles were present in the electrolyte.
- The appearance and morphological structure of the precipitation was clearly linked to the type of particles added. Between the two $BaSO_4$ types a different precipitation was clearly observed. However, a difference in the presence of the two different anode slimes was not detected.

The precipitation caused by addition of the different materials can be summarized as follows:

- SiO_2, regular with a low increase of fine and small grains
- $BaSO_4$, dendritic with small size and dense of dendrites
- $PbSO_4$, medium size and kind of dendrites
- Anode slime, rough and coarse dendrites

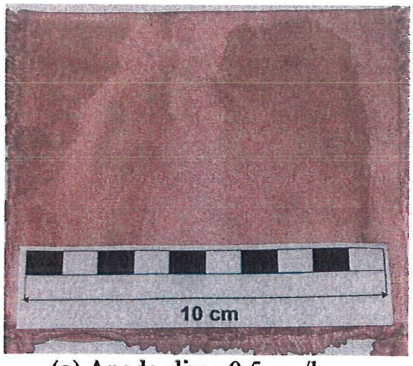

(a) Anode slime 0.5 mg/l

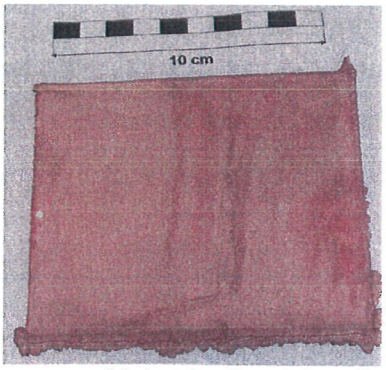

(b) Anode slime 0.8 mg/l

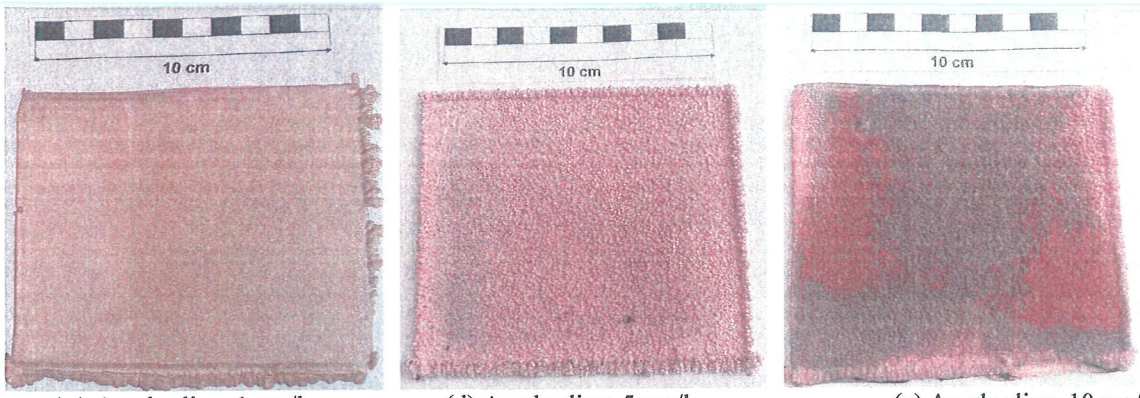

(c) Anode slime 1 mg/l (d) Anode slime 5 mg/l (e) Anode slime 10 mg/l

Figure 7-23: The deposit appearances resulted from the experiment with various anode slime particles content

Significant dendrites are obtained in the experiments using electrolyte without inhibitor at a current density of 350 A/m^2. The smoothest deposits are resulting from the experiments with the glue/thiourea ratio near to 1 (53/55 g/t_{Cu} and 75/78 g/t_{Cu}). Rough deposits are obtained from the experiments with glue/thiourea ratios of 30/60 g/t_{Cu} and 100/60 g/t_{Cu}. As indicated by polarization experiments using the potentiostat, increasing the content of glue in the electrolyte enlarged the cathodic polarization of the cathode. Higher cathode polarization by the increased glue/thiourea ratio contributes to the rise of bath voltage and consequently the specific energy consumption. High cathodic polarization, bath voltage and specific energy consumption was found in the experiments without inhibitor addition where significant dendrite formation was identified. Current efficiency, average bath voltage, average cathode polarization, and specific energy consumption for the experiments with various inhibitor dosage in the electrolyte are given in Table 7-19.

To compare the measured and calculated polarization it is necessary to use absolute figures. The polarization measurement is starting at the steady state potential (+ 200 mV). So the resulting cathodic polarization ($Up_{meas.}$) is given in Table 7-18.

	Roughness	Measurement [mV]	Up meas. [mV]
Glue/thiourea 31/53	20.2	-78	122
Glue/thiourea 30/60	12.4	-63	137
Glue/thiourea 75/78	3.5	-55	145
Glue/thiourea80/60	24.1	-82	118
Glue/thiourea100/60	45.0	-90	110
Without inhibitor	200.0	-145	55

Table 7-18: Roughness in µm and cathodic polarization measured

To produce smooth cathodes an evaluation of the cathodic polarization took place. That is why the roughness of the cathodes was measured. It is shown that a decrease of cathodic polarization resulted in an increase of roughness. As can be seen in Table 7-18 the calculated values show the same tendency.

Glue/thiourea [g/t_{Cu}]	I [A]	t [h]	$m_{theo.}$ [g]	$m_{prac.}$ [g]	η [%]	$U_{average*}$ [V]	$E_{spec.}$ kWh/t_{Cu}
30/60	3.75	47.83	212.46	211.73	99.66	0.189	160.35
80/60	3.71	47.50	208.73	208.59	99.93	0.206	174.22
100/60	3.71	48.30	212.25	208.76	98.36	0.246	211.39
31/53	3.72	48.08	211.86	211.79	99.96	0.215	181.84
75/78	3.71	47.53	208.88	208.40	99.77	0.194	163.98

Table 7-19: Current efficiency, average bath voltage, average cathode polarization, and specific energy consumption

*bath voltage, ** Cathode polarization

The experimental part of this work consists of the investigation of different influence parameters due to the cathodic precipitation at the refining electrolysis. All investigations have been done at the same standard conditions as described before. After evaluating the influence of the current density (various between 350 A/m² and 500 A/m²) different geometrical conditions have been simulated. Then the current density distribution over the total cathode surface was measured and calculated. To be able to compare these results with the different anodes of the partners, some more experiments will have to been done. In the last experiments the influence of two total different anodes in chemical quality has been investigated. Finally the solid amount behaviour in the electrolyte has been taken under cognition.

7.7 Conclusion

In the investigations under precise and constant electrolysis conditions with well controlled systems the following effects on the cathodic precipitation can be summarized:

- A variation in the current density between 350 and 500 A/m² had no influence on the cathodic precipitation.

- Geometrical variations of the electrode caused a current density distribution of more than 100 % (equivalent of up to 700 A/m²) and the uneven current density distribution over the entire cathode surface forced dendrite formation.

- The different chemical qualities of the anodes had low effects on the cathodic precipitation under these well controlled systems.

- The level of solid particles present during the investigations, including mould coating, anode slime, and $PbSO_4$, influenced the cathodic precipitation. The cathodic roughness varied between 10 and 50 µm after an electrolysis time of 24 hours. Therefore, the formation of dendrites in the regular cathode life time of more than 6 days is very possible.

8 MATHEMATICAL MODEL

As previously discussed there is a broad set of parameters that influence copper refining electrolysis. It is of principal interest to establish the effect of the individual factors and their combinations. The goal of a mathematical model of a system is to predict the effects of parameter changes. In the case of the electrolysis a quantitative statement is not possible due to the high complexity of the influencing factors. However, a significant step would be to determine a qualitative estimation and to have an indication of the level of importance of the effects and their changes. Two important points for the mathematical description of a system are the definition of the system with all the boundary conditions and restrictions and the definition of a base factor, which can be described, with reference to the mathematical description.
In the course of the work, two different mathematical models were accomplished. The first was to describe the importance of individual factors on the influence of polarization at the copper cathode and a statistical test program was used in the first part. In the second part a method was developed to calculate the influence of flow conditions in the cells on the relationship of the actual current density to the limiting current density.

The physical dimension regarding the electrical crystallization and therefore on the quality of the copper at the cathode is the polarization η. Therefore, in the first part of the mathematical modelling the size of polarization was selected as the base factor for a statistic evaluation of the effect of changing different parameters.

8.1 Polarization Measurements

Polarization measurement results were the current density vs. cathode polarization curves under various conditions.

8.1.1 Theory

The electrical potential change over the boundary layer of two electrically leading phases - for example between a metal and an electrolytic solution - is in principle caused by:

- An electrical dipole layer, which leads to a surface potential difference,
- An electric double layer which is caused by the direct transition of charge

The dipole layers occur on both sides of the phase boundary. The dipole layers and the surplus electrical charge of the electrical double layer form an electrochemical double layer due to the force of attraction. In the zero current condition the phase boundary layer corresponds to the range of the electrochemical double layer. With a current flow it results in more or less large concentration differences between single parts of the phases and the internal phases. The associated material conversion also takes place outside of

the electrochemical double layer. This forms a so-called diffusion layer. The range of the phase boundary layer gets bigger than the double layer. Therefore, the electrical potential gradient over the phase boundary layer differs to the current carrying electrode. This difference of potential is called electrode polarization or simply polarization. This defined term of polarization is typically used for the simultaneous operational sequence of several electrode reactions (multiple electrodes). If only a single electrochemical reaction takes place at the electrode, then a single electrode is presented. The potential difference between current flow and currentless electrodes is termed polarization/19/.

Following Kortüm /72/ and Vetter /73/ the same symbol η is used for the polarization and the overvoltage. It is considered that the overvoltage occurs very rarely as a special case of the polarization and cannot be easily proven. Generally, linguistic usage does not differentiate between polarization and overvoltage. Furthermore, in the following this has to be taken into account.

8.1.1.1 Partial procedures of an electrochemical gross reaction

The reason for the polarization is blocking of partial procedures of which each electrochemical gross reaction consists. Accordingly, the polarization consists of several parts, which have their specific influence on the summary reaction.

- The characteristic partial procedure of each electrochemical gross reaction is the transfer of a charge carrier, an ion or electron through the phase boundary of the electrode. Therefore, it is called transfer reaction η_T.
- With metal ion electrodes the insertion into the crystal lattice of the ad-atoms (which separated in the transfer reaction) takes place or the opposite reaction (the removal of ad-atoms out of the crystal lattice) occurs. This partial procedure is well known as the crystallization reaction η_C.
- For an electrochemical reaction the material transfer takes place by diffusion, namely an ion migration due to a concentration gradient, and convection from or to the electrode surface. A migration or a transfer, namely an ion migration due to the electrical potential gradient, can be neglected with large surplus ions in the electrolyte (η_D).
- At the boundary of the electrochemical double layer and also inside the phase a changed concentration of the charge carriers can be observed due to a slowly running chemical reaction (η_R).
- Finally an Ohm's decrease of potential can occur with the polarization or polarization measurements; however, it exerts no influence on the type and speed of electrochemical reactions. This part of polarization is known as resistance polarization. It occurs at the phase boundary layer and over surface layers on the electrode material. Although Vetter /37/ defined the resistance polarization in such a way it does not agree with the terms polarization and polarization. But this Ohm's decrease of potential must be considered (η_Ω).

8.1.1.2 The different kinds of polarization

The different kinds of polarization are discussed by Forker /20/. The following basic polarizations are according to the indicated component procedures of the electrochemical gross reaction (transfer, crystallization, diffusion and chemical reaction):

- Electron transfer polarization η_T
- Crystallization polarization η_C
- Diffusion polarization η_D
- Reaction polarization η_R
- (Resistance polarization) η_Ω

Therefore, for the total polarization the following equation results:

$$\eta_{ges} = \eta_T + \eta_C + \eta_D + \eta_R + \eta_\Omega$$

Equation 8-1

For the mathematical modelling of copper refining electrolysis the fundamental quantitative connections between the individual types of polarization and substantial measured variables of the electrolysis process have to be analysed. The relations derivable concerning the polarization should be examined more closely.

8.1.1.2.1 Electron transfer polarization

With electrodes made of metal ions the transfer reaction exists in reverse in the transition of a metal ion from electrolytes by the electrochemical double layer into the metal or contrary. Both the cathodic and the anodic electron transfer reaction requires a certain activation energy. This activation energy affects the reaction velocity and therefore the value of electron transfer polarization.

Quantitative statements can be made, if it is understandable that each electron requires a special amount of energy to make the transfer reaction. For this to occur a special amount of activating energy is necessary.

The value of the amount of energy, measured from the respective starting situation of the electron transfer, provides the activation energy $\vec{E}_{gl}$ or $\overleftarrow{E}_{gl}$ for the backward reaction in the equilibrium on. During the derivative of the following relations it is presupposed that only one depressing tension arises alone, namely diffusion, crystallization and possibly chemical reaction run completely unrestrained.

With consideration of the connection between the change of the activation energy with current flow in relation to the currentless condition and the arising electron transfer polarization η_T the following dependence results in accordance to Forker /35/ and Vetter /37/ for the current density i in the case of the kind of polarization η_T and the limiting current density i_0 in the equilibrium:

$$i = \frac{z}{|z|} \cdot i_0 \cdot \left[\exp\left(\frac{\alpha \cdot z \cdot F \cdot \eta_T}{R \cdot T} \right) - \exp\left(-\frac{(1-\alpha) \cdot z \cdot F \cdot \eta_T}{R \cdot T} \right) \right]$$

Equation 8-2

with:

i	current density
i_0	limiting current density
z	valancy
α	transfer factor
F	Faraday's constant
R	gas constant
T	absolute temperature

The electron transfer polarization cannot be indicated as the above equation explicitly. That is possible only if either sufficiently large or very small electron transfer polarizations arise, so that certain approximations can be performed.

In the first case, $|\eta_T| >> \frac{R \cdot T}{|z| \cdot F}$, it can be derived as

$$|\eta_D| = a + b \cdot \log |i|$$

Equation 8-3

with

$$b = \begin{cases} \frac{2{,}303 \cdot R \cdot T}{\alpha \cdot |z| \cdot F} & \text{at anodic currents} \\ \frac{2{,}303 \cdot R \cdot T}{(1-\alpha) \cdot |z| \cdot F} & \text{at cathodic currents} \end{cases}$$

$$a = -b \cdot \log i_0$$

Equation 8-4

Relationships of this type become general, namely linear changes of the polarizations with the logarithm of the current density as "Tafel-Gleichung" as mentioned above. From the experimentally determined constants a and b the figures α and i_0 can be derived by coefficient comparison.

Alternatively, for very small electron transfer polarizations, namely $|\eta_T| << \frac{R \cdot T}{|z| \cdot F}$ a linear connection between i and η_T results:

$$i = \frac{i_0 \cdot |z| \cdot F \cdot \eta_T}{R \cdot T}$$

Equation 8-5

respectively $$\eta_T = \frac{R \cdot T}{i_0 \cdot |z| \cdot F} \cdot i$$

Equation 8-6

With the aid of the aforementioned equations it is evident that the electron transfer polarization η_T is directly linked to the current density i, to the absolute temperature T, the valency z, which is affecting the limiting current density i_0 and the transfer factor α.

8.1.1.2.2 Crystallization polarization

First the metal atoms or ions are in the adsorbed condition on the metal surface, and therefore, different from an atom in the crystal lattice. This happens after the transfer through the double layer, where the covering hydrate or other complexing agents become "stripped". These ad-atoms arrive at a growth place on the surface only by diffusion. If this procedure is the speed determining step of the electrochemical reaction then pure crystallization polarization arises. In /74, 75/ a general relationship for the crystallization polarization is given for copper precipitation from not complex salt solutions during galvanostatic precipitation. However, this relation applies only to simplified conditions. For the practice of the electrolytic copper refining only a qualitative interpretation should be used.

8.1.1.2.3 Diffusion polarization

A diffusion polarization η_D arises if the electron transfer is inhibited. If all other parts (crystallization, transfer, and chemical reaction polarization) run without any restriction, then only diffusion polarization is present. The following dependence between current density i and diffusion polarization can be written as:

$$\eta_D = \frac{R \cdot T}{z \cdot F} \cdot \ln\left(1 - \frac{i}{i_0}\right)$$

Equation 8-7

i_0 limiting current density

Using Equation 8-7 a quantitative statement can be given if the potential determining ion concentration is very small and the concentration of ions which are not potential determining are in surplus /22/. Also this equation is usable if there is no migration and the diffusion layer is like a steady state diffusion boundary layer. Therefore, the relationship has only a qualitative character for the copper refining electrolysis.

8.1.1.2.4 Reaction polarization

A reaction polarization occurs if in parallel with the actual electrochemical reaction a purely chemical reaction exists which is speed determining. Such a reaction can be for example. the solvation of an ion, a complex formation, or a dissociation process. Both homogeneous and heterogeneous partial reactions should be considered. Homogeneous chemical partial reactions take place at the solution side outside the electrochemical double layer in the so called reaction layer. Heterogeneous chemical partial reactions take place at the boundary surface of the metal/electrolyte. Desorption or adsorption processes can be included and therefore concentration changes arise within the electrochemical double layer. Also these reactions can lead to a limited reaction behaviour and to a certain polarization.

8.1.1.3 Significant influences on the electrode potential in the copper refining electrolyses

During the copper refining electrolysis the potential determining reaction takes place as well anodically as cathodically like $Cu \leftrightarrow Cu^{2+} + 2e^-$. /74,75/ illustrate that this electron transfer reaction consists of two single steps one after the other:

$Cu \leftrightarrow Cu^+ + e^-$ (fast) Equation 8-8

$Cu^+ \leftrightarrow Cu^{2+} + e^-$ (slow) Equation 8-9

The aforementioned equation 8-9 is regarded as the speed determining step. Furthermore, electrochemical dissolution or precipitation procedures from impurities must be considered which are contained as a multicomponent alloy always in the anode copper. In addition, electrochemical secondary reactions can also take place including:

$2\,H_2O \leftrightarrow O_2 + 4H^+ + 4e^-$ Equation 8-10

As previously discussed several electrode reactions take place simultaneously which are not in equilibrium. Therefore, "mixed electrode" and "electrode polarization" should be used for the practice of the electrolytic copper refining

The following parameters concerning the electrode polarization are of interest:

- Current density
- Electrolyte composition, concentration, and temperature
- Electrolyte additives (in particular inhibitors)
- Quality and type of starter sheet blanket
- Electrolyte flow conditions
- Anode quality (physical condition and chemical composition of the anodes)
- Electrolysis duration

These numerous process variables affect the electrode polarization. Further several processes during the anode dissolving and copper precipitation are interlinked. The surface texture of anode and cathode and the electrolysis conditions are subject to constant changes. Concerning the anodic dissolution of metal a time dependence of the polarization should be considered, anode mud layer causes a resistance polarization including an increase of the diffusion polarization. Further effects are also due to the anode composition, current density as well as the temperature and composition, concentration, and circulation of the electrolyte. In relation to this matter it is also possible to achieve anodic passivation, which can affect the electrolysis very unfavourably.

8.1.2 Experimental investigations

A standard electrolyte containing 175 g/l H_2SO_4, 45 g/l Cu^{2+} and 10 g/l Ni^{2+}, was used. During the experiments the influences of copper, acid, temperature, chloride, nickel, thiourea, glue, and a mixture of all these parameters were investigated /5,7,8/. The glue was provided by G. Thiourea was a Merck product, and the HCl (37 %) was used as a chloride ion source. Distilled water was used to prepare the supporting electrolyte and the stock solution of glue 24 hours before the experiment was started.

No.	PARAMETERS					
1.	Sulphuric acid (g/l)	**155**	**165**	**175**	**185**	
2.	Copper (g/l)	**35**	**40**	**45**	**50**	**55**
3.	Nickel (g/l)	**0**	**5**	**10**	**15**	**20**
4.	Temperature (°C)	**50**	**60**	**65**	**70**	
5.	Glue (mg/l)	**2**	**4**	**8**	**12**	
6.	Thiourea (mg/l)	**2**	**4**	**6**	**8**	**10**
7.	Glue-thiourea (mg/l – mg/l)	**2-4**	**4-4**	**6-4**	**8-4**	
8	Glue-thiourea (mg/l – mg/l)	**8-4**	**8-6**	**8-8**	**8-10**	**8-12**
9.	Cl (mg/l - mg/l)	**0**	**20**	**40**	**60**	
10.	Thiourea - Cl (mg/l - mg/l)	**4-40**	**6-40**	**10-40**	**14-40**	
11.	Glue-thiourea-Cl (mg/l - mg/l – mg/l)	**4-4-40**	**6-4-40**	**8-4-40**		
12	Glue-thiourea-Cl	**8-6-40**	**8-8-40**	**8-10-40**	**8-12-40**	

Table 8-1: Investigation parameters

Investigations were performed under standard conditions with the variation of one of the parameters detailed in Table 8-1.

In the following sections a short summary of the polarization investigations is provided. More information is detailed in /6,7,8/.

8.1.2.1 Effect of copper ion concentration

Increasing the Cu^{2+} concentration from 35 g/l to 40 g/l and 45 g/l decreased the cathodic polarization at all current densities. At Cu^{2+} concentrations of 50 and 55 g/l, depolarizing effects were significantly exhibited at higher current densities (> 500 A/m^2).

The reduction of cathodic polarization during copper deposition by increasing the Cu^{2+} concentration in the electrolyte can be explained partly from the point of view of electrolyte conductivity and partly by the diffusion boundary layer. With a rise of Cu^{2+} concentration, the number of charge carriers in the electrolyte and consequently the electrolyte conductivity increases. Increasing electrolyte conductivity resulted in the decrease of cathodic polarization for the copper deposition at a certain current density. This is true for the employed parameter variations but there was a certain maximum Cu^{2+} concentration. If the Cu^{2+} concentration was higher than this maximum the polarization increased. This effect could also be seen by increasing the Ni^{2+} concentration. A higher Cu^{2+} concentration also increased the limiting current density or decreased the thickness of the boundary layer. The importance of the diffusion boundary layer in relation to the limiting current density will be discussed in detail in Section 8.2.2.

8.1.2.2 Effect of sulphuric acid concentration

Increasing the H_2SO_4 concentration from 155 g/l to 165 g/l and 175 g/l decreased the cathodic polarization at all current densities. Acids have a particularly good conductivity because of the formation of cations and anions in solution. Furthermore, the increased H_2SO_4 concentration from 175 g/l to 185 g/l did not result in further depolarizing effects and resulted significantly in the opposite effect. Repeated measurements provided the same results. It appeared that there was an optimum concentration of sulphuric acid. At higher concentrations a polarizing effect could be observed. Instead of increasing the number of charge carriers in the electrolyte, a higher H_2SO_4 concentration elevate the solution viscosity. The increased viscosity resulted in a decreased ionic mobility in the electrolyte.

8.1.2.3 Effect of temperature

An increase of the electrolyte temperature from 50 °C to 60 °C and 65 °C decreased the cathodic polarization during copper deposition. A reduced cathodic overpotential with higher electrolyte temperature was due to the copper ion mobility increase in the electrolyte. At a higher temperature, the solution viscosity was lower (the ions mobility was greater) and the conductivity of the electrolyte was getting higher. Furthermore, the diffusion coefficient increased at higher temperatures. Industrial copper refining is normally conducted at temperatures between 60 and 68 °C. However, there is a problem with glue dissociation if the electrolyte temperature is too high and a higher level of evaporation occurs .

8.1.2.4 Effect of Ni^{2+} concentration

The industrial electrolytes always contain Ni^{2+} until a certain amount at which the electrolyte should go to the purification unit. The experimental analysis revealed nearly the same effect of nickel ion concentration and copper ion concentration on the polarization behaviour of the cathode. The presence of nickel ions in the electrolyte provided the depolarizing effect for the copper deposition. The depolarizing effect occurred with the increase in Ni^{2+} concentration up to a concentration of 15 g/l. However, increasing the Ni^{2+} from 15 g/l to 20 g/l gives no further depolarizing effect and resulted in the opposite effect, although there was still a depolarizing effect compared to the solution without Ni and with 5 g/l Ni^{2+}. By further increasing the charge carrier concentration, the mobility of the ions diminished (hindering effect). From this effect it was evident that increasing the number of ions in the electrolyte was not contributing to the electrolyte conductivity, and too high a concentration of charge carriers resulted in a decrease in the electrolyte conductivity.

8.1.2.5 Effect of thiourea

Polarization measurements to investigate the influence of thiourea, glue, and chloride were conducted 30 minutes after the addition of the additives into the electrolyte.

Single thiourea additions in the electrolyte of 4 mg/l, 6 mg/l, 8 mg/l, and 10 mg/l resulted in depolarizing effects. A thiourea concentration of 2 mg/l in the electrolyte resulted in the opposite effect (polarizing effect). A limiting current density was detected in the solution containing 10 mg/l thiourea. This should be due to the inhibition effect of copper deposition by the adsorption of thiourea on the cathode surface. The limiting current density occurred at current densities of ~ 600 A/m^2 and at cathodic polarizations of 52-74 mV. Below this limiting current density, 10 mg/l thiourea resulted in a depolarizing effect whilst a significant polarizing effect was found above this limiting current density. Measurements at thiourea concentrations higher than 10 mg/l should be conducted to evaluate whether a similar phenomenon will occur. The transition from a depolarizing effect to a polarizing effect by increasing the current density was also detected in the solutions containing 4, 6 and 8 mg/l of thiourea, although limiting current densities were not identified. At industrially employed current densities of up to 400 A/m^2 even high thiourea concentrations of 10 mg/l still had a depolarizing effect.

8.1.2.6 Effect of glue

Single glue additions to the electrolyte resulted in the opposite effect of thiourea. The results showed that the addition of 2 mg/l, 4 mg/l, 8 mg/l, and 12 mg/l of glue resulted in significant polarizing effects. Increasing the glue concentrations from 8 mg/l to 12 mg/l resulted only in a slight polarizing effect at current densities of ~ 550 A/m^2 to ~ 820 A/m^2.

8.1.2.7 Effect of thiourea and glue

The effect of various glue contents at constant thiourea concentrations on the cathodic polarization of copper deposition was investigated. The results indicated that the addition of 2 mg/l glue was sufficient to eliminate the depolarizing effect of 4 mg/l of thiourea. Limiting current densities were found at the polarization curves in the solution containing glue/thiourea at 2/4, 4/4 and 6/4 mg/l, at current densities between 200 A/m^2 and 300 A/m^2. The limiting current density decreased with the glue increase from 2 to

4 and 6 mg/l. In the presence of limiting current densities, the solutions contained glue/thiourea at 2/4, 4/4; this resulted in higher polarizing effects at higher current densities compared with the solutions containing only glue at 2 and 4 mg/l.

8.1.2.8 Effect of chloride ions

The results indicated that chloride ions have slightly polarizing effects on the cathodic polarization of copper. Increasing Cl^- from 20 mg/l to 40 mg/l and 60 mg/l increased the polarization of cathodic copper deposition. The effect of the Cl^- concentration was not significant at lower current densities (up to 350 A/m^2) /76, 77/

8.2 Mathematical model of the polarization investigations

To describe the results of the cathodic polarization analyses, a mathematical model was employed. With the MODDE 7 mathematical statistic program a description of the influence of all parameters was performed. For this project the polarization modelling was performed using special software. The following section is a general description of the use of these model.

MODDE 7.0 (MODeling and DEsign) is a Umetrics AB program. The multidimensional mathematical models can be performed on the basis of actual measured data. It is only possible to answer most metallurgy questions if the background of the very complex processes with a multiplicity of influencing parameters is known. It is also an advantage to evaluate the experimental results in a systematic manner. In contrast to the usual data evaluation by means of EXCEL, which enables representation of simple dependences (e.g., a measured variable as well as a calculated variable), the possibility arises of linking measured variables with a large number of variables using MODDE 7.0. By adjusting the program algorithms it is possible to form mathematical connections between measured variables and mathematical values. However, a modelling cannot only be accomplished with the complete statistic evaluation of results of measurement with this program. This software makes it possible to determine and also plot substantial dependences. Particularly, the overview of the existing reciprocal effects within a process is one of the application advantages. Nevertheless it must be pointed out that the results of such data evaluation always represent the optimum average value of dependence and the deviations between the model and actual value. However, the complex evaluation provides an ideal overview that relates to the multidimensional dependence.

Initially it is necessary to establish the model exactness:

- R^2 is the percentage variation of the response explained by the model. R^2 is a measure of fit, namely how well the model fits the data. A large R^2 is a necessary condition for a good model, but it is not sufficient. A poor R^2 is representative of poor reproducibility (poor control over the experimental error) or poor model validity (the model is incorrect).

- Q^2 is the percentage variation of the response predicted by the model according to cross validation. Q^2 indicates how well the model predicts new data. A useful model should have a large Q^2. A poor Q^2 indicates poor reproducibility (also poor control over the experimental error) or/and poor model validity (the model is incorrect).

- If the model validity bar is larger than 0.25, there is a no "Lack of Fit" (LOF) of the model (the model error is in the same range as the pure error). A model validity bar of 1 represents a perfect model. When the model validity is less than 0.25 a significant LOF exists and the model error is significantly larger than the pure error (reproducibility).

- The reproducibility is the variation of the response under the same conditions (pure error), often at the centre points, compared to the total variation of the response.
  Reproducibility = 1 – [MS (Pure error) / MS (total SS corrected)]
  MS = mean squares or variance.

When the reproducibility bar is 1.0, the pure error is 0. This means that under the same conditions the values of the response are identical. When the reproducibility bar is 0, the pure error equals the total variation of the response. At reproducibility above 0.85, it has to be ensured that the replicated experiments have been performed at different times and that at each time the experimental set-up is started under the same starting conditions.

Evaluation of the model quality

To evaluate the accuracy of the forecast model following Figure 8-1 should be regarded.

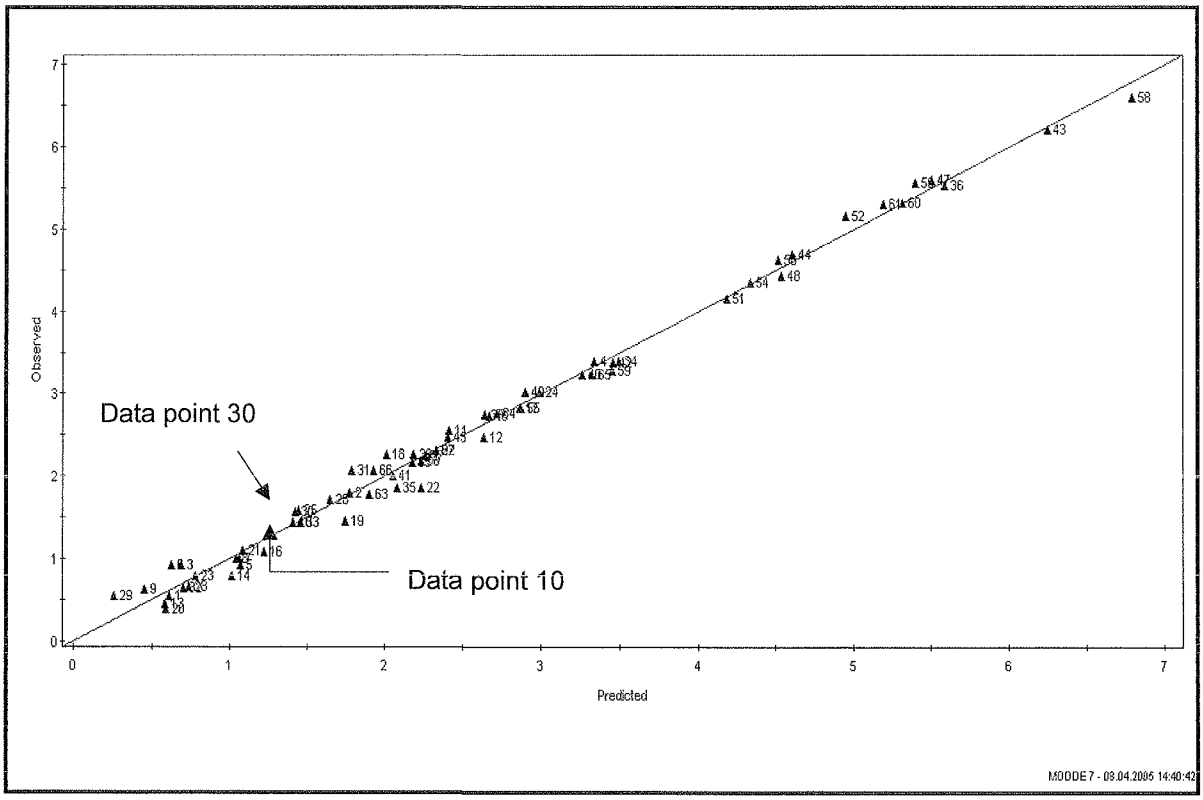

Figure 8-1: Observed versus Predicted Plot

The data points represented in Figure 8-1 indicate the difference between the so-called measured value (observed) and the relevant forecasted value (predicted) of the model for polarization. Thereby, the

measured values correspond to the base data used to produce the model. The assigned forecast values indicate how the model is able to represent the measured values. Figure 8-1 provides in a relatively simple way a general information regarding the overall quality of the forecast model. For example, if data point 30 is examined the forecast value of the model is approximately 1.43 %, assigned a measured value of 1.57 %. The absolute difference between the observed and measured value is about 0.14 %. However, the data point 10 has only an absolute difference of 0.02 % (Observed: 1.43 %, Predicted: 1.41 %). Figure 8-2 provides the statistic overview regarding the model quality.

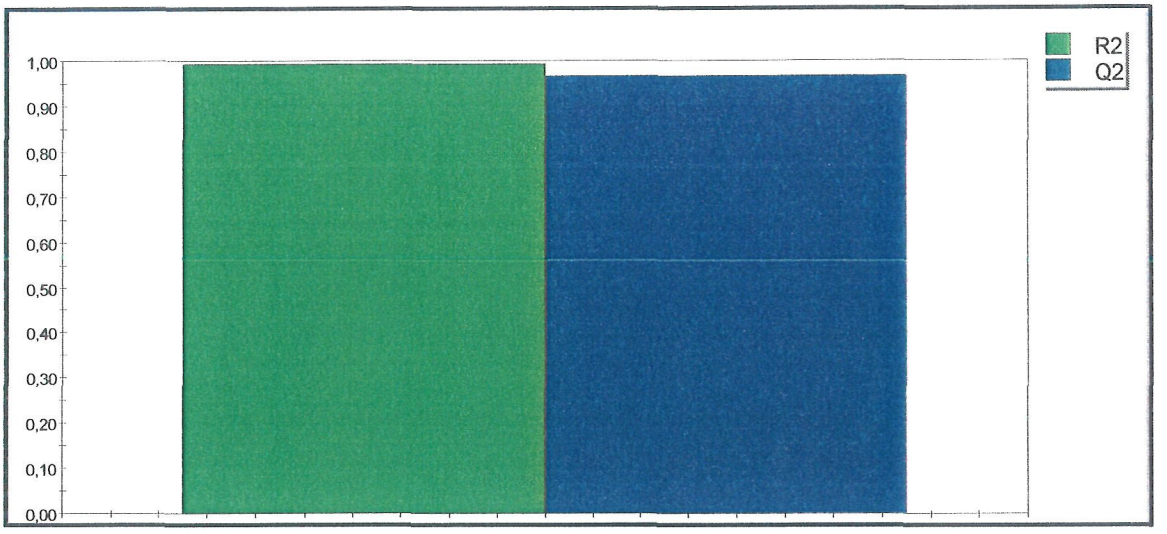

Figure 8-2: Statistic quality characteristic numbers of the model

The two characteristic values R^2 and Q^2 enable an evaluation of the forecasting ability of the model. In the following paragraphs these characteristic values are discussed briefly from the mathematical background. The characteristic value R^2 is a so-called "precision measure", and it indicates how well the adjustment of the model worked to the measured values. It is based on the dismantling the sum of the square deviations and sets the square sum of the residues SS_{res} (difference model value - measured value) in relation to the total square sum SS_{tot}, corrected around the average value.

$$R^2 = 1 - \frac{SS_{res}}{SS_{tot,korr}}$$

Equation 8-11

$$SS_{res} = \sum_{i=1}^{N} (y_i - \hat{y}_i)^2$$

Equation 8-12

$$SS_{tot,korr} = \sum_{i=1}^{N} (y_i - \bar{y})^2$$

Equation 8-13

$$\bar{y} = \frac{1}{N} \cdot \sum_{i=1}^{N} y_i$$

Equation 8-14

R^2	coefficient of determination
SS_{res}	square sum of the residues (difference measured value - model value
$SS_{tot,korr}$	total square sum of the measured values corrected around the average value
y_i	measured value in the data point
$\bar{y}$	arithmetical average value of the measured values
$\hat{y}_i$	model value in the data point i
N	number of data points

The higher the degree of the model adjustment is, the smaller SS_{res} becomes and the greater R^2. In a perfect model the total model adjustments $SS_{res} = 0$ and thus $R^2 = 1$. The disadvantage of these characteristic numbers is that their value rises in principle with the number of coefficients, due to the decrease in SS_{res}. Therefore, it is not possible to recognize a so-called "Over Fit". This results in an included modelling where the errors are taken by the model. Therefore, for the evaluation of the model quality the so-called Q_2-value, also termed PRESS-measure (Prediction Residual Error Sum of Squares), is consulted.

$$Q^2 = 1 - \frac{PRESS}{SS_{tot,korr}} = 1 - \frac{\sum (y_i - \tilde{y}_i)^2}{\sum (y_i - \bar{y})^2} \qquad \text{Equation 8-15}$$

Q^2	PRESS-value
$\tilde{y}$	model value estimated at one point which is not provided by actual measurements

Typically, the quality of this model can be objectively evaluated on the basis of these characteristic numbers. The available model for the value for R^2 is 0.996 and that for Q^2 about 0.868, this refers to an excellent model adjustment.

Parameters

To establish some central points and the boundaries of the field in which the companies are working the following additional experiments Table 8-2, had to be performed. They were necessary to describe the links between all the different parameters.

Content	Unit	Range
Ni	g/l	0 to 20
Cu	g/l	35 to 55
H_2SO_4	g/l	155 to 185
T	°C	50 to 70
Thio	mg/l	0 to 10
Glue	mg/l	0 to 12
i	A/m^2	250 to 1000

Table 8-2: Range of the investigated parameters

To describe the electrolysis conditions as accurately as possible the following range, Table 8-3, of investigated parameters was chosen.

Exp. Nr	Ni [g/l]	Cu [g/l]	H_2SO_4 [g/l]	T [°C]	Thio [mg/l]	Glue [mg/l]	i [A/m²]
1	0	35	155	70	10	12	250
2	20	35	155	50	0	12	1000
3	0	55	155	50	10	0	1000
4	20	55	155	70	0	0	250
5	0	35	185	70	0	0	1000
6	20	35	185	50	10	0	250
7	0	55	185	50	0	12	250
8	20	55	185	70	10	12	1000
9	10	45	170	60	5	6	625
10	10	45	170	60	5	6	625
11	10	45	170	60	5	6	625

Table 8-3: Experimental plan

After establishing the experimental plan and obtaining the experimental results, the model could be used to determine the significant results.

In principle the goal was to get two different results:

1) a model or equation to calculate or predict the polarization
2) coefficients for all used parameter to know their individual effects on the polarization.

It is important to understand the theory behind the software program.

To predict the polarization as accurately as possible the model must fit optimal, that means that R^2 as well as Q^2 should be as high as possible. To fit the model it could be necessary to add the square of single parameters or to add a combination of two parameters. To establish an interlink between the different parameters as exact as possible only the linear functions should be taken into consideration.

As already discussed the polarization measurements were performed as current density vs. polarization investigations /64/, that means that the current density - as detailed in the experimental plan Table 8-3 – is not an independent parameter. This means for the evaluation of the effect of different parameters due to the cathodic polarization that these current density polarization curves were used. Using this measuring system the current density was increased step by step. Therefore, these measurements did not provide any information about the influence of the current density. To ascertain this influence of the current density on the polarization it is necessary to perform investigations at stationary conditions including steady state potential measurements.

Model equation to calculate the polarization

After calculating the dependence of the single parameters, an evaluation of the main influences was performed. To fit the model it was necessary to add the square of the glue contents and the combination of glue and temperature. After these evaluations the model was checked as indicated in Figure 8-3 and it can be seen that the model fits very well; therefore, no further investigations under real conditions were necessary.

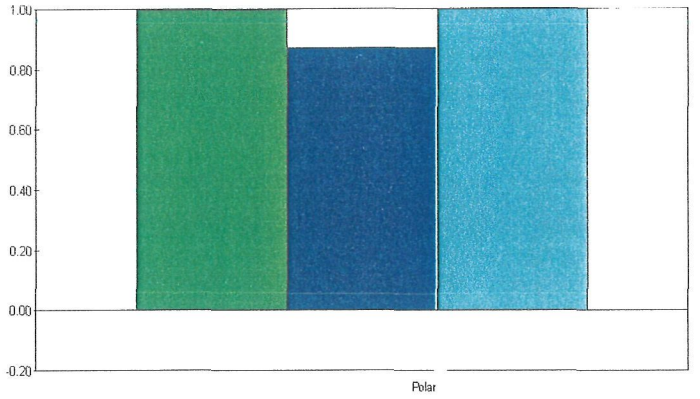

Figure 8-3: Summary of fit (Observed vs. Predicted Plot)

R^2
Q^2
Reproducibility

The plot in Figure 8-4 illustrates the observed versus predicted values of the response. By clicking on the line in the graphical toolbox one can display the regression line. With a good model all the points will fall on the 45 degree line. The plot below is an example of a good model. With worse models the points are scattered around the regression line.

Outliners in the relationship are points far away from the regression line. No points, which are demonstrating the polarization results, have to be removed. If one single parameter is picked out to describe the results and the method of evaluation it is possible to produce diagrams with polarization curves depending on all other parameters. For example the glue characteristics are illustrated. Glue has normally a polarization effect.

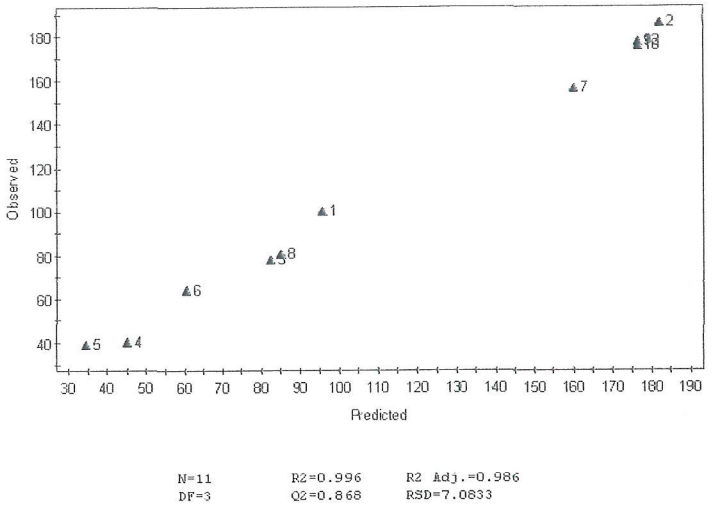

Figure 8-4: Polarization with experiment number labels

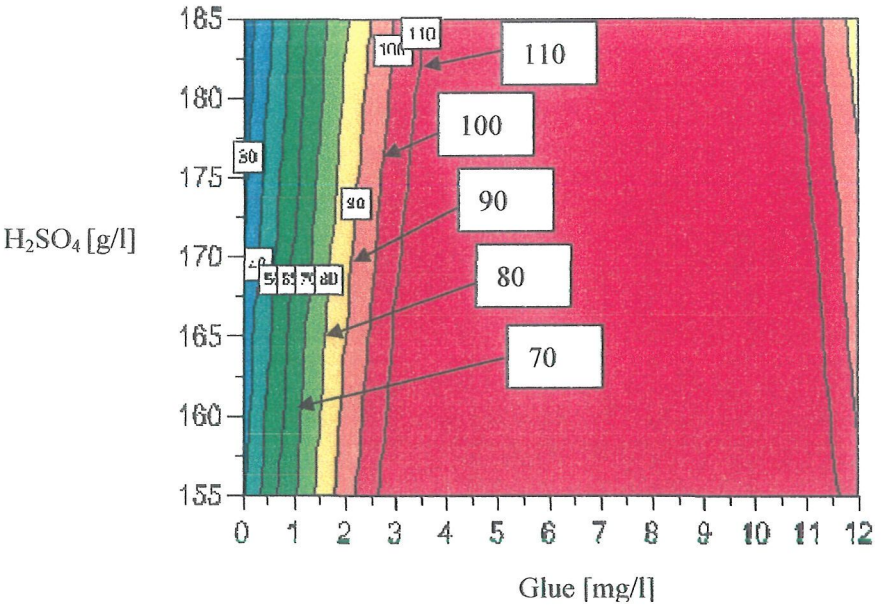

(a) T = 70 °C, Thio = 10 mg/l

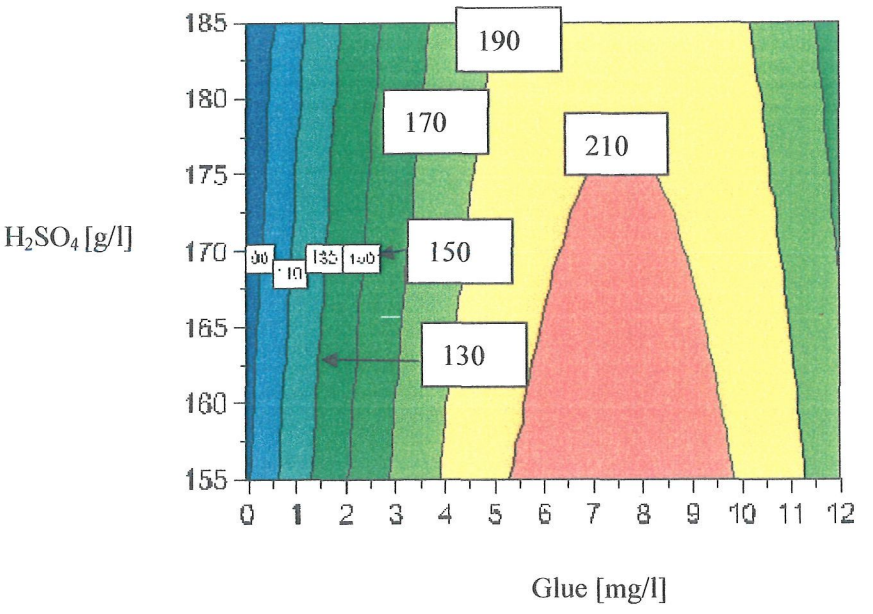

(b) T = 50 °C, Thio = 0 mg/l,

Figure 8-5: Glue effect depending on temperature, thiourea

In Figure 8-5 (a) the maximum of the thiourea content and the temperature is illustrated. It is recognisable that the polarization reaches a limiting value. After this value the polarization decreases again. The polarization values are between 80 and 110 mV. At lower temperatures and without any thiourea the cathodic polarization is between 90 and 210 mV. After reaching 7 mg/l glue content the polarization effect is also decreasing.

At low temperatures, without any thiourea and with a low concentration of acid the polarization is up to 210 mV.
By increasing the temperature and the thiourea content and increasing the acid concentration the polarization decreases, Figure 8-6.

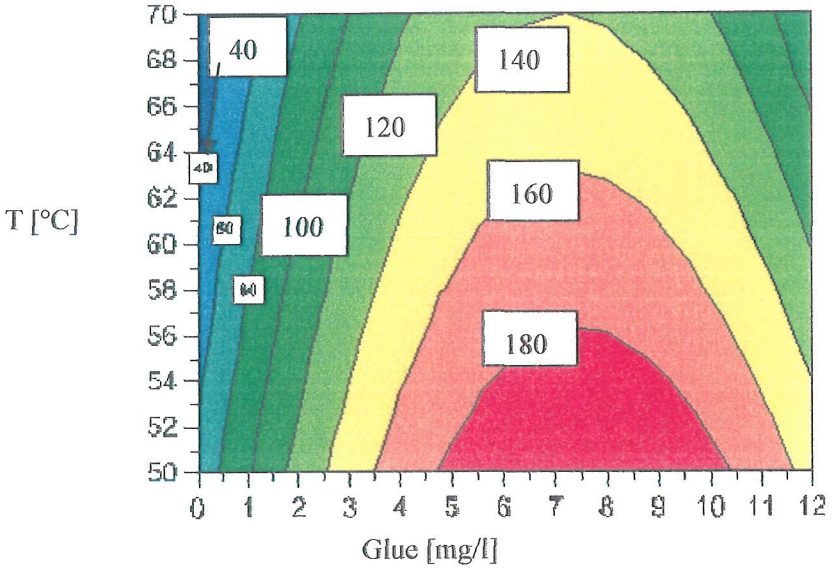

(a) Thio = 10 mg/l, H_2SO_4 = 185 g/l

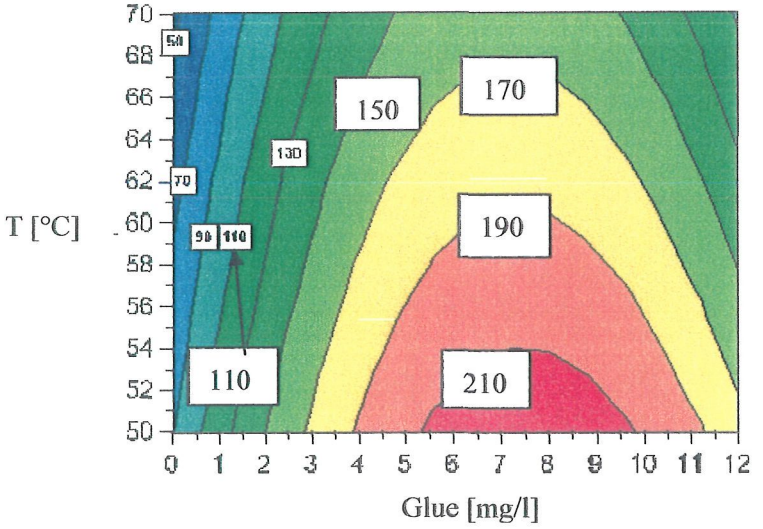

(b) Thio = 0 mg/l, H_2SO_4 = 155 g/l

Figure 8-6: Polarization depending on temperature [°C] and glue [mg/l]

At high acid concentrations the polarization effect has at 7 mg/l glue a maximum at 180 mV. By decreasing the acid concentration this maximum increases to 210 mV.

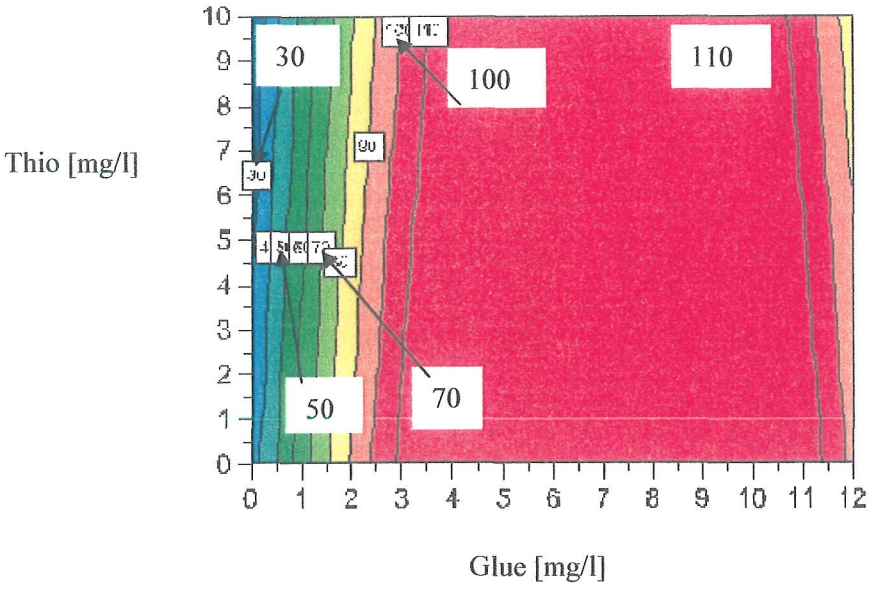

(a) T = 70 °C, H_2SO_4 = 185 g/l

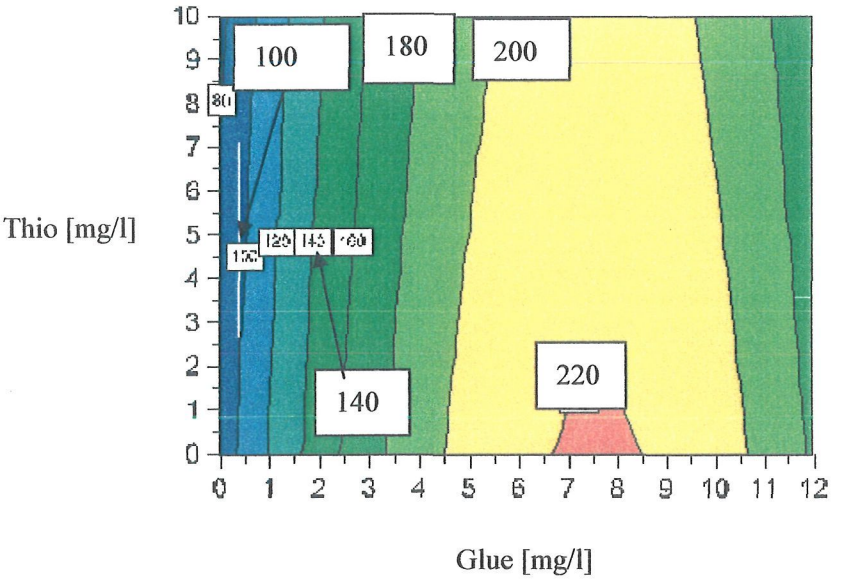

(b) T = 50 °C, H_2SO_4 = 155 g/l

Figure 8-7: Polarization effect of thiourea [mg/l] and glue [mg/l]

At lower temperatures the cathodic polarization increases tremendously.

To predict the cathodic polarization an equation was calculated. In this analysis the influence of the concentration of copper, nickel, sulphuric acid, thiourea, glue, the so-called current density (which resulted in the measuring method and is not a variable parameter), and the temperature on the cathodic polarization was calculated.

In this model the calculated polarization difference for a Cu concentration between 35 and 55 g/l and for a Ni concentration of 0 – 20 g/l was below 1 mV (investigated in /8/). In addition, the model asked for the parameter combination of temperature and glue, as well as glue squared. These combinations were necessary to fit the model more accurately.

Cathodic polarization equation: Equation 8-16

$$U = 176.567 - 7.27841 c_{H2SO4}^{*} - 25.1446\ T^{*} - 5.55104\ c_{Thio}^{*} + 33.5969\ c_{glue}^{*} + 2.4932\ i^{*} - 66.8033\ c_{glue}^{2*} - 4.965\ c_{glue}^{*} T^{*} \quad [mV]$$

c*, T*, i* standardized values

To calculate the polarization values of the companies the following equation has to be used for standardizing the single parameters:

$$\text{Stand. parameter} = 1 - 2 \bullet \frac{Max - Act}{Max - Min}$$

To ensure, that the model can be used in all different electrolyses a standardizing of the different parameters has to be done.
To get the standardized value the maximal value (Max), the actual value (Act) and the minimal value (Min) have to be used for the calculation.

An example of the polarisation calculation

Company E had c_{H2SO4} = 175 g/l, T = 63 °C, Thiourea = 53 g/t, Glue =31 g/t

Model range of H_2SO_4 155 to 185 g/l: $C_{H2SO4}^{*} = 1 - 2\frac{185-175}{185-155} = 0.333333 = \mathbf{0.33}$

Model range of T 50 to 70 °C: $T^{*} = 1 - 2\frac{70-63}{70-50} = \mathbf{0.3}$

Model range of thiourea 0 to 10 mg/l: $C_{Thiou}^{*} = 1 - 2\frac{10-6.15}{10-0} = \mathbf{0.23}$

Model range of glue 0 to 12 mg/l: $C_{Glue}^{*} = 1 - 2\frac{12 - 3.6}{12 - 0} = \mathbf{-0.40}$

Model range of the current density 250 to 1000 A/m²: $i^{*} = 1 - 2\frac{1000 - 337}{1000 - 250} = \mathbf{-0.77}$

$U = 176.567 - 7.27841 \cdot \mathbf{0.33} - 25.1446 \cdot \mathbf{0.3} - 5.55104 \cdot \mathbf{0.23} + 33.5969 \cdot (\mathbf{-0.40}) + 2.4932 \cdot (\mathbf{-0.77}) - 66.8033 \cdot (\mathbf{-0.40})^2 - 4.965 \cdot (\mathbf{-0.40}) \cdot \mathbf{0.3}$

U = 139.89 ~ 140 mV

The parameters influencing the equation are the standardized acid concentration (c_{H2SO4}*), the standardized temperature*, the standardized concentration of thiourea (c_{Thio}*), the standardized concentration of glue (c_{Thio}*) and the standardized current density (i*).

Company	H_2SO_4	H_2SO_4*	T	T*	Thio	Thio*	Glue	glue*	Ni	Ni*	Cu	Cu*	U
E	175.00	0.33	63.00	0.30	53.00	0.23	31.00	-0.40	15.00	0.50	46.00	0.10	140
B	172.00	0.13	65.00	0.50	78.00	0.81	75.00	0.45	20.00	1.00	50.00	0.50	157
C	200.00	2.00	60.00	0.00	60.00	0.39	35.00	-0.32	0.30	-0.97	42.00	-0.30	139
A	180.00	0.67	64.00	0.40	60.00	0.39	80.00	0.55	5.00	-0.50	45.00	0.00	155
F	150.00	-1.33	68.00	0.80	70.00	0.63	120.00	1.32	13.00	0.30	60.00	1.50	83
G	175.00	0.33	65.00	0.50	60.00	0.39	100.00	0.93	12.00	0.20	45.00	0.00	128

Table 8-4: Calculation of the cathodic polarization

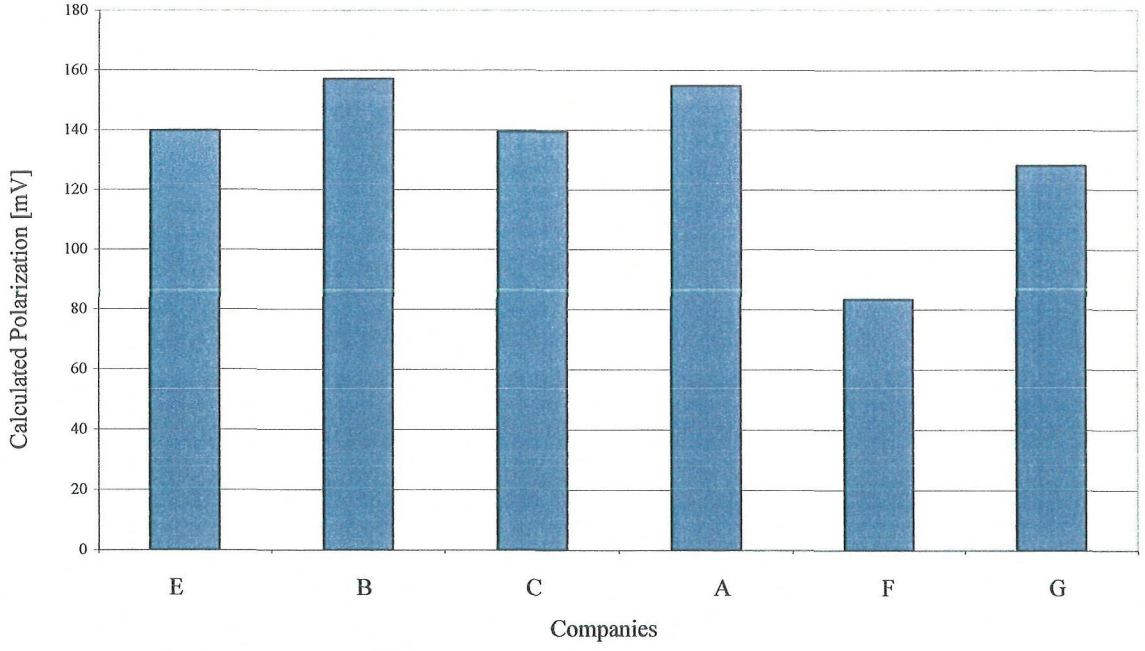

Figure 8-8: Calculated cathodic polarization [mV]

In Table 8-4 the different polarization values for the six companies are calculated. Therefore, it was necessary to change the absolute values and define the units for the model. The inhibitor amount was taken in mg/l, all other parameters in the known units (T in °C, c in g/l, i in A/m², U in mV).

The calculated cathodic polarization is between 83 mV and 157 mV. Figure 8-8 shows the calculated cathodic polarization for all investigated companies.

To show the quality of the Equation 8-16 the polarization of the experiments which are described at page 107 was calculated. In Table 8-5 it can be seen that the measured and calculated values are in good accordance.

	Up meas. [mV]	Up calc [mV]
Glue/thiourea 31/53	122	136
Glue/thiourea 30/60	137	133
Glue/thiourea 75/78	145	156
Glue/thiourea80/60	118	155
Glue/thiourea100/60	110	129
Without inhibitor	55	68

Table 8-5: Comparision of the measured and calculated polarization

8.2.1 Effect of single parameters

As mentioned, the second idea using such a mathematical model is to evaluate the effect of different parameters on a defined physical figure. During this work the influence of the concentration of copper, nickel, sulphuric acid, thiourea, glue, and the temperature on the cathodic polarization was calculated. For this work it is not allowed to use also the so-called current density due to the above mentioned reasons

$$U = 93.06 - 4.58\, c_{Cu^*} - 8.70\, c_{H2SO4^*} - 0.39\, c_{Ni^*} - 30.05\, T^* - 13.27\, c_{Thio^*} + 40.16\, c_{Glue^*} \quad [mV]$$

Equation 8-17

This equation could be read as (under the conditions of Table 8-2):

- The sign shows the polarization effects, like polarizing (+) and depolarizing (-).
- The most depolarizing effect has the temperature, which decreases the cathodic polarization by the factor 30.
- More than three times lower is the influence of the acid concentration by factor 8.7 and more than 6 times higher than the copper concentration by factor 4.6.
- Thiourea is about factor 13 and seems to have a slightly higher influence than the acid concentration.

- The nickel concentration is negligible.
- Glue is increasing the cathodic polarization by the factor 40. So it is shown the high influence of the glue concentration on the cathode precipitation.

Figure 8-9 shows the calculated effect of the mentioned parameter on the cathodic polarization.

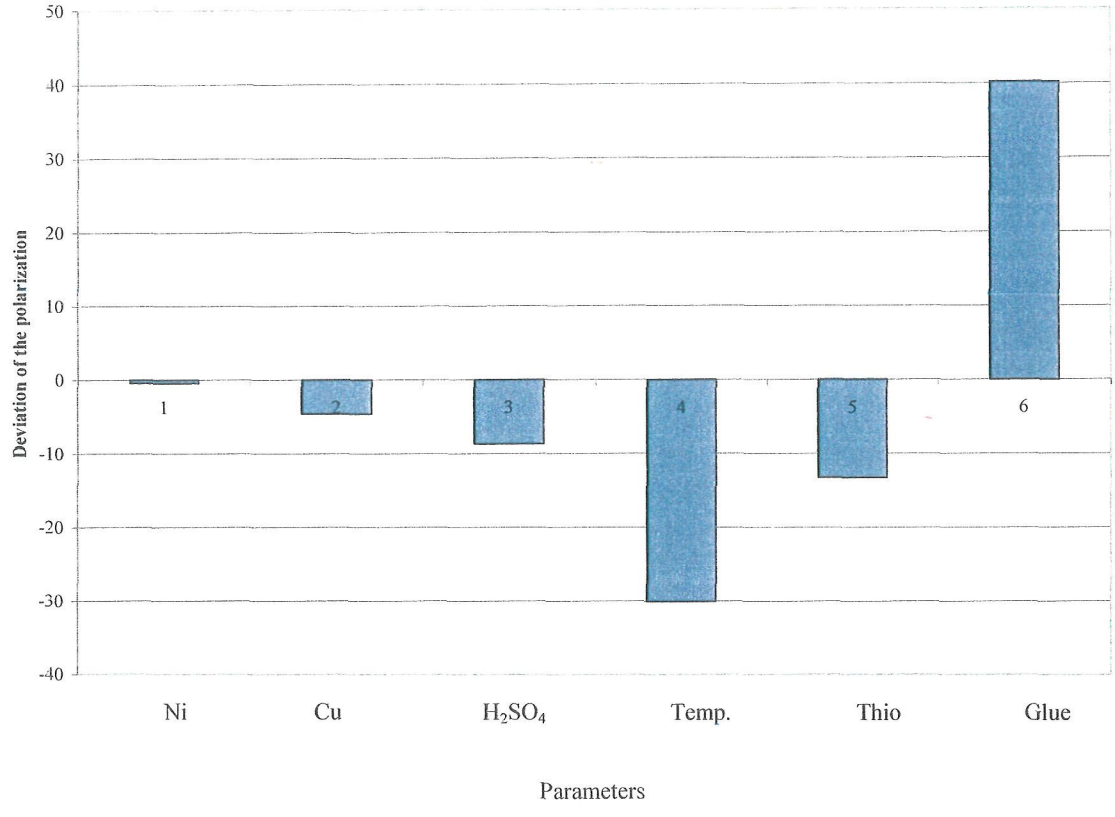

Figure 8-9: Scaled and centred coefficients for polarization

8.2.2 Discussion

Using the above calculated equations it is possible to evaluate the effect of different parameters on the cathodic polarization and to predict the cathodic polarization value for a certain electrolysis system.

For the defined parameter range the temperature, the thiourea concentration, the acid concentration, and the copper concentration have shown a depolarization effect whilst the glue concentration has increased the copper polarization.
The effect of nickel concentration was too weak in the defined parameter range.

In principle the calculated effects are in good correlation with the theoretical discussion (chapter 8.1.2).

Still there are several points which have to be considered:

a) Once again, this evaluation is calculated for the defined parameter range.

b) The polarization investigations were done in a lab scale electrolysis cell and e.g. the electrolyte flow behaviour and the inhibitor distribution in the vicinity of the electrodes are different compared to a technical cell.
c) The equation for the effects of the investigated parameters was calculated for a fixed current density. That means that one of the most important parameter wasn't included in the model. As mentioned before due to the kind of measurement – current density via potential – it was not possible to include the current density as an independent value.

Parallel to the polarization investigations experiments (see chapter 7) have been carried out. These investigations have shown the importance of the current density.
The actual current density is of course an important parameter but it is not only the current density, but also the ratio actual current density to limiting current density has to be considered.

According to Fick's law the current density is given as:

$$i = \mathrm{n} \cdot \mathrm{F} \cdot \mathrm{D} \cdot \left(\frac{\partial \mathrm{c}}{\partial \mathrm{x}} \right)_{x=0} = \mathrm{n} \cdot \mathrm{F} \cdot \mathrm{D} \cdot \frac{\mathrm{c}^0 - c^s}{\delta_N}$$

Equation 8-18

As soon as the concentration c^s becomes zero the limiting current density is reached (Equation 8-19).

$$i_o = \mathrm{n} \cdot \mathrm{F} \cdot \mathrm{D} \cdot \frac{\mathrm{c}^0}{\delta_\mathrm{N}}$$

Equation 8-19

The limiting current density increases linearly with an increase of concentration c^0, with an increasing diffusion constant and a decreasing diffusion boundary layer δ_N. Because the diffusion constant and the concentration of solute cannot be influenced extensively, an increase of limiting current density can be obtained mainly by a decrease of diffusion boundary layer. Steady state diffusion boundary layer is defined by hydrodynamic conditions in front of the electrode surface.

In the past a lot of investigations were done, especially at the Department of Nonferrous Metallurgy at the University of Leoben, Austria /85, 84, 78/. In /85/ a method is described to calculate the limiting current density for a certain electrolysis arrangement. Due to the importance of the hydrodynamic conditions in the electrocrystallization of the copper precipitation the methods for a mathematical optimizing of the electrolyte flow should be given in the next chapter.

The relation between electrolyte flow and mass transport during electrolysis is modelled by computational fluid dynamics (CFD).

8.3 CFD – Computational Fluid Dynamics Calculation

Today it is possible to describe a lot of metallurgical processes with the use of mathematical and physical models. The Finite-element-method (FEM) or the method of the finite volumes (Computational Fluid Dynamics, CFD) could be the methods for mathematical modelling.

These days the use of mathematical modelling is widely accepted in all industrial sectors. During the last years the use of CFD modelling for the copper electrolyse was developed /79, 80, 81, 82/.

8.3.1 Fundamentals of the CFD Modelling

The numerical calculation of fluid flow or heating and temperature distribution is possible, if the physical laws can be transported into mathematical equations, normally into differential equations.
Each single differential equation is linked to a certain conservation law and consists of one physical value as a dependent variable. It is assumed that the different factors influencing the physical value are in equilibrium.
The dependent variables of these differential equations are used as specific values, they are calculated of one device volume. Examples are the velocity (momentum per device volume), the mass or rule of agitation and the specific enthalpy/energy. The temperature that is often given as dependent variable is not a specific value, because it is a compound in a fundamental equation with the energy/enthalpy equation.
The single term of a differential equation shows the influence of an imaginary unit volume. An example of the continuity equation, the conservation of mass will be calculated of a two dimensional field.

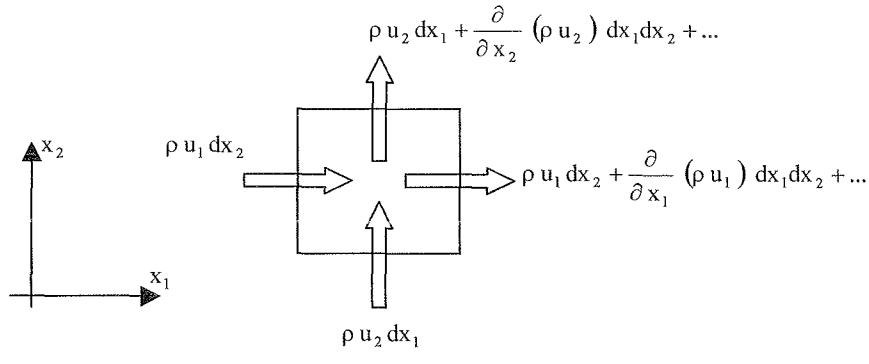

$$\frac{\partial}{\partial t}(\rho\, dx_1 dx_2) = \rho u_1 dx_2 + \rho u_2 dx_1 - \rho u_2 dx_1 - \frac{\partial}{\partial x_2}(\rho u_2) dx_2 dx_1 - \rho u_1 dx_2 - \frac{\partial}{\partial x_1}(\rho u_1) dx_1 dx_2 - \ldots$$

Figure 8-10: Two dimensional area field /83/

Looking at Figure 8-10 an element in the two dimensional space with the edge dx_1 and dx_2 is shown. The continuity equation is the result of the calculation in both directions x_1 and x_2 with taking care of the changing in time of the density– according to the mass input per volume in kg/m³.

$$\frac{\partial \rho}{\partial t} + \frac{\partial}{\partial x_1}(\rho u_1) + \frac{\partial}{\partial x_2}(\rho u_2) = 0$$

Equation 8-20

The differential equation, which describes the conservation of momentum for one direction of one volume element of a Newton 's fluid, can be calculated in a similar way like it is described before. With u for the velocity vector and u_1 as the velocity component in x_1-direction it can be described:

$$\frac{\partial \rho u_1}{\partial t} + div(\rho u u_1) = div(\mu grad u_1) - \frac{\partial p}{\partial x_1} + Bx_1$$

Equation 8-21

with μ as the viscosity, p the pressure and B as „body force" in x_1-direction, for example the gravitational acceleration. The individual parts of this differential equation describe the different kinds of momentum transportation. The first part of the term $\delta(\rho u_1)/\delta t$ means the rate of momentum exchange (changing the velocity) per time interval, the term $div(\rho u u_1)$ the convective flow of the momentum, which will be transported, caused by the general velocity field u. The term div(μ gradu_1) shows the diffuse part of the momentum transport, with the meaning of μ gradu_1 in combination with the Fick's diffusion law:
The viscosity μ corresponds to the „diffusion coefficient" of the momentum and gradu_1 to the differential of the momentum of the volume element. The term $\delta p/\delta x_1$ shows the part of the pressure force to the complete momentum calculation. The momentum conservation equation is being called Navies-Stokes-Equation.
The now described conservation of momentum equation is only working in the case of laminar conditions but turbulent flows occur in nearly all technical processes. Only in very special cases and under extreme computing time it is possible to solve the instationary turbulent flows. At numerical flow calculation it is common to use time depended and ensembled values of the dependant variables, for example velocity, density, etc.
For these calculations it is normal to think of an average because a fast and hazardous fluctuation will be present.

In the equation of conservation the current variables on a volume element through the sum of the ensemble calculated values ⟨u⟩ and the deviation u′ of the calculated value are replaced by u, for example B for the velocity component:

$$u = \langle u \rangle + u'$$

Equation 8-22

The correlation of the velocity fluctuation is not known and that's why it must be calculated with a turbulence model. This kind of solving the equation system is called closing the system. In this case it is important that the apparent transverse strain is mainly caused by the bigger turbulence conglobe. This big turbulence conglobe gives its energy to smaller whirls through vortex filament extension till the velocity gradient of the smallest turbulence elements is very steep, so that the transformation into the inner energy can take place.
This transport of energy in the turbulence energy spectrum to bigger wave numbers will be called as turbulence energy cascade.

The feed of energy into these cascades is not depending on the viscosity. It will take place through transmission of energy of the average movement of the apparent shearing strain to the big turbulence elements. This energy will be passed on from a small turbulence element to the next one till it is at the dissipation. This is also the reason that the distribution of the average velocity at turbulent flow depends only to a small extent on the Reynolds number, although the viscosity causes the loss of energy.
In case of going through the energy cascade the information of direction of the velocity will be lost. This means that the fluctuation energy in the cascade will be distributed into all directions. The smallest turbulence elements are isotropic. This is normal at turbulent flows with big velocity gradients. These flows are called locally isotropic.

The dependent variables ϕ must be transported into an average value $\langle\phi\rangle$ and the fluctuated component ϕ':

$$\phi = \langle\phi\rangle + \phi'$$

Equation 8-23

For a static stationary flow ϕ is the temporal average:

$$\langle\Phi(x_0)\rangle = \underset{t_0 \to \infty}{\text{Limit}} \frac{1}{2 \cdot t_0} \int_{t=-t_0}^{t=t_0} \phi(x_0, t)\,dt$$

Equation 8-24

Many different turbulence models are used. For practical and technical working, here the so-called k-ε-Model from Harlow and Nakayama /83/ will be taken. The k-ε-Model solves two more partial differential equations for the turbulent kinetic energy k

$$k = \frac{\overline{u_i'^2}}{2}$$

Equation 8-25

and their dissipation ε

$$\varepsilon = C_{\mu}^{3/4} \frac{k^{3/2}}{l_t}$$

Equation 8-26

In the equations which are described, l_t stands for a characterise turbulent whirl length.

8.3.2 Model description

An overview concerning different models and different fluid flow behaviour calculations is given by /84/. In /85/ also mass transport phenomena in the vicinity of the electrodes are modelled and a method to calculate the limiting current density is given.

However, all existing models are usable for an optimization of the flow conditions of an industrial electrolysis cell only to a very limited extent. The root of the problem lies in the insufficient computer achievement for the description of the three-dimensional conditions of an electrolysis cell. In the models already existing the following procedures have been chosen:

- either the selected computation area was too big, then the solving of the procedures very close to the electrode was not possible,
- or the phenomena in front of the electrodes were dissolved and therefore it was possible only to consider a very small range with a two dimensional calculation.

The total height of the computed system in /85/ is only 25 cm, but the layer thickness of the cells in front of the electrodes was just 0,057 mm. At that time 5000 cells were used for the description of the system. At this time (in the year 2000) the commercially available CFD software of programs could dissolve approximately 250,000 cells. Today's programs manage about 10 times as much.

Therefore it was undertaken to attempt a model that makes it possible to describe the procedures in electrolysis mathematically and enables to accomplish an optimization of the procedures.

Soon it had to be recognized that due to the complexity of this system it must be differentiated between a general view of the electrolyte and a specification of the procedures close to the electrode. The unification into one model due to insufficient computer achievements is not purposeful.

The considerations must proceed from an accurate description of the individual processes:

8.3.2.1 Detailed modelling of the copper refining electrolysis

The most substantial point of the mathematical modelling is to describe the physical and physicochemical procedures of the copper refining electrolysis in a mathematical way. The physical dimension, to which the electrical crystallization leads, is the polarization. A mathematical representation of the polarization value of the cathode at each individual point in dependence of the electrolysis parameters is the goal of the detailed modelling.

In the following part of this work the dependence of the polarization on the electrolysis parameters will be discussed. Their mathematical modelling shall be checked.

As already described in cap. 8.1.1.2 the polarization consists of:

$$\eta_{ges} = \eta_T + \eta_C + \eta_D + \eta_R + \eta_\Omega$$

Evaluating the single terms (see chapter 0) the following conclusions are made:

The transfer polarization η (8.1.1.2.1) is mathematically described as a function of:

T absolute temperature, which can be calculated for each point at the cathodic surface,

i current density, which can be chosen as one of the boundary condition for the model,

i_0 limiting current density, which itself is a function of the diffusion constant (which is a function of the absolute temperature T), the copper concentration, and the diffusion boundary thickness. The diffusion boundary thickness and therefore the limiting current density is strongly influenced by the electrolyte flow conditions.

For the crystallization polarization η_C (see chapter 8.1.1.2.2) there is no formula available. Of course the crystallization polarization is influenced by the content and distribution of the inhibitors, and by the electrolyte composition in general. These factors are part of the polarization equation which is given in chapter 8.1.1.2. That means that the crystallization polarization is just part of the general polarization and no explicit calculation will be done.

The diffusion polarization η_D (Equation 8-7) is again a function of the absolute temperature T, the current density i, and the limiting current density i_0.

For the mathematical model it is assumed that the reaction polarization is just part of the general polarization.

The resistance polarization is now used to calculate the current density distribution of the cathodic surface. The current density can be chosen as a boundary condition. Due to an uneven temperature distribution and uneven geometrical conditions a certain current density distribution occurs. Using the model it is possible to calculate the temperature at each single point and also a certain resistance polarization based on the distance between the electrodes. The correlation between the current density distribution and the distances between the electrodes is linear.

Using the calculated polarization equation (see page 129)

$$U = 176.567 - 7.27841 c_{H2SO4}^* - 25.1446\ T^* - 5.55104\ c_{Thio}^* + 33.5969\ c_{glue}^* + 2.4932\ i^* - 66.8033\ c_{glue}^{2*} - 4.965\ c_{glue}^* T$$

the general polarization can be calculated in each single point at the cathodic surface. As discussed in chapter 8.2.2 the very important parameters current density and limiting current density are not included. There are two possibilities to consider these parameters:

a) the polarization investigations have to be done under different current densities and different electrolyte flow conditions which are directly related to different limiting current densities or
b) the limiting current density will be calculated using a method as described in /85/.

To do the above mentioned polarization investigations for different current densities under different electrolyte flow conditions in a lab scale cell is not really useful because the link to the reality cannot be done. That means that at present calculating it is the best way to include this parameter by the limiting current density separately. Based on such a calculation a ratio between the actual current density and the limiting current density has to be calculated and a factor has to be defined.

The final polarization can be calculated as

$$\eta_{calc} = \eta_{ges} \cdot f_i \qquad \text{Equation 8-27}$$

The f_i factor can be written as:

$$f_i = k \cdot (i/i_0)^x \qquad \text{Equation 8-28}$$

k is a constant which has to be defined in a further work, i/i_0 means the ratio between actual current density and limiting current density, and x has to be defined also.

To calculate the so-called calculated polarization in each point of a cathode a detailed model has to be used. To calculate the limiting current density the gradients in the vicinity of the electrodes have to be calculated and therefore a lot of cells are necessary. Furthermore, the calculation should be done using a one-phase solver calculating all necessary Navies-Stokes-Equations. To describe the relation between dissolved and precipitated copper in front of the electrodes and the electrolyte density and to calculate the polarization in each volume element in the model so-called user functions have to be defined. Commercially available software programs provide only a very limited possibility to do this. That is the reason why for the detailed model an open (private) code should be used.

With such a fine calculation grid it is not possible to calculate the whole electrolyte behaviour using such a model. Therefore, a second simplified model should be used also.
The calculation with the simplified model should describe the electrolyte velocity between the electrodes, the temperature distribution, and the inhibitor distribution all over the electrolysis cell.

8.3.2.2 Simplified model

To optimize the electrolyte flow in a technical cell the whole cell has to be calculated. Although the available software programs can handle more than a million of grid cells the dimension of the single cells are too big to calculate the phenomena in front of the electrodes as already discussed.

The goal of the simplified calculation is to describe and to optimize the electrolyte flow in the whole electrolysis cell. The commercial CFD software Fluent was used. To do the calculation as simple as possible (which means as fast as possible) an already existing Navier-Stokes-equation was used to define the correlation between copper concentration in the electrolyte and the density.

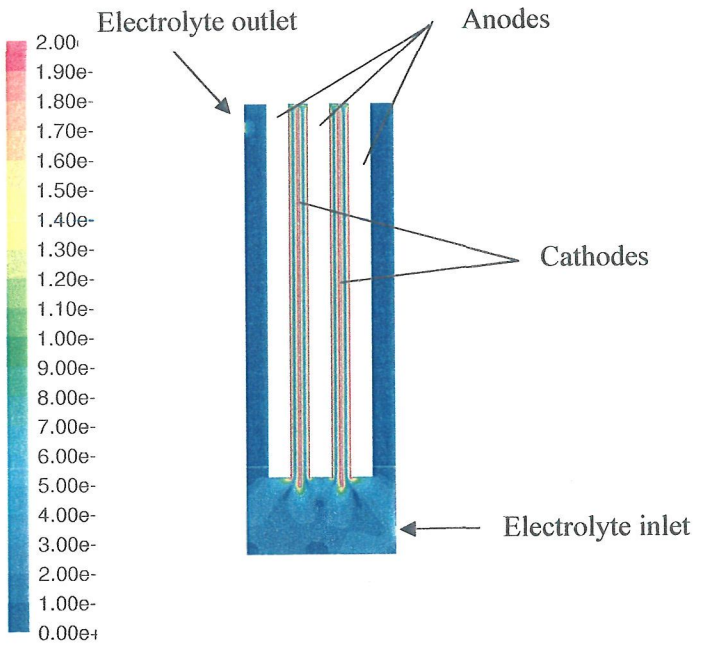

Figure 8-11: Velocity distribution in m/s in the near technical cell.

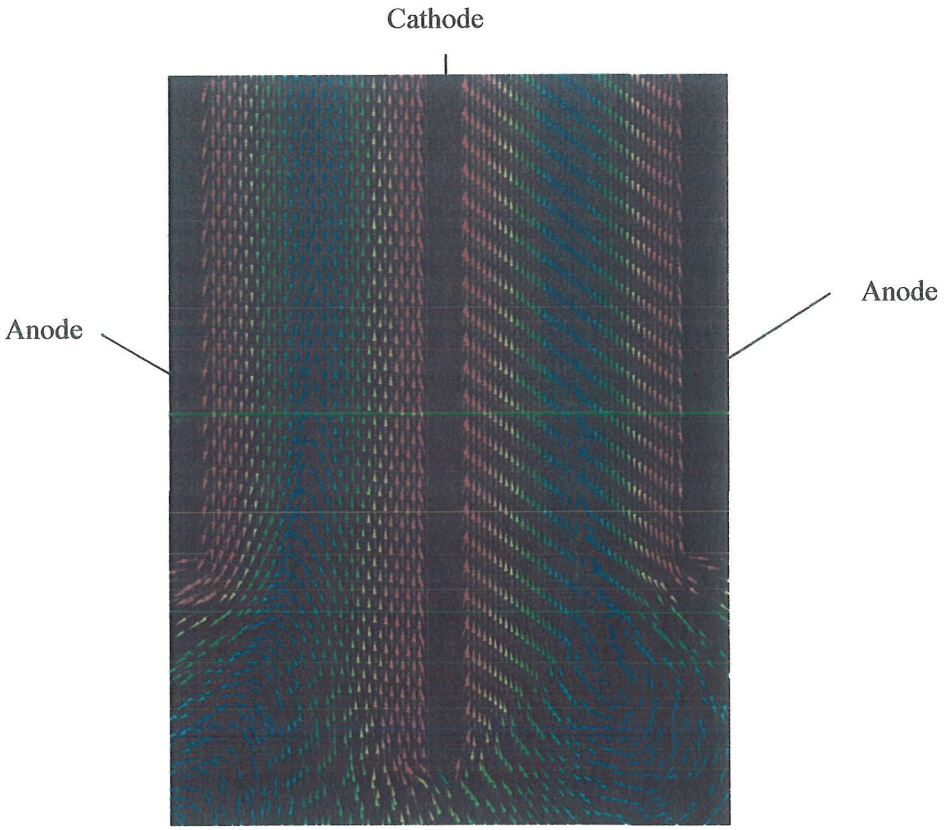

Figure 8-12: Velocity distribution in front of the cathode

In principle a potential field was defined and linked with a density. To calculate the density change due to the anodic copper dissolution and to the cathodic copper precipitation the change of the scalar value of the potential field has to be calculated.

As a first trial for this potential field the Navier-Stokes-equation for the temperature profile was used. To allow just the movement which is driven by convection the diffusion term of the heat transfer term was switched off.

Figure 8-11 shows the velocity distribution in m/s for the near technical cell arrangement. It can be seen, that the electrolyte goes down in front of the anodes and goes up in front of the cathodes. It can be seen also, that the natural convection is much more important than the forced convection. The forced convection was calculated according to the parameters which were used in the near technical scale investigations.

Figure 8-12 shows the velocity distribution between the central cathode and the two anodes more in detail. The absolute velocity in front of the electrodes and also the velocity distribution over the electrode gap was in good correlation with /79/. The calculation time was minimized because no additional equation had to be solved.

Such a simplified model can be used for an electrolyte flow optimization because it is possible to model a whole cell three-dimensionally. The informations which are generated by the simplified model e.g. velocity field between the electrode, can be used to calculate the limiting current density and afterwards the polarization on the cathode surface.

A full mathematical modelling of an electrolysis cell has to be done in three steps.

a) Calculation of an optimized velocity distribution in a technical electrolysis cell using the simplified model. The temperature distribution and the inhibitor distribution should be optimized in the same step.
b) Calculation of the limiting current density in front of a cathode using the detailed model.
c) Calculation of the polarization value in each point of a cathode.

Knowing that a current density distribution variation of more than 100 % is quite normal in a tankhouse the potential of an optimized cell could be seen by 50 % at least. That means that current densities up to 500 A/m^2 could be possible in an optimized copper refining cell.

At the very first beginning a CFD calculation was also used to find out the best possible cell arrangement to be as comparable as possible to real technical cells

8.3.3 Optimization of the flow conditions

The target was to construct and build a cell where the flow conditions are simulated to be very close to the conditions of a cell used in industry.

In order to carry out near industrial tests a semi-technical experimental plant was built. In this installation the height of the test electrodes corresponds to that of industrial ones. The width was chosen to be 10 cm for the anodes and 11 cm for the cathodes. To find out the best cell/electrode arrangement two variants have been calculated using the CFD software Fluent:

I: One cathode between two anodes

II: Three cathodes with two anodes in between

The evaluation was done by the following criteria: All experiments have to be performed as near as possible to industrial scale; that means that the arrangement of the electrodes leads to similar fluid flow conditions as industrially. The different behaviour of the anode air side and mould side and its influence on the cathodic copper deposition must be reflected. For a systematic investigation of this effect it has to be taken into consideration that a mixing-up of the electrolyte between cathode and anode air side on the one hand and between cathode and anode mould side on the other hand has to be minimized. The cathodic current density - one of the most important parameters – must be set exactly
($\pm$ 0.5 A/m^2).

The advantage of variant I is that the difference in electrolyte composition between cathode – air side and cathode - mould side should be more pronounced, because the active anode surface is lower than with variant II. The disadvantage, however, is that one side of each anode has to be deactivated. In the first tests this was done by covering with a foil. But problems arose due to the insufficient durability of foil and glue. The latter dissolved in the acid electrolyte and went into the electrolyte as an impurity.

In case of variant II it is necessary to cover the outsides of the two cathodes to achieve industrial conditions. These sides could be covered by a Macrolon® plate without glue. For the test results only the cathode in the middle was used and no inaccuracies could occur since the two outer cathodes did not influence the current density at this cathode surface.

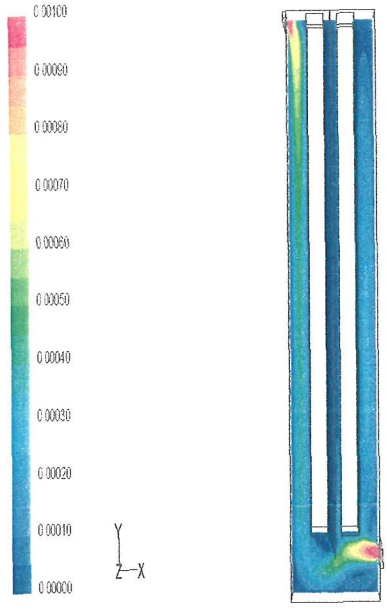

Figure 8-13 : Cell with one cathode

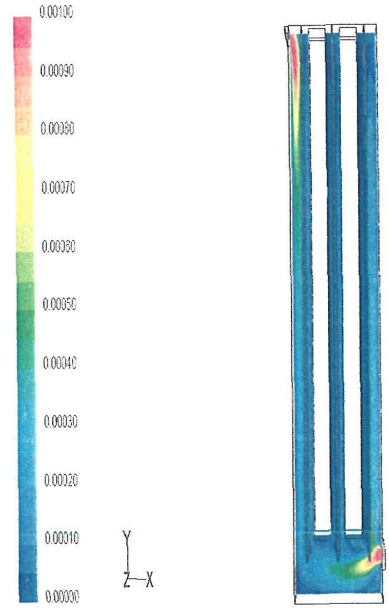

Figure 8-14: Cell with three cathodes

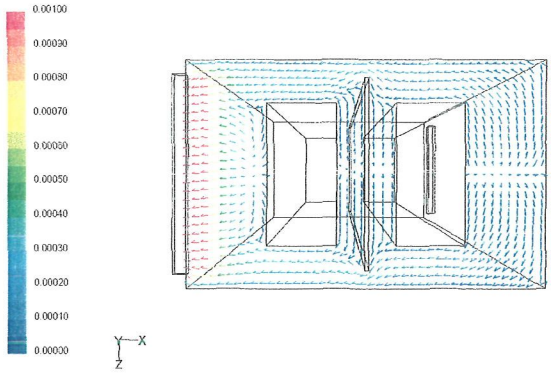

Figure 8-15: Fluid circulation [m/s²] at the top in I

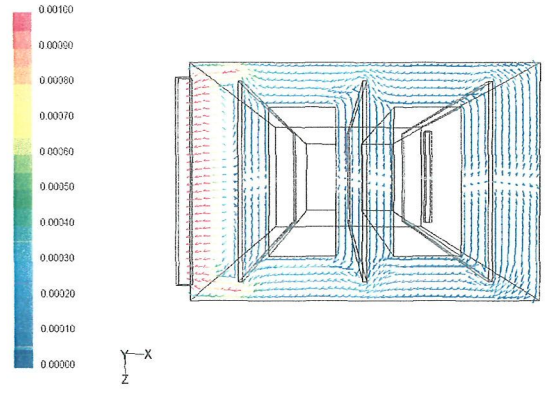

Figure 8-16: Fluid circulation [m/s²] at the top in II

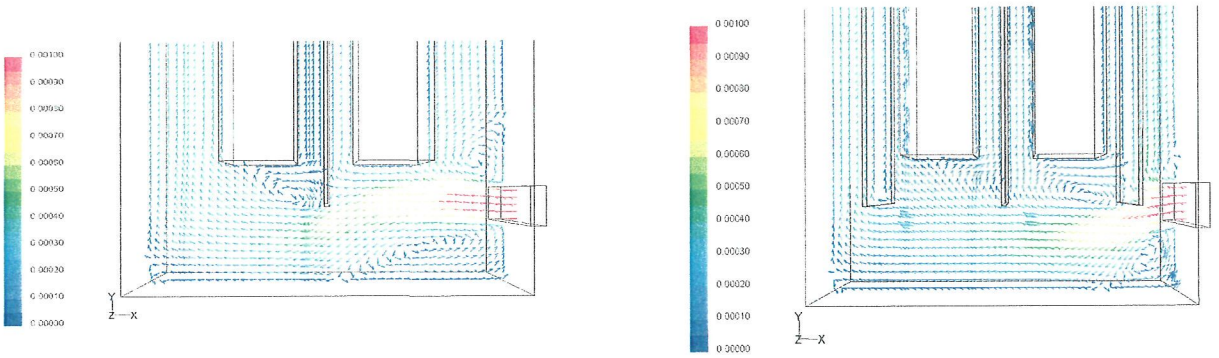

Figure 8-17: (a) Fluid circulation [m/s²] at the bottom in I (b) Fluid circulation [m/s²] at the bottom in II

To get a better understanding of the fluid flow dynamics in the semi-technical cells a fluid flow simulation was done for both variants.
The experimental equipment was modelled (scale 1:1). The volumes of the CFD calculation were built up by 200,000 single cells. The following limiting conditions have been assumed: Only the forced convection was taken into consideration. Furthermore a pure steady streamline flow was taken into account. For the upper surface of the electrolyte (a "free" surface) the term "specified shear stress = 0" was used, which represents a wall without shear stress.
The electrolyte density was taken as 1181.81 kg/m³ and its viscosity as 0.00112586 kg/ms /86/.
In Figure 8-13 the cell arrangement with one cathode and two anodes is shown, whereas, in Figure 8-14 three cathodes and two anodes were used. In both cells the electrolyt inlet were at the right side at the bottom of the cell and the electrolyte outlet was an overflow on the left side (top part). In these figures the general flow vectors are seen.
In Figure 8-15 and Figure 8-16 the fluid circulation at the top layer of the electrolyte is predicted. Here are no significant differences are recognizable. In Figure 8-17 (a) the fluid flow at the bottom of the cell is shown. The electrolyte flow goes mainly along the outside of the two anodes. At the first cathode face (right side) the electrolyte flow achieves as high as at the anode side, whereas at the left side of the cathode a quite lower flow rate exists. So no regular electrolyte distribution can be guarantied by this cell arrangement. In Figure 8-17 (b) the equal electrolyte flow at each available space between anode and cathode is shown. So the transportation of fresh electrolyte is fixed by using this cell system.

8.4 Conclusion

After measuring the cathodic polarization a mathematical evaluation was performed. This resulted in an equation that makes it possible to calculate the polarization with in a defined framework of the electrolysis parameters. The resulting equation for the calculation of the polarization (mV) is:

$$U = 176.567 - 7.27841 c_{H2SO4}^* - 25.1446\ T^* - 5.55104\ c_{Thio}^* + 33.5969\ c_{glue}^* + 2.4932\ i^* - 66.8033\ c_{glue}^{2*} - 4.965\ c_{glue}^* T$$

Furthermore, such a mathematical model has been used to evaluate the effect of the different electrolysis parameters on a defined physical parameter, the polarization. The influence of the concentration of copper, nickel, sulphuric acid, thiourea, glue, and the temperature on the cathodic polarization was calculated. The difference between these two equations is that for the second equation only linear terms were employed.

$$U = 93.06 - 4.58\ c_{Cu^*} - 8.70\ c_{H2SO4^*} - 0.39\ c_{Ni^*} - 30.05\ T^* - 13.27\ c_{Thio^*} + 40.16\ c_{Gluc^*} \qquad [mV]$$

This equation can also be written as:

- The sign shows the polarization effects, for example polarizing (+) and depolarizing (-).
- The most depolarizing effect was the temperature, which decreased the cathodic polarization by a factor of 30.
- More than three times lower was the influence of the acid concentration with a factor of 8.7 which was more than 6 times higher than the copper concentration with a factor of 4.6.
- Thiourea was about a factor of 13 and seemed to have a slightly higher influence than the acid concentration.
- The nickel concentration was negligible.
- Glue showed polarizing effects. Glue increased the cathodic polarization by a factor of 40. Thereby, the high influence of the glue concentration on the cathode precipitation in the electrolysis system was demonstrated.

The calculated polarization has not included the influence of the ratio of current density and the limiting current density.

After using the mentioned mathematical program to describe the polarization as a mathematical equation the electrolysis cell was calculated with the CFD software Fluent. The goals of the simplified calculation were to describe and to optimize the electrolyte flow in the whole electrolysis cell which was separated into:

- Forced convection:
  A calculation of the forced convection which is influenced by the position of the electrolyte inlet, outlet, and electrolyte flow rate was performed.
- Natural convection
  The natural flow of the electrolyte caused by the variation in the copper concentration in the electrolyte and the density was calculated.

9 SUMMARY

A statistical evaluation of the different tankhouse parameters was performed to evaluate their influence of the tankhouse parameters to the formation of shorts, which are the result of irregular cathodic precipitation

The range of working parameters is listed as follows:

Casting weight tolerance:	4 to 15 kg
Anode thickness:	37 to 50 mm
Cathode crop:	5 to 12 days
Anode-cathode distance:	18.5 to 33.5 mm
Current density:	242 to 337 A/m^2
Glue to thiourea ratio:	0.58 to 1.71 g/t of cathodic copper
Glue:	31 to 120 g/t
Thiourea:	45 to 70 g/t
Chlorine:	35 to 50 mg/l
Temperature:	60 to 68 °C
Electrolyte flow rate:	15 to 40 l/min
Content in the anodes of Ni:	24 to 4100 ppm,
Oxygen:	1140 to 3500 ppm.
MFRI in the anodes:	0.77 to 17.88
MFR II in the anodes:	0.42 to 3.92

Altogether 150 cross sections, that means 150 cathode samples with one or more dendrites were examined.

The influence on the cathodic precipitation can be described as:

- Impurities like anode slime particles, mould coating particles, and particles on the cathode surface from outside cause a polarization modification at the cathode. It was seen clearly that after the formation of holes and leaks dendrites started to grow.
- Too much mould coating on the anode does not dissolve in the electrolyte and these particles can be transported to the cathode. At the cathode surface they are nuclei for dendrites. If a dendrite is already formed, the insoluble mould wash can be mounted into the copper precipitation.
- The influence of the inhibitor on the cathode precipitation was:
  A relative high glue/thiourea ratio resulted in a fine grain size of the copper crystals due to the polarization increase.
  A relative low glue/thiourea ratio caused fine clefts over the entire copper precipitation.
  If the inhibitor dosage varied during the cathode crop, crystallization layers with different sizes of copper crystals were detected.
- The anode slime particles at the cathode surface form a nucleus for irregular crystal growth and/or the anode slime particles influence the cathodic polarization and furthermore the crystallization behaviour.

A clear allocation of the cross sections to the conditions in the tankhouse was seen. That's why the occurrence of the dendrites at the cathodes can be attributed to operating conditions in the cells.

Investigations on the anode

Anode roughness:	differences up to nearly 7 mm
Anode thickness:	up to 6 mm variation
Oxygen content in the anode:	0.234 % at the air side and 0.192 % at the mould side
Pb, As, Ag, and Se content:	differences up to 100 ppm between air side and mould side.

Investigations in different electrolysis cells

- Current densities between 350 and 500 A/m² have no influences.
- Geometrical variations showed a current density variation of more than 100 % (that means up to 700 A/m²) and the uneven current density distribution over the whole cathode surface forced the dendritic copper growth.
- The chemical qualities of the anodes have shown low effects, but only at well controlled systems.
- The amount of solid particles (anode slime, mould coating and $PbSO_4$) influenced the roughness of the cathodic precipitation between 10 and 50 µm in 24 hours.

After measuring the cathodic polarization the mathematical description of the different parameters was done.

This results in two equations. The first equation makes it possible to calculate the polarization in a special frame of electrolysis parameters and is listed in mV

$$U = 176.567 - 7.27841 c_{H2SO4}^{*} - 25.1446\ T^{*} - 5.55104\ c_{Thio}^{*} + 33.5969\ c_{glue}^{*} + 2.4932\ i^{*} - 66.8033\ c_{glue}^{2*}$$

The second mathematical equation has been used to evaluate the effect of the different electrolysis parameters on the defined physical figure, the polarization. The influence of the concentration of copper, nickel, sulphuric acid, thiourea, glue, and the temperature on the cathodic polarization was analysed as

$$U = 93.06 - 4.58\ c_{Cu^{*}} - 8.70\ c_{H2SO4^{*}} - 0.39\ c_{Ni^{*}} - 30.05\ T^{*} - 13.27\ c_{Thio^{*}} + 40.16\ c_{Glue^{*}} \quad [mV]$$

This second equation could be read as:

- The sign shows the polarization effects, like polarizing (+) and depolarizing (-).
- The most depolarizing effect has the temperature, which decrease the cathodic polarization with the factor 30.
- More than three times lower is the influence of acid concentration with factor 8.7 and more than 6 times higher than the copper concentration with factor 4.6.
- Thiourea is about factor 13 and seems to have a slightly higher influence than the acid concentration.
- The nickel concentration is negligible.
- Polarizing effects show glue. Glue is increasing the cathodic polarization with the factor 40. So it is shown the high influence of the glue concentration on the cathode precipitation at the electrolyses system.

After using the mentioned mathematical program to describe the polarization as a mathematical equation the electrolysis cell has been calculated with the CFD software Fluent. The goals of the simplified calculation were to describe and to optimize the electrolyte flow in the whole electrolysis cell which was separated into

- Forced convection
  The calculation of the forced convection which is influenced by the position of the electrolyte inlet, outlet and electrolyte flow rate has been done
- Natural convection
  The natural flow of the electrolyte caused by the variation of the copper concentration in the electrolyte and the density has been calculated.

The above mentioned calculated polarization has not included the influence of the ratio of the current density and the limiting current density. To be able to modify the calculation of the polarization the following equation has to be added.

$$\eta_{calc} = \eta_{ges} \cdot f_i$$

The dependence of the final polarization of the current density is maintained by the f_i factor. This factor is suggested as $f_i = k \cdot (i/i_0)^x$ and has to be evaluated in further investigations.

The best way to calculate the limiting current density as a function of the electrolyte flow is the CFD calculation. To be able to model a real electrolysis cell it is necessary to split the calculation into two parts:

- a simplified general calculation of the velocity field inside the cell
- a calculation of the reactions in the close electrode layers.

The target was to evaluate the influencing parameters on the electrolysis system in a mathematical describable way. With a combination of the CFD calculation and the polarization equation this can be done.

10 APPENDIX

Chapter 1

E^0	[V]	standard potential

Chapter 3

A, B, C, D, E, F, G, H		companies
CI, CII, CIII,		different qualities C
GI, GII, GIII		different qualities of G
L	[mm]	length
W	[mm]	width
T	[mm]	thickness
D	[mm]	depth
A/A	[mm]	distance anode-anode
A/C	[mm]	distance anode-cathode
MFR	[-]	mole fraction ratio
MFR A	[-]	anode mole fraction ratio
MFR AS	[-]	anode slime mole fraction ratio
MFR C	[-]	cathode mole fraction ratio
MFR E	[-]	electrolyte mole fraction ratio

Chapter 4

FT		field-oriented texture type
FI		field-oriented isolated crystal type
BR		basis-oriented reproduction type
Z		twinning intermediate type
UD		unoriented dispersion type
σ		[N/mm²] surface tension metal-electrolyte
S		[mm²] surface of the nucleus being formed
η	[V]	polarization at the metal ion discharge
z	[-]	number of electrons involved
F	[As/mol]	Faraday constant
i_0	[A/m²]	standard exchange current density
i_K	[A/m²]	cathodic current density
i_{Gr}	[A/m²]	limiting current density
c_0	[mol/l]	concentration of dischargeable ions in the electrolyte
R	[J/kgK]	ideal gas constant
Ψ_1	[V]	external electric potential
MFR I	[-]	mol fraction ratio As/(Sb+Bi)
MFR II	[-]	mol fractin ratio Ag(Se+Te)
SEM		scanning electron microscopy
EDX		energy dispers x-ray analysis

Chapter 5

MS		mould side
AS		air side
R_z	[mm]	Roughness
K		distribution coefficent
c_S	[mol/l]	concentration in the solid phase
c_L	[mol/l]	concentration in the liquid phase
K_{Cu}		equilibrium distribution coefficient of the minor elements in copper
ICP-AES		inductively coupled plasma atomic emission spectrometry
E^0	[V]	standard electrode potential

Chapter 6

CC		copper cathode
T		temperature
U		voltage
U_P		polarization voltage

Chapter 7

i_w	[A]	Amperage by the cube
j	[A/m²]	the current density
a^2	[mm²]	area of the cube of the edge length a
δ_N	[mm]	the final copper deposition layer thickness
κ	[1/Ωm]	specific electrical conductivity
ρ	[Ωm]	specific electrical resistance
R	[Ω]	electrical resistance
L	[m]	the electrode distance
A	[m²]	he effective electrode surface
c	[val/l]	concentration
PS		parallel and same distance
PD		parallel and different distance
CT		canted top to bottom
CL		canted left to right
BT		bent top to bottom
BL		bent left to right
CLD		canted left to right different distance
CTD		canted top to bottom different distance
CC		copper cathode
A	[mm²]	area
i	[A/mm²]	current density
U	[V]	voltage
m	[g]	mass
$m_{theor.}$	[g]	theoretical mass
I	[A]	current

Up	[V]	polarization voltage
$E_{spec.}$	[kWh/t_{Cu}]	specific energy
η	[%]	efficiency
t	[h]	time
$m_{prac.}$	[g]	practical mass
$U_{average}$	[V]	average bath vpltage
Up meas.	[V]	measured polarization voltage
Up cal.	[V]	calculated polarization voltage

Chapter 8

η_T	[V]	electron transfer polarization
η_C	[V]	crystallization polarization
η_D	[V]	diffusion polarization
η_R	[V]	reaction polarization
η_Ω	[V]	resistance polarization
η_{ges}	[V]	total polarization
$\vec{E}_{gl}$		activation energy for the forward reaction
$\overleftarrow{E}_{gl}$		activation energy for the backwards reaction
i_0	[A/m²]	limiting current density
z		valancy
α	[–]	transfer factor
F	[As/mol]	Faraday's constant
R	[J/kgK]	ideal gas constant
T	[°C]	absolute temperature
R^2	[-]	coefficient of determination
Q^2	[-]	PRESS-value
LOF		lack of fit
MS		mean squares, or variance
R^2	[-]	coefficient of determination
SS_{res}		square sum of the residues (difference measured value - model value
$SS_{tot,korr}$		total square sum of the measured values corrected around the average value
y_i		measured value in the data point
$\overline{y}$		arithmetical average value of the measured values
$\hat{y}_i$		model value in the data point i
N		number of data points
c*		standardized concentration
T*		standardized temperature
i*		standardized current density
c_{Thiou}*		standardized concentration of thiourea
c_{Glue}*		standardized concentration of glue
U	[V]	polarization
Max		maximal value

Act		actual value
Min		minimal value
c^s	[mol/l]	concentration in the inner electrolyte
c^0	[mol/l]	concentration on the electrode surface
δ_N	[mm]	diffusion boundary layer
n	[-]	valency
D	[cm^2/s]	molecular diffusion coefficient
CFD		computational fluid dynamics
FEM		the finite element method
x_1, x_2		cartesian coordinate
u	[mm/s]	the velocity vector
u_l	[mm/s]	velocity component
μ	[m^2/s]	viscosity
p	[N/m^2]	pressure
B		„body force“ in x_l-direction
$\langle\rangle$		average value
ϕ	[-]	general dependent variable
k		the turbulent kinetically energy
ε	[m^2/s^3]	dissipation of the turbulent energy
l_t	[m]	characterise turbulent whirl length
η_{calc}	[V]	calculated polarization
η_{ges}	[V]	total polarisation
f_i	[-]	filzwieser iris factor

11 REFERENCES

/1/ Davenport, W.D.: Extractive Metallurgy of Copper at the New Millennium. Metallurgical Review of MMIJ, Vol.16, no.2, Dec. 1999, 151 - 168

/2/ Biswas, A.K., W. G. Davenport: Extractive Metallurgy of Copper. 2nd ed., Pergamon Press, Oxford-New York, 1980

/3/ Ullmans Encyclopädie der technischen Chemie. 4. Auflage, Band 3, Verlag Chemie, Weinheim, 486 - 487

/4/ Torben, E., D. Hannemann: New casting moulds for anode copper. Converter and Fire Refining Practices, TMS, 2005, 159 - 165

/5/ Hein, K.: Theoretische Grundlagen elektrochemischer Prozesse der Metallgewinnung. Skriptum, TU Bergakademie Freiberg, 1975

/6/ Paschen, P., I. Filzwieser: Final Report 2002. Department of Nonferrous Metallurgy, Sponsor Group, 2002

/7/ Paschen, P., I. Filzwieser, Z. Mubarok: Final Report 2003. Department of Nonferrous Metallurgy, Sponsor Group, 2003

/8/ Paschen, P., I. Filzwieser, Z. Mubarok: Final Report 2004. Department of Nonferrous Metallurgy, Sponsor Group, 2004

/9/ Davenport, W.D., J. Jenkins, B. Kenedy, T. Robinson: Electrolytic Copper Refining 1999 World Tankhouse Operating Data. See(15), 3

/10/ Abe, S., Y. Takasawa: Prevention of floating slimes in copper electrorefining. Symposium, Proceedings Denver, 1987

/11/ Noguchi, F., M. Yano, T. Nakamura, Y. Ueda: Form of antimony dissolved into electrolyte during copper electrorefining. Journal of the Minng and Materials Processing, Vol. 109, no. 2, 1994, 121-125

/12/ Kuxmann, U., U. Meyer: Untersuchungen über das Verhalten von Silber und Selen bei der Kupferraffinationselektrolyse. Erzmetall 46 (1993), 346 – 355

/13/ Schab, D., H. Bombach, K. Hein: Untersuchungen zum Verhalten von Silber bei der Kupferraffinationselektrolyse unter praxisnahen Bedingungen, Erzmetall 50 (1997), Nr. 10

/14/ Winand, R.: Electrocrystallization of copper, Manuscript (1975), 67 – 75

/15/ Dutrizac, J.E., T.T. Chen: A Mineralogical Study of Nodulated Copper Cathodes. See(15), p. 383

/16/ Grujicic, D., B. Pesic: Electrodeposition of copper: the nucleation mechanisms. Electrochimica Acta 47, 2002, 2901 - 2912

/17/ O'Keefe, T. J., R. Winand: Proc. P. E. Queneau International Symposium, TMS, 1993 Vol. 1, ISBN 0-87339-218-3

/18/ Winand, R.: Electrocrystallization – theory and applications. Hydrometallurgy 29, (1992), 567 – 598

/19/ Schab, D., K. Hein: Wachstumsstrukturen und Oberflächenformen von Kupferkathoden Einfluss von Leim und Thioharnstoffzusätzen bei erhöhten Stromdichten. Metall, 42. Jahrgang, Heft 11, November 1988, 1086-1091

/20/ Forker; W.: Elektrochemische Kinetik. 2nd Ed. Akademie-Verlag Berlin, 1989, ISBN 3-05-500486-8

/21/ Dutrizac, J.E., J. Ji, V. Ramachandran (Edts.): Electrorefining and electrowinning of copper. Proc. Copper99/ Cobre99 Internat. Conference, Vol. III, TMS, 1999

/21/ Lange, H.J., K. Hein, I. Bauer, D. Schab: Aspekte der Elektrodenkinetik bei Metallelektrolysen. GDMB Heft 81: Elektrolyseverfahren in der Metallurgie, 1997, 137-160

/22/ Winand, R.: Electrocrystallization. Process metallurgy 3: Application of polarization measurements in the control of metal deposition, Elsevier Science Publishers B.V, Amsterdam, 1984, 47-83

/23/ Fischer, H.: Elektrolytische Abscheidung und Elektrokristallisation von Metallen. Springer-Verlag, Heidelberg, 1954

/24/ Li, Jun, Ting-Ke Zhong, Milton E. Wadsworth: Application of mixed potential theory in hydrometallurgy. Hydrometallurgy, 29 (1992), 47-60

/25/ Forsen, O.: The role of organic additives on the quality of copper in electrorefining process. Proceedings of the Conference of Copper 90. Refining, Fabrication, Markets, Sweden, 1990, 189 – 197

/26/ Knuutila, K., O. Forsen, A. Pehkonen: The effect of organic additives on the electrocrystallization of copper. The electrorefining and winning of copper, edited by J.E. Hoffmann et. All, The Metallurgical Society, 1987, pp. 129 -143

/27/ Suarez, D.F., F.A. Olson: Nodulation of copper cathodes by electrorefining addition agents thiourea, glue and chloride ions. The electrorefining and winning of copper, edited by J.E. Hoffmann., The Metallurgical Society, 1987, 145 – 170

/28/ Winand R.: Industrial electrodeposit of copper. Problems connected to the behaviour of organic additions. Process Metallurgy 3, Application of Polarization Measurements in the Control of Metal Deposition, Elsevier, 1984, 133 – 145

/29/ Winand R.: Electrocrystallization of copper. Transaction of Mineral Processing & Extractive Metallurgy, vol. 84, 1975, C 67 – C 75

/30/ Schab, D.: Elektrolytischer Stoffübergang und Elektrokristallisation bei der Kupferraffinationselektrolyse mit erhöhten Stromdichten. Dissertation, TU BAF, 1981

/31/ Langner, Bernd. E., Peter Stantke: The use of COLLAMAT-system for measuring glue activity in copper electrolyte in the laboratory and in the production plant. EPD Congress 1995, edited by G.W. Warren, The Minerals, Metals & Materials Society, 1995.

/32/ Cooke, A.V., J.P. Chilton, D.J. Fray: Electrode mass transfer under conditions of natural and forced convection. Met. Trans. B. Vol 20 B, no.1, 1989, 21-29

/33/ Ibl N., Y. Barranda, G. Trümpler: Zur Kenntnis der natürlichen Konvektion bei der Elektrolyse: Interferometrische Untersuchungen der Diffusionsschicht. I Helvetica Chimica Acta 37 (1954), 583 - 597

/34/ Awakura Y., Y. Kondo: Concentration profile in the cathodic diffusion layer. Journal of Electrochem. Society 123 (1976), 1184 - 1193

/35/ Starsinzky H., K. Hein, D. Schab: Strömungsbedingungen in Elekrolysezellen für die elektrolytische Kupferraffination. Neue Hütte 18 (1973), 346 - 352

/36/ Milazzo, G.: Elektrochemie. Springer-Verlag, Wien 1952

/37/ Chen, T.T., J.E. Dutrizac: The mineralogy of copper electrorefining. JOM, August 1990.

/38/ Virtanen, H., T. Marttila, R. Pariani: Outokumpu moves forward towards full control and automation of all aspects of copper refining. See (12), p. 207

/39/ Geenen, C., J. Ramharter: Design and Operating Characterization of the New Olen Tankhouse. See (15), p. 95

/40/ Hein, K: Theoretische Grundlagen elektrochemischer Prozesse zur Metallgewinnung. Vorlesungsunterlage, Bergakademie Freiberg 1976

/41/ Fischer, M.: Beitrag zur Bildung und zum Verhalten des Anodenschlammes bei der Kupfer-Raffinationselektrolyse. Dissertation, Bergakademie Freiberg, 1998

/42/ Hein, K., E. Buhrig: Kristallisation aus Schmelzen. VEB Deutscher Verlag für Grundstoffindustrie, Leipzig, 1983

/43/ Anzinger, A., J. Wallner, H. Wöbking: Spezielle Effekte, beobachtet in der Kupferraffinationselektrolyse der Montanwerke Brixlegg AG. Vortrag auf der Kupferfachausschusstagung Fulda, März 1998

/44/ Moats, M.S., J.B. Hiskey: Post-passivation reactions occurring at the anode during copper electrorefining. See (15), p. 405

/45/ Backs, A., Feneau C., Tougarinoff B.: Anodenprobleme bei der elektrolytischen Kupferraffination. Erzmetall, 22 (1969) Beiheft, 120-127

/46/ Buhrig, E., Hein K., Baum H.: Verteilung von Fremdelementen bei der Kristallisation von Kupfer. Metall, 33 (1979) 6, 592-596

/47/ Chen T.T., Dutrizac J.E.: Application of electron microscopy to the electrorefining of copper. Scanning Microscopy, 2 (1988) 2, 735-746

/48/ Forsen O., Tikkanen M.H.: On the disolution of copper anodes in electrolytic refining. Part I: The behaviour of nickel in oxygen-bearing copper anodes. Scandinavian Journal of Metallurgy, 10 (1981), 109-114

/49/ Klose M: Untersuchungen über das Verhalten insbesondere von Nickel und Antimon bei der Kupferraffinationselektrolyse. Dissertation TU Clausthal(1990)

/50/ Chen T.T., Dutrizac J.E.: A mineralogical overview of the behaviour of nickel during copper electrorefining. Metallurgical Transaction B, 21B (1990), 229-238.

/51/ Chen T.T., Dutrizac J.E.: Mineralogical characterisation of anode slimes-4. Copper-Nickel-Antimony Oxide("Kupferglimmer") in CCR anodes and anode slimes. Canadian Metallurgical Quarterly (28), 1989 p. 127 - 134

/52/ Abe S., Burrows B.W., Ettel V.A.: Anode passivation in copper refining. Canadian Metallurgical Quarterly, 19 (1980), 289-296.

/53/ Chen T.T., Dutrizac J.E.: Mineralogical characterisation of anode slimes-7. Copper anodes and anode slimes from the Chuquicamata Division of Codelco Chile. Canadian Metallurgical Quarterly (30), (1991) 2, p. 95- 106

/54/ Bombach H., Hein K.: Beitrag zum chemischen Verhalten von Arsen und Antimon im schwefelsauren Kupfersulfatelektrolyten. Neue Hütte, 29 (1984) 4, 144-146

/55/ Claessens P.L., Baltazar V.: Behaviour of minor elements during copper electrorefining. Verlag Chemie Int. Symp. 1983, 253-265

/56/ Chen T.T., Dutrizac J.E.: Mineralogical characterisation of anode slimes-2. Raw anode slimes from Inco's Copper Cliff Refinery. Canadian Metallurgical Quarterly (27), (1988) 2, p. 97- 105

/57/ Ringel L., Hein K., Schab D.: Untersuchungen zum elektrolchemischen Verhalten von Cu-Ag-Legierungen. Neue Hütte, 19 (1974) 4, 193-197

/58/ Abe S., Goto S. :Effect of anode impurities upon Passivation of copper anodes, Journal of the Mining and Metallurgical Institut of Japan, Vol. 100 (1984), 429 - 433

/59/ Brugger G., Jeglitsch F., Wöbking H., Wallner J.: Ursachen von Passivierungserscheinugen während der Kupfer-Raffinationselektrolyse. Erzmetall, 48 (1995) 10, 691ff

/60/ Graumann D., Fischer-Bartelk Ch., Schab D.: Untersuchungen zum Verhalten von Silber bei der elektolytischen Kupferraffination. Neue Hütte 17 (1982), 71-76

/61/ Henning U., Pawlek F.: Untersuchungen über die Konstitution von Kupferelektrolytschlämmen. Erzmetall Bd. 13, Heft 5, 1960, S205ff

/62/ Westhoff F.J.: Untersuchungen über das Verhalten von Zinn und Blei bei der Kupferraffinationselektrolyse; Dissertation, TU Clausthal 1990.

/63/ Weise P.: Zeitschrift für Elektrochemie 28(1922), S.327

/64/ Autorenkollektiv: Untersuchungen über das Verhalten von Zinn, Nickel, Antimon und Blei bei der Kupferraffinationselektrolyse; Schriftenreihe der GDMB, H.57, 1990

/65/ Bacher, I.: Untersuchung der gasblaseninduzierten Zwangskonvektion in der Kupfer-Hochstrom-Gewinnungselektrolyse. Diplomarbeit, Montanuniversität 2002.

/66/ Tipler, A.P.: Physik. Spektrum akademischer Verlag GmbH Heidelberg, Berlin, 1994.

/67/ Baimakov, J.W., A.I. Churin: Elektrolyse in der Hydrometallurgie. Übersetzung aus dem Russischen,Moskau 1963, S.2-118

/68/ Hanko, G.: Untersuchung und Bestimmung der Hydrodynamik einer Kupfergewinnungselektrolyse mittels LDA. Diplomarbeit, Leoben Montanuniversität, 2000

/69/ Grossinger, A.: Die Beeinflussung des kathodischen Niederschlages durch die chemische Anodenqualität in der Kupferraffinationselektrolyse, Diplomarbeit, Montanuniversität 2004

/70/ Kothmaier, M.: Untersuchungen des Einflusses der Anodenqualität und der geometrischen Bedingungen auf die kathodische Stromdichteverteilung in der Kupferraffinationselektrolyse, Diplomarbeit, Montanuniversität 2003

/71/ Ettl R., T. Omer, J. Wundersamer: Influence of solid materials in the electrolyte, HTL Diplomarbeit, Montanuniversität Leoben, 2003

/72/ Kortüm, G., Lehrbuch der Elektrochemie, Verlag Chemie, Weinber/Bergstraße, 1966

/73/ Vetter, K. J., Elektrochemische Kinetik. Springer-Verlag, Berlin/Göttingen/Heidelberg, 1961

/74/ Eichkorn, G., H. Fischer, H. R. Mache, Kristallisationsvorgänge bei der elektrolytischen Kupferabscheidung auf polykristalline Kupferunterlagen I. Bestimmung der Kristallisationsüberspannung in Abwesenheit von Inhibitoren. Berichte der Bunsen-Gesellschaft 75, (1971) 5, 482-488

/75/ Eichkorn, G., H. Fischer, H. R. Mache, Kristallisationsvorgänge bei der elektrolytischen Kupferabscheidung auf polykristalline Kupferunterlagen II. Einfluss eines primären Grenzflächeninhibitors auf die Kristallisation, Keimbildungsprozesse. Berichte der Bunsen-Gesellschaft 76, (1972) 12, 1264 - 1270

/76/ Kotzschmar A.: Electrochemical characterization of the influence of organic additives in copper electrorefining. Diploma thesis, Department of Materials Science and Rock Engineering, Faculty of Process Engineering and Material Science, Helsinki University of Technology, Finland.

/77/ Jin S., E. Ghali: Effects of gelatine, thiourea and chloride ion on the copper cathode polarization behaviour in acidic copper sulphate at 65°C. Canadian Metallurgical Quarterly, Vol. 40, No. 4, pp. 433-440, 2001

/78/ Meyer, R.: Kupferfolienherstellung bei Stromdichten > 1000 A/m². Diplomarbeit, Leoben Montanuniversität, 2000

/79/ Filzwieser, A., A. Lackner, K. Hein: Möglichkeiten zur Strömungsberechnung in Elektrolysezellen unter besonderer Berücksichtigung des Stofftransportes. Schriftenreihe der GDMB, Heft 81 (1997), 161 – 172

/80/ Hein, K., G. Hanko, A. Filzwieser, M. Stelter: Untersuchungen zur Hydrodynamik bei der Kupfergewinnungselektrolyse. BHM 144 (1999), 6 – 13

/81/ Filzwieser, A., K. Hein, G. Hanko, H. Grogger: Application of two phase hydrodynamic modeling to an electrowinning cell. Proc. of the 4th Int. Conference „Copper 99 – Cobre 99", Vol. III, Phoenix, Arizona, USA, October 1999, 695 – 709

/82/ Hanko, G., K. Hein, A. Filzwieser: Visualisierung und Quantifizierung der Strömungsverhältnisse in einer Kupfergewinnungselektrolyse. Erzmetall 52 (1999), 226 – 235

/83/ F. Harlow, P. Nakayama: Transport of turbulence energy decay rate. Report LA-3845, Los Alamos Science Lab., University of California

/84/ Lackner, A.: Strömungssimulation in verschiedenen Reaktoren der NE-Metallurgie, Dissertation; Montanuniversität Leoben, Österreich, 1996

/85/ Filzwieser, A.: Modellierung der kathodennahen Vorgänge in der Kupferelektrolyse, Dissertation, Montanuniversität Leoben, Österreich, 2000

/86/ Price, D.C., W.G. Davenport: Densities, electrical conductivities and viscosities of $CuSO_4/H_2SO_4$ solutions in the range of modern electrorefining and electrowinning electrolytes. Metall.Trans. 11B (1980), 159 - 163